UNIVERSITÄT ZU LÜBECK

From the Priority Research Area Infections of the

Research Center Borstel

Programm - Direktor: Prof. Dr. Ulrich E. Schaible

Aerosol Particle Analysis of Airborne Human Pathogens, Represented by *Mycobacterium bovis* BCG and Influenza A virus.

Inauguraldissertation

zur

Erlangung der Doktorwürde

der Universität zu Lübeck

Aus der Sektion Naturwissenschaften

vorgelegt von

Karoline Elisabeth Pfrommer

aus Frankfurt am Main

Lübeck, 04.04.2020

Dissertationsgutachter / *dissertation reviewer:*

1. Gutachter / *first reviewer*: **Prof. Dr. Ulrich E. Schaible**

Department of Cellular Microbiology, Leibniz Lung Center Borstel, Borstel, Germany

2. Gutachter / *second reviewer*: **Prof. Dr. Christian Hübner**

Institute for Physics, University of Lübeck, Lübeck, Germany

vorgelegt von / *submitted by*: **Karoline Elisabeth Pfrommer**

vorgelegt am / *submitted:* 10th of April 2020

Mündliche Prüfung/ *oral examination*:

1. Gutachter/ *first reviewer*: **Prof. Dr. Ulrich E. Schaible**

Department of Cellular Microbiology, Leibniz Lung Center Borstel, Borstel, Germany

2. Gutachter/ *second reviewer*: **Prof. Dr. Christian Hübner**

Institute of Physics, University of Lübeck, Lübeck, Germany

Prüfungsvorsitzender/ *chair of examination:* **Prof. Dr. Norbert Tautz**

Institute of Virology and Cellbiology, University of Lübeck, Lübeck, Germany

Prüfling/ *Examinee:* **Karoline Elisabeth Pfrommer**

am/ *on the:* 11th November 2020

Diese Arbeit wurde im Zeitraum vom
01. September 2015 bis zum 30. Dezember 2019 im Rahmen des interdisziplinären Forschungsverbundes INFECTION'S 21 an den folgenden Instituten angefertigt:

1. Forschungszentrum Borstel, Leibniz Lungenzentrum (Direktor: Prof. Dr. Stephan Ehlers, Fachbereich Experimentelle Medizin) unter Betreuung von Prof. Dr. Thomas Gutsmann und Prof. Dr. Ulrich Emil Schaible.
2. Heinrich-Pette-Institut, Leibniz-Institut für Experimentelle Virologie (Direktor: Prof. Dr. Thomas Dobner, Fachbereich Biologie der Universität Hamburg), unter Betreuung von Prof. Dr. Gülşah Gabriel.
3. TROPOS, Leibniz Institut für Troposphären Forschung (Direktor: Prof. Dr. Andreas Macke, Fachbereich Physik der Atmosphäre der Universität Leipzig) unter Betreuung von PD Dr. Kerstin Schepanski.

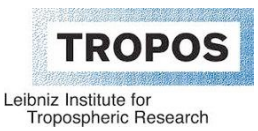

Table of Content

Index of Abbreviations

ACI	Andersen Cascade Impinger
AH	absolute humidity
ALI	air liquid interface
APS	aerosol particle spectrometer
BAL	broncho-alveolar lavage
BCG	*Mycobacterium bovis* Bacillus Calmette Guerin
cDNA	copy deoxyribonucleic acid
CD	cluster of differentiation
CDC	climate data center
CFU	colony forming unit
DNA	deoxyribonucleic acid
FA	formaldehyde
FCS	fetal calf serum
GA	glutaraldehyde
H_2O_2	hydroperoxide
HA	hemagglutinin
HA assay	hemagglutination assay
HMDS	hexamethyldisilazan
IAV	influenza A virus
IFN	interferon
IgG	immunoglobulin G
IgG-HRP	immunoglobulin G coupled horse reddish peroxidase
IL	interleukin
LDH	lactate dehydrogenase
M	matrix protein
MDCK	madin-darby canine kidney cells
M.tuberculosis	*Mycobacterium tuberculosis*
mRNA	messenger RNA
NA	neuraminidase
NaCl	natriumcloride
NLS	nuclear localization signal
NP	nucleoprotein

NS	non-structural protein
OD	optical density
ORF	open reading frame
PFU	plaque-forming unit
PA	polymerase acidic protein
PB1	polymerase basic protein 1
PB2	polymerase basic protein 2
PBS	phosphate-buffered solution
PCR	polymerase chain reaction
PFA	paraformaldehyde
PMN	polymorphonuclear cell family (neutrophils)
pH1N1	pandemic H1N1
PPRs	pattern recognition receptors
RH	relative humidity
RNA	ribonucleic acid
RPMI cell medium	roswell park memorial institute cell medium
RNS	reactive nitrogen species
ROS	reactive oxygen species
SA	sialic acid
TAE	TRIS-Acetat-EDTA buffer
TB	Tuberculosis
TLR	toll-like receptors
TNF-α	tumor necrosis factor- α
UV light	ultraviolet light
vRNA	viral RNA
WHO	world health organization

Glossar

	Name	Definition
A		
	A/Hamburg/05/09(H1N1)	Nomenclature: Virus serotype/Place of first isolation/consecutive number assigned by the WHO/ year of isolation/HA- NA- subtype combination.
	Aerosol	An aerosol is a colloid of fine solid particles, in our case pathogens. They can transmit through the air both via aerosols (>5 µm) and droplets (<5 µm). In our definition aerosol is an umbrella term for both.
	Aerodynamic diameter	Abstract measure for airborne particles, that dismisses the individual shape of the particle.
	AFM	Atomic Force Microscopy (AFM) allows imaging of the three-dimensional topography of a sample at high resolution, thus AFM will be used to define the surface, the volume and height of aerosols and pathogens.
	Airborne particle	Particles isolated from the air and is part of an aerosol.
B		
	BAL	Broncho alveolar lavage: flushing of the lung with isotonic buffer.
	BCG	*Bacillus Calmette- Guerin*: Mycobacterium which structurally is quite close to *Mycobacterium tuberculosis*, but is only pathogenic in humans with severe immune deficiency and classified as BSL1. It can therefore be used without fixation.
	BSL 1-4	Biosafety level: A biosafety level is a set of biocontainment precautions required to isolate dangerous biological agents in an enclosed laboratory facility. The levels of containment range from the lowest biosafety level 1 (BSL-1) to the highest at level 4 (BSL-4).
	BSL 1-3 facility	Facility with required security measurements to work with BSL classified pathogens.

C		
	CFU	Colony Forming Unit: Method which allows the determination of bacterial numbers in a sample. Each bacterium will form a colony which then can be counted.
H		
	H1N1	Subtype of influenza A virus which can be found in human, pigs and water fowl. Most prominent epidemic caused by H1N1 type, is the Spanish flu.
I		
	IAV	Influenza A Virus
	Impinger	Instrument in which fine particles in a gas (ambient air) are analyzed by blowing them through a jet onto a suitable plate (glas, mica, Cu2+ grids). Andersen is the inventor of the multistage Impinger in which sizing is possible.
	Impactor	Instrument in which fine particles in a gas/air are collected by blowing them through a liquid, in which they are washed out.
K		
	Köppen climate classification	The Köppen climate classification divides climates into five main climate groups, with each group being divided based on seasonal precipitation and temperature patterns. The five main groups are *A* (tropical), *B* (dry), *C* (temperate), *D* (continental), and *E* (polar). All climates are assigned a main group (the first letter) as well as a seasonal precipitation group and temperature subgroup. For example, *Cfb* indicates an oceanic climate with warm summers as indicated by the ending *b*.
M		
	MDCK cells	Madin-Darby Canine Kidney cells were originally isolated from a kidney of a dog, which is highly susceptible to IAV infection.
	Mucus	Mucus is a slippery secretion produced by, and covering, mucous membranes. Mucous fluid is rich in

		glycoproteins and water and is typically produced from Goblet cells found in mucous glands.
P		
	PFU	Plaque Forming Unit: Method to determine the numbers of viable virus in a solution.
S		
	Soluble particle	Pathogens which were isolated by flushing the respiratory tract with an isotonic-fluids like nasal washes and BAL.
T		
	TEM	Transmission Electron Microscope: Particle morphology will be analyzed by TEM, which allows high resolution imaging of particles. An image is formed from the interaction of the electrons transmitted through the specimen and then magnified and analyzed with certain software. This will allow to understand the structure of aerosols and their embedded pathogen particles.

List of Tables

List of Figures

Abstract

Airborne pathogens include a wide variety of highly infectious and dangerous microbes. Two prominent airborne pathogens are *Mycobacterium tuberculosis* (*M. tuberculosis*) and influenza A virus (IAV). Both cause important respiratory infections, are proliferating in hosts cells and are transmitted via the airborne route between humans.
Studying underlying biophysical properties of pathogens and the influence of the infected cells and tissues in the respiratory tract involved in the infectious process on properties of aerosols containing pathogens, will help to understand the mode in which pathogens can be transmitted through the air.
As a pathogen overarching results, analyses of mycobacteria and IAV containing aerosols indicate an average aerodynamic diameter, that would allow long distance transmission. However, viability of airborne pathogens while airborne is quickly lost in both mycobacteria and IAV. By analyzing pathogen-containing aerosols from infected cells to mimic aerosol formation of infected patients experimentally, we found an increase in aerodynamic diameter for both pathogen containing aerosols increased, indicating short distance transmission between infected and sentinel host as aerosols are quicker settling down.
Mycobacteria-infected necrotic neutrophils, predominant in active tuberculosis patients, revealed similar particle sizes and viability rates as free mycobacteria, but in addition, larger aggregates of viable mycobacteria. These mycobacteria are shielded multi-bacillary aggregates from necrotic neutrophils from environmental stresses such as drying out. Analysis of viral aerosol particles generated from a primary nasopharyngeal tissue model in comparison to cell line-derived viral particles, revealed a direct correlation between the thickness of the mucus corona around the virus particle and the aerodynamic diameter. Influenza transmission is influenced by environmental, ecological and evolutionary processes shaping the transmission potential of airborne IAV particles. Considering fluctuating environmental conditions including specific humidity as a key driver, we analyzed their effect on the infection dynamic during the influenza season between 2010 and 2018 in Germany. The intensity of the influenza season as well as season onset and progression were driven by climatic conditions. But as wind is not influencing the geographical distribution of IAV incidence, we postulate a short distance transmission for IAV particles in a wind independent likely indoor environment.
A better understanding of physicochemical properties and airborne transmission modalities of pathogen containing aerosol particles and the required pathology will enable us to better define risks of infection, to improve protocols to protect risk groups like care takers or house hold contacts and to, ultimately, develop measures to prevent pathogen spreading.

Zusammenfassung

Krankheitserreger, die über die Luft übertragen werden können, umfassen eine Vielzahl für Menschen hochinfektiöser und gefährlicher Mikroben.
Zwei der bekanntesten luftgetragenen Krankheitserreger sind der Tuberkuloseerreger (*Mycobacterium tuberculosis*) und das Influenza A Virus (IAV). Beide verursachen Infektionen der Atemwege, wo sie sich in Wirtszellen vermehren und werden von Mensch zu Mensch unter anderem auf dem Luftweg über Pathogenen-beladene Aerosole übertragen.
Unsere Studien zeigten, dass die biophysikalischen Eigenschaften und der aerodynamische Durchmesser dieser Aerosole eine weiträumige Verbreitung erlauben würden. Der reduzierte Verbreitungsradius der Pathogene ist dennoch eingeschränkt, was an der mangelnden Überlebensfähigkeit der Pathogene in der Umwelt liegt.
Anhand der experimentellen Nachahmung der Aerosolbildung aus infizierten Zellen, wie sie im infizierten Patienten erfolgt, stellt die wichtigste Erreger-übergreifende Erkenntnis dieser Arbeit das Ergebnis dar, dass der aerodynamische Durchmesser solcher Erreger-haltigen Aerosole im Vergleich zu Aerosolen, die nur mit dem reinen Pathogen beladen waren, zunahm.
Bei der aktiven Tuberkulose sind mit Mykobakterien infizierte nekrotische Neutrophile in der Lunge vorherrschend. Diese zeigen ähnliche Partikelgrößen und Überlebensraten wie freie Mykobakterien, jedoch werden in den Aerosolen aus mit Mykobakterien infizierten nekrotischen Neutrophilen zusätzlich große Aggregate mit lebenden Mykobakterien gefunden. Vermutlich schützen die durch die nekrotischen Neutrophilen gebildeten multibazilliären Aggregate die Mykobakterien vor schädlichen Umwelteinflüssen wie das Austrocknen.
Durch die Analyse viraler Aerosolpartikeln aus in Kultur infiziertem primärem Nasenpithelgewebe im Gegensatz zu in Zelllinien generiertem Virus konnte auch für IAV gezeigt werden, dass ein erhöhter Schutz vor Umwelteinflüssen, hier durch eine dickere Mukusschicht der Epithelzellen, mit einem vergrößerten aerodynamischen Durchmesser einhergeht, der die Verweildauer in der Luft verkürzt.
In diesem Zusammenhang wurde dann die geographische Ausbreitung von IAV im Hinblick auf Umwelteinflüsse wie Temperatur, Luftfeuchtigkeit und Wind anhand der Daten über die Grippewellen der Jahre 2010 - 2018 modelliert. Die Tatsache, dass der Wind keinen Einfluss auf die geographische Verbreitung von IAV hat, deutet auf eine kurze Verweildauer in der Luft und eine Verbreitung in vom Wind unbeeinflussten Innenräumen hin.
Ein besseres Verständnis der physikalisch-chemischen Eigenschaften und der Übertragungsmodalitäten von Aerosolpartikeln in der Luft für Krankheitserreger und die erforderliche Pathologie wird es uns ermöglichen, Infektionsrisiken besser zu definieren, Protokolle zum Schutz von Risikogruppen wie Betreuern oder Haushaltskontakten zu verbessern und letztendlich Maßnahmen zu entwickeln die die Ausbreitung von Krankheitserregern zu verhindern.

Preamble

Understanding the survival and decay of airborne microorganisms is essential for public health measures aiming to reduce the spread of pathogens transmitted through the air. Prominent airborne bacterial and viral pathogens are *M. tuberculosis* (*Chapter 1)* and IAV (*Chapter 2 and 3* respectively). Both pathogens cause important respiratory infections in humans and are transmitted via the airborne route from human to human.

After an *Introduction* to bioaerosols in the context of human pathogens, the biophysical properties of human pathogens, the effects on airborne pathogens of exposure to ambient environmental elements and the underlying aerobiology that allow airborne transmission will be discussed *(Chapter 1 and 2).* After determination of probability for both pathogens of either short- or long- distance transmission, we modelled the effects of weather conditions on particle transport of IAV (*Chapter 3*). Finally, common findings for both pathogens and their correlation to the situation of other aerosol transmitted pathogens are concluded (*Conclusion)*.

1 INTRODUCTION: Airborne Transmission of Diseases

Transmission of diseases from human to human can result from either direct contact with an infected person or indirect contact through intermediate medium, including air. Direct contact transmission is accomplished by large infectious aerosols, also called droplets, which travel over a short distance from an infected person to a not infected one[1]. Some pathogens are able to transmit indirectly and are not dependent on close proximity of hosts[2]. An important mode of indirect contact transmission is airborne transmission. Airborne transmission can occur via the spread of fine aerosol particles in ambient air over long distances and time scales.

The term airborne is conceived by the medical profession as aerosols that are transported by airflows over long time periods (minutes) and large distances (>1 m)[3]. As reviewed before by Owen *et al.*, most papers define aerosols that contribute to airborne infection as smaller than 5 µm in aerodynamic diameter, an abstract measure for airborne particles[4]. There are hundreds of airborne communicable pathogens falling into three major categories: i) viruses are the smallest with a diameter of 0.02 – 0.3 µm , ii) bacteria with diameter ranges of 0.5 – 10 µm and iii) spores with diameters in the range of 0.5 – 30 µm[5,6].

1.1 Bioaerosols

Bioaerosols are airborne particles, that originate biologically from either plants, animals or humans and are defined as suspensions of fine solid or liquid particles in gas. Shapes of bioaerosols can be sorted into three basic categories i) particles that are perfectly or approximately spherically shaped ii) particles of rod or filamentous shape and iii) particles that are disk and platelet shaped[7]. Those different shapes determine the behavior of particles in air. Dismissing the individual shape of the airborne particle, the aerodynamic diameter of a particle is defined as sphere, whose density is 1 g/cm^{-3} and settles in still air at the same velocity as the particle in question[8]. The aerodynamic diameter is therefore a good measure, as it allows comparison between biological particles of different origins.

The aerodynamic diameter of bioaerosols is defined not only by the size of a particle itself but rather by the complex mixture of various components, that strongly influence the ability of an airborne particle to take water up. Thus, swelling of the aerosol particle by water uptake changes the aerodynamic diameter. Those components include salts, proteins and other organic and inorganic matters with hygroscopic properties.

Velocity properties of a bioaerosol depend on the counter play of its mass density and buoyancy. Thus, larger particles tend to settle faster than smaller particles. The settling velocity of 0.001 µm particles is $6.75*10^{-9}$ m/s while 10 µm particles already settle at $3.06*10^{-3}$ m/s and 100 µm particles drop at $2.49*10^{-1}$ m/s[8].

When studying bioaerosols generated by humans, different aspects of the bioaerosol biogenesis should be considered (Figure 1). Airborne transmission of pathogens is mainly influenced by four factors: i) the target organ, i.e. the respiratory tract ii) the pathogen induced pathology, which is based on virulence and host response associated to inflammatory processes promoting cell death, exacerbated pathology and the expelling of the pathogen as aerosol droplets[9]; iii) the aerobiology of pathogen-containing aerosols, which facilitates airborne transmission and is determined by size and other physicochemical characteristics of the aerosol particles[10] as well as environmental factors and iv) aerosol deposition in the respiratory tract and the availability of a susceptible host.

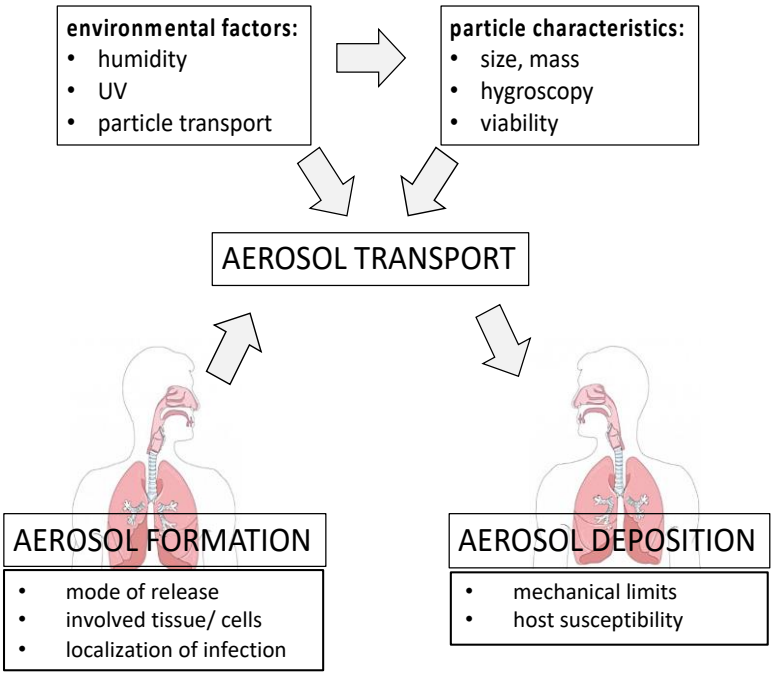

Figure 1: Biogenesis of Human Pathogen-Containing Aerosols. The human lung can function as bioaerosol generator and collector. The formation of aerosols depends on the mode of release and the involved tissue. Released particles show certain characteristics that will enable the airborne transmission. The tenacity of an airborne pathogen is therefore dependent on particle characteristics like size and mass density of the pathogen and its resilience to environmental factors. Those can either enhance transmission, as they enhance transport efficiency of the particle or reduce transmission by limiting pathogen viability. The circle of successful transmission is completed, when the pathogen is inhaled by a susceptible host and deposited at the preferred site for infection.

1.2 The Human Lung as Bioaerosol Generator

Natural human respiratory activities include breathing, sneezing and coughing, which produce expiratory droplets. The human as source of pathogen containing aerosols is particularly important in the spread of airborne infection between humans as the species barrier is not given[11].

Several mechanisms of particle generation from these activities have been postulated. During normal breathing conditions aerosols are broken down through a process of condensation and air stream turbulences. When warm and wet gas transits from the alveolar region to the upper respiratory tract, the containing water condensates and the turbulent airflows expels liquid aerosols during exhalation[12]. Coughing or sneezing increases air turbulence, thus a higher proportion of liquid is broken down and lager particles are expelled. At colder temperatures more water evaporates from the respiratory tract during breathing and thus it can be assumed that more aerosol particles are produced[13].

Production of infectious respiratory particles depends on the type and frequency of respiratory activity, type and side of infection and pathogen load. Different types of respiratory activities will produce different numbers and sizes of exhaled particles (Table 1). In addition, the frequency of the activity is important and even though one sneeze produces multiple amount of particles compared to breathing, breathing occurs constantly and therefore overall more airborne particles are exhaled[12]. Additionally, different activities of the respiratory tract will generate particles at different sites of the respiratory tract. While sneezing and coughing mainly produces particles in the upper respiratory tract, breathing produce particles from the lower respiratory tract[13,14]. Comparing results from Table 1, we can observe a large variation in reported droplet size. This can be attributed to three major causes: i) the sensitivity of different measurement techniques, ii) the unrepeatable nature of coughs and sneezes for each subject as well as the variability of coughs and sneezes among different subjects, and iii) the evaporation of droplets at different time scales according to the given environmental conditions.

Besides particle size and number also the initial velocity distribution differs between the various respiratory activities. Velocities of aerosol particles during sneezing have been analyzed before and a wide variability has been reported. While Jennison *et al.* reported a sneezing determined aerosol particle velocity of 46 m/s, Wells *et al.* even suggested an estimate of 100 m/s and Tang *et al.* at 4 m/s[15–17]. Velocities of aerosol particles during

coughing were described by Kwonn *et al.* and found at 15.3 m/s (male) / 10.6 m/s (female) and speaking velocity was about 22 – 27 % of coughing velocity[18].

Table 1: Aerosol Sizes Generated by the Human Lung

Author, Date	**Sampling method**	**Infection status of partipicant**	**Predominant particle size range [µm]**			**# of expelled particles**
			Breathing	Coughing	Sneezing	
Han *et al.* 2013[19]	Laser particle size analyser	Healthy			74-360	
Milton *et al.* 2013[20]	slit impactor	IAV H1N1	0.01-100	<0.1-500		$1.3*10^5$ [copies in 30 min]
Lindsley *et al.* 2010[21]	two stage aerosol sampler	IAV H1N1	0.005-5	1-4		15.8 (SD29.3) [per cough]
Holmgren *et al.* 2010[22]	SMPS	Healthy	0.01-2			10.8 ± 22.3 [#/cm^3]
Fabian *et al.* 2011[14]	Optical particle counter	Human rhinovirus	0.3-10 (82 % at 0.3-0.49)			0.1 – 7200 [#/l]
Fabian *et al.* 2008[23]	Optical particle counter	Influenza	87 % under 1 µm			67 – 8500 [#/l]
Papineni und Rosenthal 2009[24]	Solid impaction and optical counter	Healthy	98 % under 1 µm			14 – 3230 [#/l]

1.3 Airborne Pathogens in the Atmosphere

The fate of an aerosol in the environment is governed by several physical variable's endemic to the infectious particle. Pathogens can persist in the atmosphere as individual cell or can be associated with other particles like soil dust, leaf fragments, spores or other microbes[25–27]. Due to their size they can remain in the atmosphere for a prolonged time period. In fact, even intercontinental transport has been observed, like transport of *Neisseria meningitis*, the cause of meningococcal meningitis, with dust plumes[28].

Once aerosolized, microbes are substantially influenced by environmental conditions. Especially temperature and air humidity are considered as determining factors in successful transmission as they influence the viability of pathogens[29–37].

1.3.1 Influence of Temperature

Pathogens are very differently impacted by varying temperature. In general, low temperatures have been suggested to be ideal for airborne transmission. IAV survival decreases progressively with increasing temperatures[38]. In contrast, for successful *M. tuberculosis* transmission, a dependency on higher temperatures was described[34].

1.3.2 Influence of Humidity

Ambient air contains a certain amount of water vapor, which can be described as either absolute humidity (AH) [kg/m^3] or as relative humidity (RH) [%]. The ambient water content influences directly the tenacity of airborne microbes. Airborne particles are expelled from the human respiratory tract and interact with this water vapor, during their time in air. Depending on their inherent hygroscopicity, airborne particles uptake water, which usually leads to increased particle mass density, particle volume and settling velocities. In reality, compared to the respiratory tract with a 100 % humidity, all exhaled particles will primarily lose in size, as water evaporates, the moment they leave the respiratory tract. Dehydration may either lead to a reduction in viability and thus, decreases the tenacity of airborne pathogens or as volume, mass and aerodynamic diameter decrease, prolong their ability to stay airborne. Interestingly, for IAV particle a lower RH seems to be favorable for transmission[34,36]. In contrast for *M. tuberculosis* seems to have a higher RH favorable for transmission[34,36,38,39].

1.4 Depostion of Bioaerosols in the Human Respiratory Tract

The human respiratory tract is organized in regions, the upper respiratory tract (URT), including nasal cavity, nasopharynx, laropharnyx and trachea and the lower respiratory tract (LRT). The LRT that can be subdivided into air conducting zone, including bronchi and non-alveolated bronchiolae and the gas exchange zone including the respiratory bronchiolae and alveolae inclosing sacs (Figure 2).

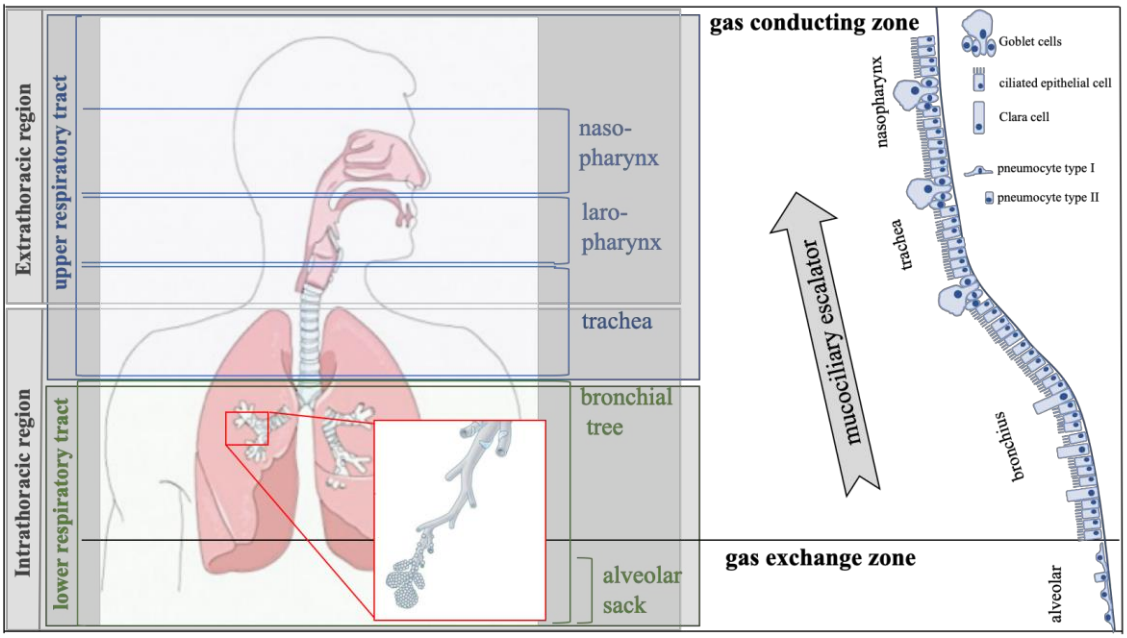

Figure 2: Schematic Overview of the Respiratory Tract. The respiratory tract can be described either by its anatomical location as extra-thoracic and thoracic region or by its functional differences as gas exchange zone and gas conduction zone. While the gas conduction zone includes nose, nasopharynx, laropharynx, trachea and most of the bronchial tree, the gas exchange zone includes the respiratory bronchioles and alveolus. The gas exchange zone lined by specific type I and type II alveolar cells. While type I allows gas transfer, type II produces the so-called surfactant that prevents that the alveolar collapse. The gas conducting zone is lined by respiratory epithelia, that contains mainly ciliated epithelial cells and goblet cells providing the mucus for the mucociliary escalator (modified after Löffler[40]).

Besides epidemiological evidence that describes the settlement of certain airborne particles in certain parts of the human respiratory tract, experimentally approaching inhaled infections aerosol particle deposition in the human lung is difficult due to biohazard and ethical reasons. Thus, computational modelling of bioaerosol deposition has been performed. The actual morphometric of the respiratory tract is taken into account by applying the variability of airway geometry in specific lung branches[41]. The airway is considered as cylindrical space and the alveoli are modelled as spherical space. Besides inherent particle sedimentation and Brownian motion determine the fate of a particle in alveoli's, also the inertial impaction needs to be considered in airways[7]. Inertial impaction

usually occurs in the first 10 generations of the lung, where air velocity is high and airflow is turbulent[42].

The deposition of airborne particle in the human respiratory tract is defined by a wide spectrum of physicochemical characteristics of the particle as well as physiological factors of the respiratory tract. Whereas ultrafine particles (aerodynamic diameter <0.001 μm) and large particles (aerodynamic diameter >3 μm) mainly deposit in the extra thoracic part of the respiratory tract, intermediate size particles (aerodynamic diameter 0.1–3 μm) are enabled to penetrate the outmost lung generations, where they finally may settle down in the aveoli[7]. Most particles that are inhaled are also exhaled and only a small fraction of inhaled particles will deposit in the lower respiratory tract[7]. Even though viruses and bacteria are very different in their size scale, they both have the potential to reach the lower part of the respiratory tract[6].

1.5 Lung Mediated Defense Responses to Exogeneous Particles

The lung encounters numerous amounts of foreign, potentially dangerous, particles on a daily basis. In response to these challenges, humans have developed a series of defense mechanisms to protect the airways from this potential insult.

Immediately after particle deposition in the respiratory tract, most particles are subjected to different defense mechanism including inertial forces, anatomical barriers, aerodynamic changes and immune system-based responses. Particles that deposit on the nasopharynx and tonsillar region are caught by mucus and cleared by inertial forces like coughing and sneezing or are swallowed. Inhaled particles that reach conducting airways and settle on the epithelium coated with mucus will be cleared by mucocilliary movement, allowing the transport of particles out of the lung[43,44]. The mucocilliary clearance is performed by ciliated epithelia cells that line healthy airway surfaces. When particles become entrapped in the surface mucus layer, in a synchronized matter, beating cilia propels entrapped particles toward the pharynx so that they can be swallowed[43]. The airway surface layer has two functions, first it entraps inhaled particles and second lubricates airway surface, so ciliary beating for efficient mucus clearance is possible[45].

Pathogens, that escape those mechanisms, are met by alveolar macrophages. Macrophages are the resident innate immune cells of the airway and are in the first line of defense against microbes. Alveolar macrophages along with their role in effecting and propagating the inflammatory response by phagocytosing microbes secret proinflammatory mediators can also facilitate resolution of inflammatory processes. This

is achieved by production of anti-inflammatory mediators and finally efferocytosis[46,47]. Attracted by proinflammatory mediators, neutrophils arrive to the interstitium within minutes of a pathogenic challenge. Activated neutrophils clear fungi, bacteria and viruses through pathocytosis of microbes and degranulation mediated release of reactive oxygen species and antimicrobial peptides[46,47].

1.6 Sampling of Airborne Pathogens

Various sampling devices can be used to recover airborne pathogens. Most of those air sampling devices use aerodynamic diameter, velocity properties and adhesion properties of the airborne particle for particle separation. Most commonly used sampling devices are liquid and solid impactors as well as filters. Different sampling methods are suitable for different research questions and need to be selected accordingly[48].

Analyzing the aerodynamic diameter of airborne particles, will help to understand the health impact of those aerosols, as it will determine their ability to penetrate the human respiratory tract. Commonly used are multistage impactors, including the Andersen Cascade Impinger (ACI) or multistage liquid impactors. The ACI accelerates the particles through small holes and moves them towards a solid surface and then abruptly changes their direction. The velocity of the particle deviates them from the airstream and impacts them on the given surface, which usually holds Petri dishes with a culture medium. The ACI contain a number of stages, each of which traps particles with a certain aerodynamic diameter range[49]. The multistage configuration is designed to accelerate incoming particles by using different sized holes[49]. While the first stage induces moderate acceleration so that only the largest particles deviate from their trajectory, the second stage accelerates a little more and with each level, acceleration increases. The different stage configurations are modelled on the human respiratory tract and allow the simulation of aerosol deposition[48,49]. Multistage liquid impactors accelerate airborne particles through a narrow opening, placed at a fixed distance from the bottom of a flask, filled with liquid. Mimicking the particle transport through the nose, the tube curves and trapes larger particles based on their inertial impactions. Remaining particles are impacted onto the liquid, which prevents desiccation and facilitates for example extraction of genetic material for further analysis.

Different sampling methods are available to test the viability of airborne pathogens. Some studies on sampling airborne viruses indicate that the liquid impactor has a lower recovery potential than other samplers, such as the electrostatic precipitators[50], the ACI[51] and the

slit sampler[52]. But in other studies it was suggested that the liquid impactor recovers concentrations of viruses that are equivalent to those with the electrostatic precipitator[53], greater than those with the ACI[54], and greater than[55] or equal to[56] those with the slit sampler.

A more recent development is the swirling aerosol collector. Here the air is forced not only through a single nozzle but has three tangential sonic nozzles and is less destructive and violent to the particle than other samplers[57].

In field settings, where large volumes of ambient air with low concentrations of airborne pathogens have to be analyzed, the sampler needs to be able to facilitate a large air volume. Here electrostatic precipitators are preferred in those settings as they can filter up to 10,000 liters/min through a high voltage corona, where the particles are charged and precipitated onto a grounded rotating disk[8]. The rotating disk allows determination of pathogen concentrations as a function of time[48].

Since most previously mentioned samplers cannot collect aerosols with an aerodynamic diameter smaller than 500 nm, filters are frequently used to sample airborne viruses. The efficiency of filters is based on the interception, inertial impaction, diffusion, gravitational settling and electrostatic settling of a filter and differs depending on the used material[8,48].

2 Methods

In our studies we focused on two prominent respiratory diseases, Tuberculosis and influenza. Both pathogens are airborne transmitted. The reactive agent of Tuberculosis is *M. tuberculosis*; influenza is caused by influenza A virus. Thus, protocols are needed to meet the different requirements of the pathogens.

To allow the analysis of pathogens containing aerosols, different steps including pathogen maintenance, varying pathogen origin, biophysical characteristics and aerosol production and collection (Figure 3).

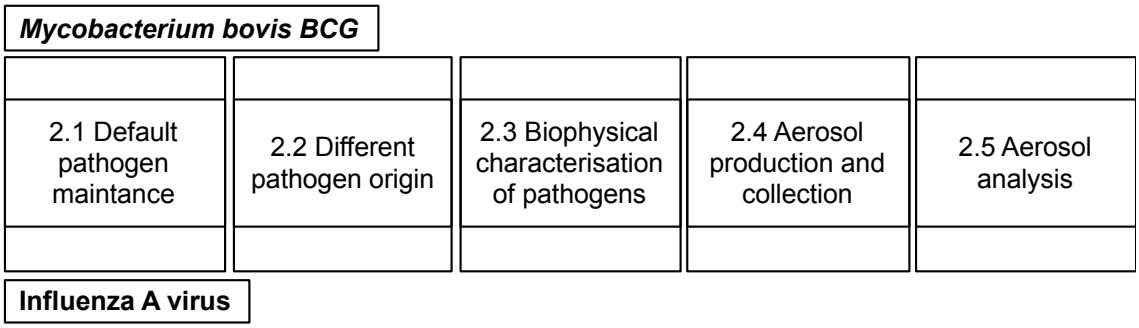

Figure 3: Overview Over Used Methods. For both analyzed pathogens, five different method packages were applied, eventhough in detail applied methods differ fundamentally. In the following the default pathogen maintenace (2.1) as well as the introduction of different pathogen origin systems will be discussed in 2.2. Methods to analyze the biophysical characteristics of pathogens are explained in 2.3. The new established Aerosol Collecting Device is presented in 2.4 and the analysis of those collected aerosols is discribed in 2.5. Differences between BCG and IAV are descripted in the following subchapters.

2.1 Default Pathogen Maintenance

Pathogens are grown usually in well-established systems and can be stored in stocks at -80°C. All experiments were performed in an BSL2 lab in a biosafety cabinet.

2.1.1 *Mycobacterium bovis* BCG

2.1.1.1 Mycobacteria Strains and Growth

To grow *Mycobacterium bovis* BCG strains Pasteur (BCG; a generous gift by Camille Locht (Institute Pasteur, Lille, France) for our experiments, mycobacteria were incubated in Middlebrook 7H9 broth (BD Bioscience, Franklin Lakes, New Jersey), 0.05 % Tween 80 (Serva, Heidelberg, Germany) and 10 % OADC (BD Bioscience, Franklin Lakes, New Jersey). Frozen mycobacteria stock was thaw and washed with Middlebrook 7H9 broth by bringing the stock into 10 ml of broth, gently pipetting bacteria up and down to allow homogenization of bacteria solution. Subsequently the bacteria solution was centrifuged (800 g for 10 min) and bacteria pellet was up taken in 1 ml broth. After transferring the bacteria solution to cell culture flask with 9 ml Middlebrook 7H9 broth, they were incubated for 4 days in an incubator at 37 °C/ 5 % CO_2. Bacteria cultures were passages by inoculating 9 ml of fresh broth with 1 ml of bacteria culture (OD = 0.6 - 0.7). The culture was passaged for maximum of 5 cycles, to minimize cell culture effects. The optical density was determined by transferring 1 ml of stock to a cuvette and measuring in a spectrophotometer (LabGenius, London, UK) at 650 nm.

2.1.1.2 Mycobacteria Stock and Storing

In order to store mycobacteria for a prolonged time period, they were kept at -20 °C. Mycobacteria culture was transferred to 50 ml Falcon and centrifuged for 10 min at 800g. Bacteria were taken up in freezing broth containing 10 % glycerol. 1 ml of mycobacteria solution was transferred to freezing vial and transferred to the freezer in a cooling box (Mr Frosty^{TM}, ThermoFisher Scientific, Walthalm, Massachusetts).

2.1.2 Influenza A virus

2.1.2.1 MDCK Cell Culture

MDCK cells are suitable to grow H1N1 IAV *in vitro*. MDCK cells were kept in a CO_2 incubator at 37 °C, 5 % CO_2 and 95 % RH and split according to the application needed or once they reached 80 - 90 % confluence. For MDCK cells, 10 % FCS (Sigma-Aldrich, St. Louis, Missouri), 1 % penicillin and streptomycin (Sigma-Aldrich, St. Louis,

Missouri) and 1 % L-glutamine (Sigma-Aldrich, St. Louis, Missouri) was added to the MEM cell culture medium (Sigma-Aldrich, St. Louis, Missouri). When passaging the cells, they were washed with 1x PBS and incubated with Trypsin-EDTA (Sigma-Aldrich, St. Louis, Missouri) at 37 °C until the cell layer dispersed. By adding the MEM cell culture growth medium containing FCS, the Trypsin-EDTA was inactivated and the cells were sub-cultivated as needed.

2.1.2.2 Virus Stock

Virus stocks used for *in vitro* experiments were passaged at most two times in order to minimize the occurrence of random mutations appearing due to the missing proofreading capacity of the viral polymerase[58]

All H1N1 virus stocks were grown in MDCK cells and 1 µg/ml TPCK-Trypsin (Sigma-Aldrich, St. Louis, Missouri) was added as all virus stocks have a monobasic cleavage site.

For successful virus propagation MDCK cells were seeded one day before in a 75 cm^2 cell culture flask. If the cells were 80 - 90 % confluent, they were washed with PBS and infected with 1.5 ml virus dilution aiming a MOI of 0.1. After 30 min of incubation at 37 °C, the virus inoculum was removed and 6 ml infection medium were added to the flask. After infection, cells were incubated and regularly checked for cytopathic effects (CPE) greater than 50 % (approximately after 24 - 36 h) or positive hemagglutination with chicken erythrocytes in a HA assay. Cell culture supernatant was then harvested and centrifuged at 1000 g for 5 minutes to remove cells and cell debris. The supernatant was aliquoted in 100 µl aliquots and stored at -80 °C.

2.1.2.3 Hemagglutination Assay

The hemagglutination assay (HA assay) is based on the ability of the viral HA protein to bind red blood cells. The binding of virus to the erythrocytes is mediated by α2,3- and/or α2,6-linked sialic acid on the cells surface as receptor. The present virus prevents erythrocytes sediment to the ground of the plate. The HA assay was performed in 96-well V-bottom shaped (conical) plates (Nunc™, ThermoFisher Scientific, Walthalm, Massachusetts). 100 µl sample (i.e. cell culture supernatant from virus growth fluid) was pipetted into the first well of the 96-well plate, followed by a 2-fold serial dilution in 1x PBS (Sigma-Aldrich, St. Louis, Missouri). Next, 50 µl of 1 % chicken erythrocytes (Lohmann Tierzucht, Cuxhaven, Germany) suspension (chicken erythrocytes were

diluted in 0.9 % NaCl) were added to each well and the suspension was incubated for 30 minutes at 4 °C. Following the incubation time, agglutination patterns were observed – agglutination causes the red blood cells to not settle at the bottom of the well, giving it a cloudy appearance. If no agglutination occurred, the red blood cells settle at the bottom of the well as a "button" or circle of cells. The titer was then calculated by determining the HA titer per milliliter in each dilution step.

2.1.2.4 Plaque Forming Assay

In order to determine the titer of infectious virus particles in a virus suspension, a plaque assay was performed (modified from[59]). MDCK cells were seeded into a 6- well plate and were kept in culture overnight. If the cells had a confluence of 70 - 80 %, they were washed with PBS (Sigma-Aldrich, St. Louis, Missouri) and the cells were inoculated with 333 µl of the relevant virus dilution. In case of virus titer determination, a ten-fold dilution in PBS of the unknown sample or virus stock was performed for inoculation. Following inoculation the cells were kept for 30 minutes at 37 °C in the incubator and occasionally carefully tilted to avoid drying-out of the cells. Next, 3 ml of avicel-overlay medium including 1 µg/ml TPCK-Trypsin was added and incubated for 72 h at 37 °C. After 72 h the avicel-overlay medium was removed, the cells were washed with PBS and fixed for at least 30 minutes with 4 % PFA (Sigma-Aldrich, St. Louis, Missouri) at 4 °C.

The viral plaques were made visible via immunostaining of the viral NP protein. Cells were washed with PBS and permeabilized for 30 minutes with 0.3 % Triton-X (Sigma-Aldrich, St. Louis, Missouri) on a tumbling table. Cells were then incubated with 500 µl per well of the primary antibody, an anti-NP antibody (Abcam, Cambridge, UK), for one hour at room temperature. Plates were then washed three times with PBS-Tween (0.05 %) and 500 µl of the secondary antibody, an anti-mouse IgG-HRP conjugated antibody (SouthernBiotech, Birmingham, Alabama), were added for another hour. The primary antibody was diluted 1:1000 in superblock, the secondary 1:2000. Following this incubation step, the plates were washed three times with PBS-Tween. The detection of the viral plaques was carried out by applying True-Blue (KPL, Seracare Lifescience, Milford, Massachusetts) which serves as a substrate for the HRP conjugate of the secondary antibody.

With this method viral plaques could be detected in the cell layer. The titer was then calculated by determining the *plaque forming units* per milliliter (PFU/ml) in each dilution.

2.2 Different pathogen origin

In the course of our experiments, we were interested in the effect of other participants, of either the immune system or tissue of origin, on the formation and composition of pathogens containing aerosols.

2.2.1 Neutrophils

Neutrophils play a crucial role in re-activating Tuberculosis and are commonly found in smear samples of TB patients[60–62]. But their role in aerosol formation is not understood yet.

2.2.1.1 Ethical Approval, Isolation, Culture and Infection of Neutrophils

Human neutrophils were isolated from heparinized peripheral blood from healthy donors. Written consent approving and authorizing the use of the blood from healthy donors (22-202A). Neutrophils were separated by centrifugation by first using a Histoplaque 1199 (Sigma-Aldrich, St. Louis, Missouri) gradient and second a Percoll gradient (Sigma-Aldrich, St. Louis, Missouri) as described before (van Zandbergen *et al.,* 2002). Neutrophils were cultured in RPMI medium (Invitrogen, Carlsbad, California) supplemented with 10 % FCS (Sigma-Aldrich, St. Louis, Missouri), 2 mM Glutamine (Invitrogen, Carlsbad, California) and infected at MOI 1. For that, BCG were opsonized with autologous serum from healthy donors and incubated for 30 min at 37 °C. Infected neutrophils were incubated for 36 h at 37 °C/ 5 % CO_2. In some experiment's neutrophils were treated with 0.3 % H_2O_2 (Omnilabs, Hamburg, Germany) to induce necrosis.

2.2.1.2 Necrotic Cell Death Induction and Lactate Dehydrogenase Assay

When using BCG as a *M. tuberculosis* surrogate, artificial necrosis induction required addition of a reactive oxygen intermediate (ROI) donor to the cell cultures. Treatment of BCG-infected human neutrophils by hydrogen peroxide (H_2O_2) robustly initiated necrotic cell death as determined by measuring the activity of lactate dehydrogenase (LDH) in neutrophil cultures: LDH is a strictly cytoplasmic enzyme that is detected in supernatant after plasma membrane rupture.

To experimentally drive infected neutrophils into necrotic cell death, cells were treated with 0.3 % H_2O_2. The 100 % reference was determined by lysing neutrophils with the detergent Triton X-100 (0.1 % in PBS, Omnilabs, Hamburg, Germany). For measuring necrotic cell death, neutrophil culture supernatants or total cell lysates were transferred to 96-well plates and serially diluted 1:2. A good measure for necrosis is the measurement

of Lactate Dehydrogenase (LDH) activity. LDH activity was measured using a mixture of diaphorase/NAD+ and Iodotetrazolium chloride/sodium lactate following the manufacturer's instructions (Roche, Mannheim, Germany). Samples were analyzed by measurement of optical density using an Opsys MR ELISA reader (Dynex Technology, Chantilly, Virgina) at 490 nm wavelength.

2.2.1.3 Scanning Electron Microscopy of Neutrophils

Isolated neutrophils were fixed with 2.5 % Glutaraldehyde (EMS, Hatfield, Pennsylvania) in PBS (Sigma-Aldrich, St. Louis, Missouri). Subsequently stained with 2 % Osmium (EMS, Hatfield, Pennsylvania) in PBS on ice (Sigma-Aldrich, St. Louis, Missouri) and washed with ddH_2O. Samples were dehydrated in ethanol solutions of 30 %, 50 %, 70 %, 90 % in ddH_2O and three times 100 % each for 3 min (Carlroth, Karlsruhe, Germany). All steps were performed in the 12-well plate. In order to dry samples with hexamethyldisilazane (HMDS, Sigma-Aldrich, St. Louis, Missouri), samples were immersed for 3 min in 50 % HMDS in ethanol and 3 min in 100 % HMDS and dried over a filter (Whatman, GE Healthcare, Chicago, Illinois). Dried samples were mounted on stubs and sputter coated with 10 nm gold (Q150R Quorum Technologies, Lewes, GB). Samples were examined with Philips XL30ESEM (Philips, Hillsboro, Oregon), equipped with a DISS5 digital scanning system (point electronic GmbH, Halle, Germany).

2.2.2 Re-differentiated Nasopharyngeal Tissue-based Cell System

IAV are grown by default in MDCK cells, but IAV bud from the host cell surface and thus their physiology may differ drastically when using a more natural cell system of the nasopharynx.

The isolation of adult tissue stem cells from patient material and re-differentiation of those to nasopharyngeal tissue on air liquid interfaces (ALI) was performed by Wilhelm Ching. He obtained adult stem cells from several patients with very different backgrounds, as shown in the following table (Table 2) and was able to keep them in culture.

Table 2: Patient Information Used to Isolate Adult Stem Cells

Patient	Diagnosis	Gender	Age
NaP6	Adenoid	female	52 years
NaP7	Non-Hodgkin	male	72 years
NaP13	Adenoid	male	6 years
NaP14N	Nasopharynx carcinoma	female	64 years

2.2.2.1 Visual Analysis of Re-differentiated Nasopharyngeal Tissue-based Cell Model

The re-differentiated nasopharyngeal tissue model was yet uncharacterized, thus we used four different microscopy approaches to get the best overview of this cell model. This was necessary as all different techniques show slightly different aspects of the model. For the visual analysis of the nasopharyngeal tissue culture model, the samples were fixed with 2.5 % Glutaraldehyde (EMS, Hatfield, Pennsylvania) for 30 min at room temperature after they were washed with PBS. After fixation, samples were again washed in PBS twice. Each transwell insert was removed from its holder and cut into 2 pieces, each piece going either to electron microscopy or histology analysis.

2.2.2.1.1 Histology analysis

After fixation, inserts were dehydrated using a graded series of ethanol concentration. Samples were incubated for 8 minutes each in 35 %, 50 %, 70 %, 95 % and two times 100 % ethanol (Carl Roth, Karlsruhe, Germany) in ddH_2O. In order to remove the alcohol, samples were incubated for 10 min in Roticlear® (Carl Roth, Karlsruhe, Germany). After removing Roticlear®, samples were embedded in paraffin (Sigma Aldrich, St. Luis, Missouri) and kept for 1 hour in warm oven at 60 °C. Subsequently the paraffin was replaced by new paraffin and kept another hour in the warm oven. Samples could then be embedded in a paraffin boat, placing the sample perpendicular to the cutting direction. Paraffin blocks were kept at either 4 °C or -20 °C depending on the time span till they were cut.

To cut the sample containing paraffin block, samples were kept at 4 °C and mounted in the microtome (Leica Biosystems, Wetzlar, Germany). After adjusting the blade to the block, aiming for a parallel cut, samples were cut 5 µm thick and mounted on starfrost glass slides (Sigma Aldrich, St. Luis, Missouri) and dried over-night in ventilated oven at 37 °C. The slides were kept at 4 °C for long term.

In order to enable antibody-based and hematoxylin and eosin (H&E) stainings of the samples, paraffin was removed, by first incubating the slides at 60 °C for 30 min. Then the paraffin was washed out using xylene (Sigma Aldrich, St Luis, Missouri) (3x times), and an ethanol series from 100 % to 90 %, 80 %, 70 % and 50 % ethanol for 3 min each (Carl Roth, Karlsruhe, Germany). After that slides were washed in PBS for 2 times for 3 min. For heat induced epitope retrieval, a citrate-based epitope retrieval solution (Leica, Wetzlar, Germany) was used and the slides were incubated for 30 min in a pressure cooker in a microwave. After cooling down, the slides were transferred to PBS. Once

slides were dried the sample was surrounded by PAP pen (Sigma- Aldrich, St. Luis, Missouri) to allow incubation with different solutions. 5 % natriumdodecylsulfat (Carl Roth, Karlsruhe, Germany) was used as a detergent and incubated for 5 min at room temperature. Subsequently samples were washed 4 times with PBS and 100 µl blocking solution, containing 5% BSA (ThermoFisher Scientific, Walthalm, Massachusetts), 0.1% Triton (Carl Roth, Karlsruhe, Germany) was added in the encircled area for 60 min at room temperature or overnight on ice. After incubation period, the solution was taken off and samples were washed with PBS. The first antibody, targeting certain proteins, was incubated for 1 hour at 4 °C and then washed with PBS plus 1% Tween (Merck, Darmstadt, Germany) (PBST) 3 times. Afterwards, the samples were incubated for 45 min with the secondary antibody in the dark at 4 °C and washed again with PBST for 3 times. After drying, samples were mounted with Fluoroshield Mounting Medium (Abcam, Cambridge, UK) and covered with cover slips and sealed with nail polish.
When performing a H&E staining, sections were incubated for Hematoxalin (Abcam, Cambridge, UK) for 3 min and rinsed with tap water for 10 min. Subsequently, sections incubated with Eosin (Abcam, Cambridge, UK) for 30 sec and then washed for 3 times with 95 % ethanol and 3 times with 100 % ethanol. Slides were then transferred to Xylene (Sigma Aldrich, St. Luis, Missouri) and incubated for 15 min for 3 times. Probes were then mounted with Permount (ThermoFisher Scientific, Walthalm, Massachusetts) and covered with coverslips.

2.2.2.2.2 Transmission Electron Microscopy and Serial Block Face Imaging (3 view).

Samples were fixed on ice with 2.5 % Glutaraldehyde (EMS, Hatfield, Pennsylvania) in PBS (Sigma-Aldrich, St. Louis, Missouri), stained with 2 % Osmium (EMS, Hatfield, Pennsylvania) in PBS on ice (Sigma-Aldrich, St. Louis, Missouri) and washed with ddH_2O three times. Samples were dehydrated in ethanol solutions of 30 %, 50 %, 70 %, 90 % and three times 100 %, each for 3 min (Carl Roth, Karlsruhe, Germany). In order to embed samples in Epon (Epoxy plus hardener), they were first incubated for two hours in 50 % Epon in ethanol (Carl Roth, Karlsruhe, Germany). Subsequently samples were transferred again in 50 % Epon in ethanol and incubated overnight. Next morning, samples were transferred to 100 % Epon and incubated at least for two hours. This step was replicated 3 times. Next, samples were embedded in Epon in desired molds (Electron Microscopy Sciences (EMS), Hatfield, Pennsylvania) and polymerized at 65 °C for 3 days. Subsequently samples were either trimmed for serial block face imaging, or

sectioned using the ultra-microtome (Leica, Wetzla, Germany) and transferred to 400 mesh copper grids (Electron Microscopy Sciences (EMS), Hatfield, Pennsylvania). The sections were then stained with 2 % Uranylacetate for 1 min (EMS, Hatfield, Pennsylvania) and analyzed in a transmission electron microscope (Philips CM120/ Gatan MSC 794, Hillsboro, Oregon). 3D datasets were obtained by serial block face imaging in a Jeol JSM-7100 microscope (Jeol GmbH, Munich, Germany) equipped with a 3View XP2 System (Gatan, Pleasanton, USA).

2.2.2.2.3 Scanning Electron Microscopy

Samples were fixed on ice with 2.5 % Glutaraldehyde (EMS, Hatfield, Pennsylvania) in PBS (Sigma-Aldrich, St. Louis, Missouri), stained with 2 % Osmium (EMS, Hatfield, Pennsylvania) in PBS on ice (Sigma-Aldrich, St. Louis, Missouri) and washed with ddH_2O. Samples were dehydrated in ethanol solutions of 30 %, 50 %, 70 %, 90 % and three times 100 % each for 3 min (Carl Roth, Karlsruhe, Germany). For hexamethyldisilazane (HDMS, Sigma-Aldrich, St. Louis, Missouri) drying, samples were immersed for 3 min in 50 % HMDS in ethanol and 3 min in 100 % HMDS and dried. Dried samples were mounted on stubs and sputter coated with 10 nm gold (Q150R Quorum Technologies, Lewes, GB). Samples were examined with a Philips XL30ESEM microscope (Philips, Hillsboro, Oregon), equipped with a DISS5 digital scanning system (point electronic GmbH, Halle, Germany).

2.3 Biophysical Characterisation of Pathogens

2.3.1 Aldehyde Fixation

Infectious pathogens are by default inactivated by aldehydes. They form cross links between the aldehyde and uncharged reactive amino groups, leading to the inactivation of pathogens.

2.3.1.1 Influence of Aldehyde Fixation on Mycobacteria

M. tuberculosis is an obligate human pathogen and therefore can only be handled in a BSLS-3 facility. But, as most of our analyzing techniques are located in a BSLS-2 facility, probes needed to be inactivated when leaving the S3 laboratory. By default, aldehydes are used for that. To analyze the effect of inactivation 1 ml of the mycobacteria culture was centrifuged at 800g for 10 min and the bacteria pellet up taken in fixation solution. In our experiments we compared the effects of different aldehydes including 4 % Formaldehyde (FA, EMS, Hatfield, Pennsylvania), 2.5 % Glutaraldehyde (GA, EMS, Hatfield, Pennsylvania) and 10 % Paraformaldehyde (PFA, EMS, Hatfield, Pennsylvania). The inactivation with GA, FA, PFA led to an increased volume in *Mycobacterium bovis* Bacillus Calmette Guerin (BCG), determined by the Atomic Force Microscopy (Figure 4A).

As samples were measured in air, the influence of aldehydes on the volume of mycobacterium in PBS was also analyzed, using dynamic light scattering method (ZetaSizer, Malvern Panalytical Ltd, Malvern, UK). The dynamic light scattering method allows the analysis of particle sizes in solution. First, we used an Abbe refractometer (A. Krüss Optronic GmbH, Hamburg, Germany) to determine the refractive index of mycobacteria. Unfortunately, the refractometer only allows wet measurements, but in order to measure the mycobacteria and not the surrounding liquid, a preferably viscous bacteria solution was used for the measurements. The average of the defined refraction index (1.56 ± 0.3) was implemented in measurements by the dynamic light scattering method. For that mycobacteria were taken up in PBS and adjusted to the optical density of 0.05. The results indicate that the refractive index varies strongly, but since the size of mycobacteria is not homogeneous in one probe, this was expected. In comparison to measurements of *E. coli*, where a mean value of 1.3387 was published, mycobacteria have a higher index[63]. Analyzing the effect of aldehyde fixation on the particle size in solution, no difference was observed between treated and non-treated mycobacteria (Figure 4B). This suggest a change of water translocation across the membrane of

mycobacterium when they are inactivated with aldehydes. We therefore decided to work with non-human pathogenic *M. bovis* BCG, a bacterium structurally comparable to *M. tuberculosis,* which would allow the usage of native material.

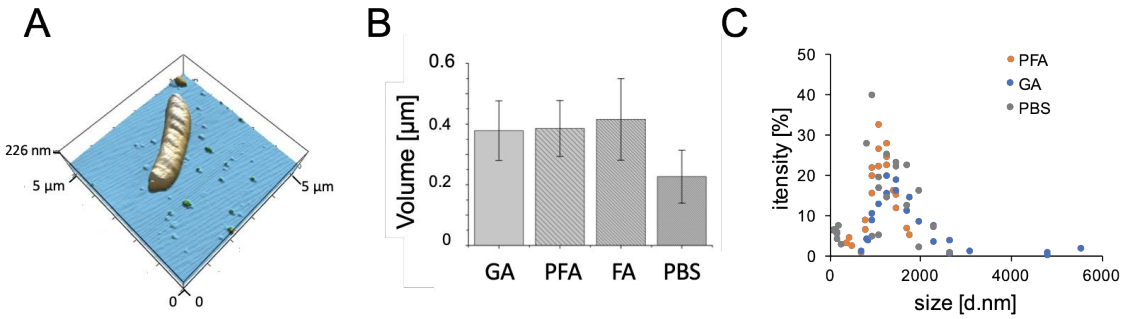

Figure 4: Effects of Aldehyde Fixation on Mycobacteria. (A) Representative of AFM iamge to determine the volume of single BCG. **(B)** Samples were inactivated for at least 30 min with different aldehydes (GA = Glutaraldehyde; FA = Formaledhyde; PFA = Parafomaledyde)and then analyzed by AFM (non-contact mode, AC165TS cantilever). Different aldehydes effect on the volume of BCG, leading to an increased volume compared to native particles (mean and standart deviation of 20 independent experiments are shown). **(C)** Analysis of either fixed or native BCG solution with dynamic light scattering (mean and standart deviation of three independent experiments are shown).

2.3.1.2 Influence of Aldehyde Fixation on IAV Particles

The influenza strain used here is human pathogenic and thus can only be handled in BSL-2 safety facilities. To analyze the effect of aldehyde fixation, virus stock was mixed with either cell medium, PFA (4 %), FA (4 %) or GA (2.5 %) and then brought onto mica. Probes were analyzed by AFM and the volume was reconstructed from the obtained data of topography. When samples were not inactivated, they were handled in a closed chamber. Aldehyde fixated IAV particles were significantly smaller than non-treated particles. Interestingly, the variability of volume in fixed particles was also reduced compared to the unfixed particle (Figure 5).

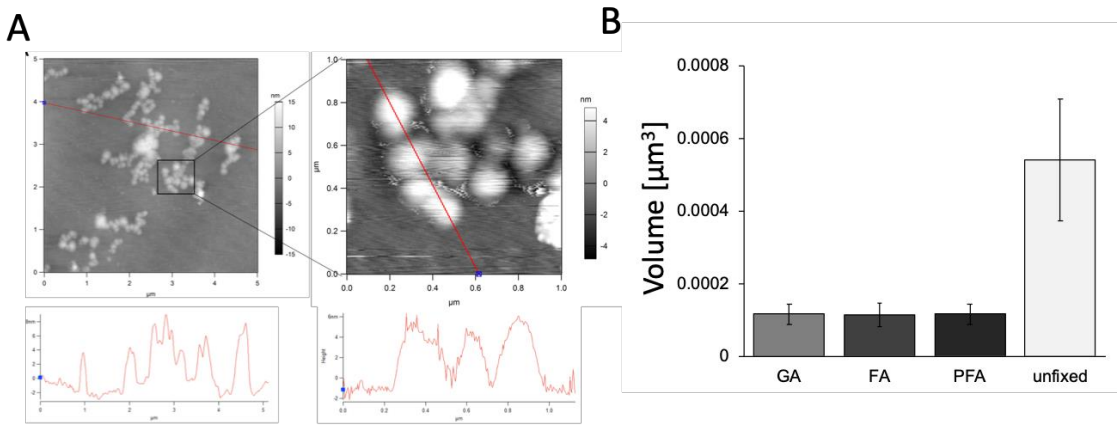

Figure 5: Influence of Aldehyde Fixation on IAV Particles. (A) Volume of single IAV particles determined by AFM. Probes were inactivated for at least 30 min with different aldehydes, tranferred to mica and then analyzed by AFM (non-contact mode, AC165TS cantilever). **(B)** For each aldehyde types (GA = Glutaraldehyde; FA = Formaledhyde; PFA = Parafomaledyde), nine different virus particles, from three independet experiments were analysed. Different aldehydes effect on the volume of IAV particles, leading to a reduced volume compared to native particles (mean and standart deviation of 24 particles for each group).

2.3.2 Hygroscopicity of Pathogens

Hygroscopicity is defined as the ability to absorb water from ambient air. The amount of available water is depended on the relative humidity. BCG in PBS (Sigma-Aldrich, St. Louis, Missouri) was brought on coverslips by centrifugation (200g for 20 minutes). On MDCK cells grown IAV particles were harvested and brought and dried on freshly sliced mica. For measurements of hygroscopicity samples were transferred to a closed fluid chamber in which the RH was adjusted by in saturated salt solutions-soaked tissues. The volume of single pathogen particles was determined by AFM under different RH´s. The RH was adjusted by deliquescence salts inside a closed chamber using saturated salt solutions of potassium chloride (85 % RH), sodium nitrate (65 % RH) and lithium chloride (20 % RH) (ThermoFisher Scientific, Waltham, Massachusetts).

2.3.3 Determination of Mass density of Mycobacteria

The following formula was used to calculate mass density of one single bacterium: Mass density = Volume of bacterial cell/ weight of bacterial cell. The volume of one bacterium was determined using Atomic Force Microscopy (AFM, Oxford Instruments, Asylum Research, Santa Barbara, California; Cantilever OMCL-AC160TS, Olympus, Tokyo, Japan) at 65 % relative humidity (RH). For that mycobacteria culture was transferred to PBS by centrifuging bacteria (10 min/ 800 g) and uptake of pellet in PBS. Obtained bacteria - PBS solution was adjusted to an OD of 0.2 and subsequently, 200 µl of solution were centrifuged on glass cover slips by using the cover slide centrifuge for 20 min at

100 g. The weight of one bacterium was determined by defining the number of single bacteria in culture samples, using a sperm counting chamber (Marienfeld, Lauda Königshofen, Germany), and weighing of BCG culture, after drying and adjusting to 65 % RH. This allows the calculation of the weight of one bacterial cell (weight of total bacteria/ numbers of bacteria).

2.4 Production and Collection of *in vitro*-produced Pathogen Containing Aerosols

Successful transmission of pathogens through the air depends on several factors, including their aerodynamic size, aerosol composition and their ability to survive airborne transmission by resisting environmental influences. Our set up allows a simultaneous assessment of viability of airborne pathogens, their composition and their aerodynamic size. Airborne particles will settle on the different levels of the ACI, dependent on their velocity. Thus, particles with a lower aerodynamic diameter will settle on lower levels compared to aerodynamically bigger particles. In each level different solid supports were provided to allow the analysis of viability as well as composition (Figure 6B). To be able to produce and subsequently analyze aerosols, an aerosol collecting chamber was established in our lab (Figure 6A).

The home-built Aerosol Collecting Devise (ACD) contained a small clean-box (27 l) connected to the ACI. Intake air flow was cleaned by a HEPA filter (SF-HA 50 HEPA AirClean, Miele, Gütersloh, Germany). All experiments using the ACD were performed under a sterile class II biosafety cabinet. Aerosols were expelled into the small clean-box using two different nebulizers. The jet nebulizer (IH18, Beurer, Ulm, Germany) used compressed air flow with a high velocity to produce aerosols, whereas the ultrawave nebulizer (U22 Microair, Omron, Kyoto, Japan), produced aerosols by an oscillatory membrane (Figure 5A). Aerosols were expelled for the whole sampling time of 10 min and thus aerosols were sampled during nebulization. From the clean-box, ambient air was pumped either through an ACI consisting of 8 levels (-2 to 5) collecting aerosols at 28 l/min (Copley Scientific, Nottingham, UK) or, in the case of mycobacteria, an Aerodynamic Particle Spectrometer (APS 3221, TSI, Shoreview, Minnesota). The APS provides information about the aerodynamic and optical diameter of airborne particles as dN/dlogDp value. dN (or ΔN) is the number of particles in a certain range channel (total concentration of particles) and dlogDp (or ΔlogDp) is the difference in the log of the channel width. Air was pumped by a vacuum pump (Copley Scientific, Nottingham, UK)

and airflow was measured by an airflow-meter (Copley Scientific, Nottingham, UK). Ambient ACD air was filtered before entering the pump by HEPA filter (Patronenfilter-HS- Mikroseal JG-S, HS-Luftfilterbau GmbH, Kiel, Germany).

To allow the analysis of mycobacterium containing aerosols, BCG was grown and transferred to either PBS (Sigma-Aldrich, St. Louis, Missouri) or RPMI medium (Invitrogen, Carlsbad, California), set to an OD of 0.6 - 0.7. As we were interested in the confirmation of airborne BCG, we did not single the mycobacteria with a cannula.

IAV particles were harvested from either MDCK cells or nasopharyngeal tissue culture model. The harvest was transferred to the nebulizer. To assess the titer before aerosolization, we performed PFU assay.

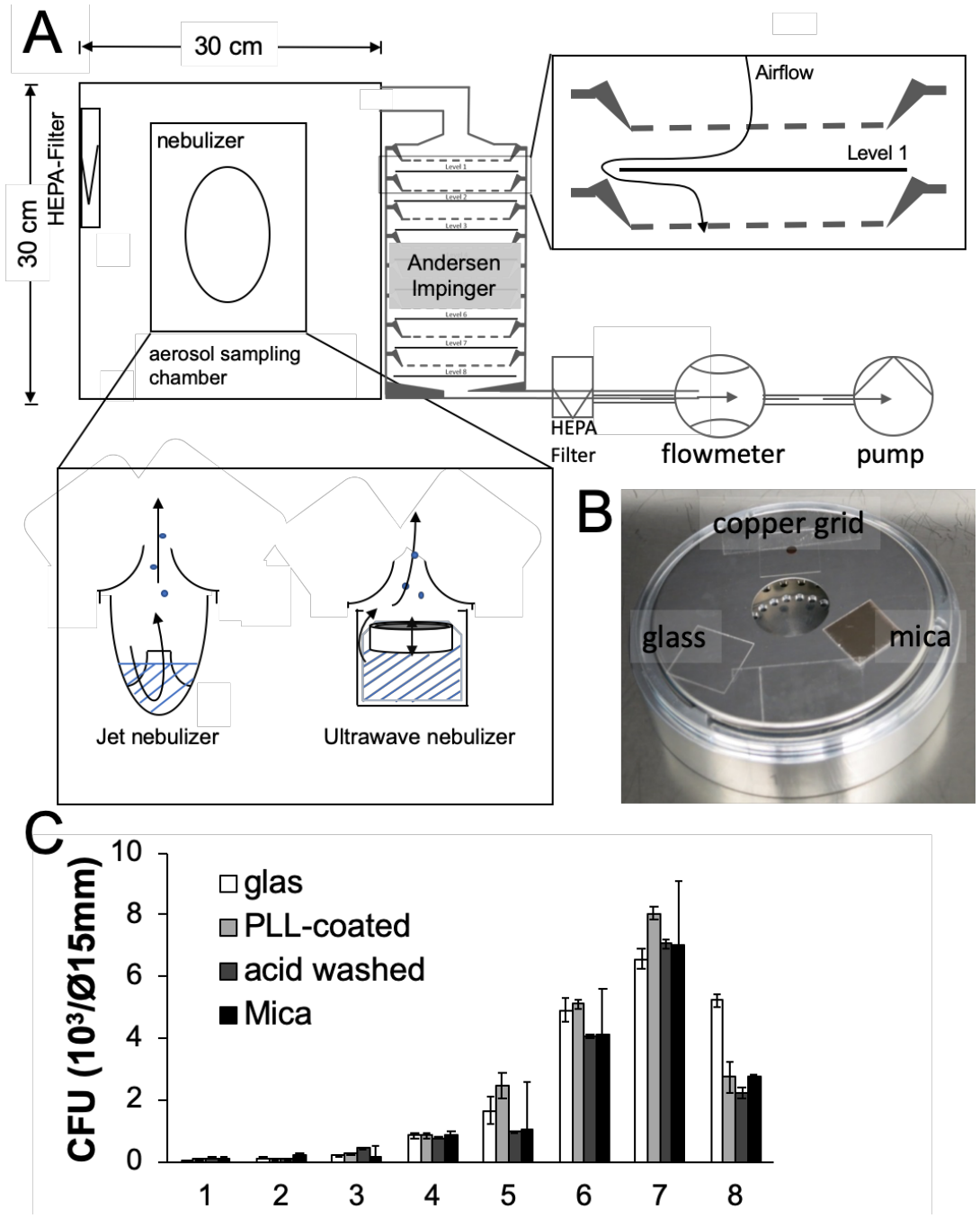

Figure 6: Schematic Overview of Aerosol Collecting Device. (A) Device consists of an acrylic glass chamber of 27 l including a HEPA filter to remove particles from incoming air. The ACD was connected to nebulizers, which used either jet or ultrasound to generate aerosols. The air containing these aerosols was actively pumped by a pump through the Multi Stage Impactor. The airflow was measured by a flowmeter and set to 28 l/min. The HEPA filter in front of pump and flowmeter protected the equipment. **(B)** A photography of Level 1 of the Impinger, equipped with three different surfaces to collect settling aerosols, i.e. i.) glass coverslip for viability testing ii.) copper grid for Electron Microscopy analysis iii.) Mica for Atomic Force Microscopy. **(C)** Different solid supports were tested to find the most robust solid supports for sampling viable airborne mycobacteria. Samples were collected at 28 l/min for 10 min using all different solid supports in the same run. After collecting, samples were washed with PBS and viability was tested on cultivation plates (mean and standart deviation of three independent experiments are shown).

2.5 Analysis of Pathogen Containing Aerosols

The viability of airborne transmitted pathogens can be determined by CFU/PFU as well as live/dead staining. Additionally, different solid supports were supplied in each level, allowing the analysis with both electron microscopy and atomic force microscopy.

2.5.1 Transmission Electron Microscopy (from ACD)

Aerosols were sampled on carbon-coated, sputtered 400 mesh copper grids (Electron Microscopy Sciences EMS, Hatfield, Pennsylvania) in the ACD and subsequently stained with 2 % Uranylacetat (EMS, Hatfield, Pennsylvania). Grids were analyzed in transmission electron microscope (Philips CM120/ Gatan MSC 794, Hillsboro, Oregon). For every grid 100 bacteria were analyzed. As the virus samples did contain far less particles each grid (1-2 particles), all particles were analyzed.

2.5.2 Atomic Force Microscopy (from ACD)

AFM analysis was only performed for mycobacteria, as IAV particles concentration did not allow the analysis. Freshly cut mica was placed on each level of the ACI. Samples were brought into a closed chamber, to avoid contamination and dehydration during transport. Samples were then analyzed by AFM in non-contact mode using the AC165TS cantilever (AFM, Oxford Instruments, Asylum Research, Santa Barbara, California; Cantilever OMCL-AC160TS, Olympus, Tokyo, Japan).

2.5.3 Analysis of BCG containing Aerosols

The most suitable solid support to collect viable mycobacteria-containing aerosols was determined by comparing different solid supports. Most robust result was found while using glass and in the following it was proceeded with glass (Menzelgläser, VWR, Radnor, Pennsylvania) (Figure 6C).

2.5.3.1 Viability of Mycobacteria (after Aerosolization)

To assess the concentration of viable mycobacteria, the colony-forming units (CFU) were determined by plating BCG-containing solutions, after separating bacteria with cannula (∅ 0.9 mm, B. Braun, Melsungen, Germany), on sterile 7H11 agar plate. Colonies were counted after 4 weeks of culture at 37 °C. Additionally, the ratio between live and dead bacteria was analyzed using the LIVE/DEAD™ BacLight™ Bacterial Viability Kit (ThermoFisher Scientific, Waltham, Massachusetts). Slides were observed using an

inverted Zeiss LSM 510 fluorescent confocal microscope (63x objective; Zeiss, Oberkochen, Germany). Images were analyzed by Zeiss LSM Image Browser software.

2.5.4 Analysis of IAV containing Aerosols

2.5.4.1 Airborne Virus Titer Determination by Plaque forming assay

In order to determine the titer of infectious virus particles after airborne transmission, a plaque assay was performed. Sampled aerosols were washed with ice cold 350 µl PBS and kept on ice. Plaque forming assay was performed as described in *Chapter 2.1.2.4*.

2.5.4.2 Reverse Transcription and PolyChainReaction (PCR) for Detecting IAV

The presence of viral RNA was detected by performing a reverse transcription, followed by amplifying poly chain reaction. For that sampling glass plates were washed with 140 µl of the RNA isolation buffer from the QIAamp Viral RNA Mini Kit (Quiagen, Venlo, Netherlands) and RNA was isolated following the instructions of the kit. Isolated RNA was then transcripted to cDNA by using the SuperScript™ III Reverse Transcriptase Kit (Quiagen, Venlo, Netherlands). For that, universal primers were used, which bind to highly conserved promoter regions of the viral genome. Freshly transcripted cDNA was then amplified by PCR using the viral NP sequence as target for primers. For amplification the HotStart II polymerase kit was used (Thermofisher, Waltam, Massachusetts, US). Amplificated cDNA was then separated using a 1 % agarose gel in 1x TAE buffer. DNA SYBR™ green (Thermofisher, Waltam, Massachusetts, US) was added to the agarose gel to allow the detection of double stranded DNA by UV light. All probes were mixed with 6x loading buffer. To allow for identification of mass, the mass ruler DNA mix (Thermofisher, Waltam, Massachusetts, US) was used. The gel was run for 10 min at 110 V and additionally for 70 min at 120 V. DNA bands were visualized by UV light.

2.6 Statistics

All data analysis and statistics were performed using Excel. Data were entered into a standard table, with one row representing one sample. Statistical analysis was done by determining the average and standard deviation and analysis of variance (ANOVA) and all significant differences were reported at 95% confidence intervals. Significant differences with a p-value <0.01 are represented by one asterix, two asterix represent a p-value <0.001 and three asterix represent a p-value <0.0001.

CHAPTER 1: Enhanced Tenacity of Mycobacterial Aerosols from Necrotic Neutrophils

1 Introduction

At a global level, Tuberculosis (TB) continues to be a major cause of morbidity and mortality and belongs with 1.2 million deaths in 2018 to the top ten causes of death worldwide[64]. Even though in Germany the number of TB cases decreased over the last century, approximately one fourth of the world's population is latent infected[64]. 10 % of these people will likely develop active TB during their lifetime and become capable of transmitting the disease. The increasing spread of drug resistant TB with more than 186 772 cases in 2018 highlights the importance to understand transmission properties of its agent, *Mycobacterium tuberculosis* (*M. tuberculosis*)[64].

1.1 Clinical Aspects of Tuberculosis

The lung is the predominant side of TB manifestation. Infection with *M. tuberculosis* almost exclusively arises from inhaling aerosols containing the bacilli. Inhalation might lead at first to symptomatic primary pulmonary TB. In adults secondary TB can result, after a variable time span, in a clinically asymptomatic latent stage, from which TB can reactivate[65]. In some cases *M. tuberculosis* spreads directly, from the lungs via the lymphatic or blood system to other body sites causing various extrapulmonary TB manifestations, including TB in bones, kidney, spleen and in the central nervous system[65]. Even in immunocompetent patients, the latent primary complex reactivates in 5 – 10 %. Host responses important in controlling the latent infection may include macrophage activation, maintenance of granuloma structure, CD4 T cells, CD8 T cells, IFN-γ, and TNF-α[66]. Severe immunosuppression, including HIV[64] or anti-TNF-α treatment, can only explain part of active tuberculosis. Most reactivations are caused by comorbidities like diabetes[65] and chronic renal failure[67], a pro-inflammatory environment induced by smoking[68] and genetic prospensity[69].

1.2 Classification of *Mycobacterium tuberculosis* Complex

The mycobacteria grouped in the *Mycobacterium tuberculosis* complex are characterized by 99.9% similarity at the nucleotide level and identical 16S rRNA sequences but differ widely in terms of their host tropisms, phenotypes, and pathogenicity. Even though they

are derived from a common ancestor, some strains infect exclusively human, specific *Mycobacterium tuberculosis*, *Mycobacterium africanum*, *Mycobacterium canettii,* whereas others are zoonotic and have an animal reservoir as for example *Mycobacterium bovis*[70,71] and Lineage 5 and 6[72]. It was shown that the *M. tuberculosis* complex evolved in Africa, most probably on the Horn of Africa and was distributed by human migration[72]. The main species infecting human have been classified into seven lineages and since lineage 2 (Bejing group), 3 (Central Asian group) and 4 (Euro-American group) share a unique deletion event, they form a monophyletic group. Lineage 5 and 6 (*M. africanum*) are closely related to animal strains of the *M. tuberculosis* complex[72].

1.3 Virulence Factors of *Mycobacterium tuberculosis*

Virulence is referred as the ability of a pathogen to successfully infect the host, grow and reproduce inside the host and evade the hosts immune system under the use of virulence factors[73]. Mycobacteria associated virulence depends on their ability to reside within host cells and evade the microbicidal mechanisms of macrophages and neutrophils[73]. The mycobacterial genome encodes bacterial factors that reflect a highly evolved and coordinated program that allow the evasion of both innate and adaptive immunity causing disease in the host[73]. Mycobacterial virulence can be measured through i) the ability of the bacteria to survive the host immune response, ii) their capacity to cause lung damage and iii) to be successfully transmitted to infect a susceptible host[73].

M. tuberculosis is a fairly large, nonmotile rod shaped bacterium. The rods are 2 - 4 µm in length and 0.2 - 0.5 µm in width. *M. tuberculosis* is an obligate aerobe and thus can be found in the well-aired upper lobes of the lung. The bacterium is a facultative intracellular parasite and has a slow generation time for up to 35 hours[74]. *Mycobacterium* species are classified as acid-fast bacterium, due to their impermeability for certain dyes and stains. The cell wall structure of *M. tuberculosis* is unique among prokaryotes and is a major determinant of bacterial virulence. The cell wall is hydrophobic waxy and rich in lipids and protects the mycobacterium against cationic proteins, lysozymes and oxygen radicals. The cell wall of mycobacteria itself can be considered as virulence factor.

It was shown, that the highly cross-linked peptidoglycan shows differential cross-linking patterns when the bacterium is either actively growing or in a dormant state[75]. This potentially allows the bacterium to survive through a variety of physiological and metabolic phenotypes. Several lipids and glycolipid components make up the cell wall or

outer membrane and contribute uniquely to the pathogenesis and virulence of the bacillus capsule[73].

Molecular migration of substances across the mycobacterial cell wall, are important for environment and host cells interaction. The mycobacterial waxy cell envelope controls the molecular movement and the secretion of substances across this structure is dependent on specialized protein systems[76–80].

1.4 Pathogenisis of *Mycobacterium tuberculosis* Infection

A circle of events leads to airborne human-to-human *M. tuberculosis* transmission. This circle is initiated when *M. tuberculosis* aerosol particle enwrapped in water droplet is inhaled and deposited onto the alveolar surface[81]. As the immune system cannot eliminate *M. tuberculosis*, it controls the pathogen and thus induces, in contrast to normal "resolving" outcome of infections, persistent inflammation[82].

The mycobacterium is first recognized by the innate immune system through pattern recognition receptors, by macrophage pattern recognition receptors (PPRs) that can be found on the surface of innate immune system cells like macrophages, dendritic cells natural killer cells and neutrophils[83,84]. The recognition of the bacterium by PRRs induces a network of coordinated signaling pathways that leads to distinct gene expression profiles in infected immune cells at different stages of infection as reviewed by Liu *et al.* (2017)[84]. During *M. tuberculosis* infection, the host orchestrates signaling from those PRRs and launches a variety of cellular functions, such as phagocytosis, autophagy, apoptosis and inflammasome activation, to control or eliminate *M. tuberculosis*. Macrophages have a dual role in TB infection. While the bacterium resides in resting macrophages, activated macrophages deliver the antimicrobial arsenal required to limit the pathogen[84]. Mycobacteria-induced apoptosis of infected macrophages releases mycobacterial antigen-containing apoptotic vesicles. These vesicles are engulfed by dendritic cells, which process the antigenic cargo for subsequent presentation to CD 8^+ T cells[85]. In particular TLR-2 plays a pivotal role in the induction of an innate immune response to mycobacterium infection, by upregulating tumor necrosis factor-α (TNF-α)[86] and interferon-γ (IFN-γ).

Furthermore *M. tuberculosis* are able to inhibit the phagosome-lysosome fusion of macrophages, and thus persists within the immature phagosomal compartment[81]. Some *M. tuberculosis* strains show a diminished capacity to tolerate phagosomal stress but are

able to translocate to the cytosol. By that the virulence of the *M. tuberculosis* strain is rescued[87]. Following the engulfment, alveolar macrophages transport *M. tuberculosis* into the interstitium and the mycobacterium replicates intracellularly within the phagocytes, and eventually burst out of the cell and infect new phagocytes[81]. Interestingly, *M. tuberculosis* limits the occurrence of apoptosis in macrophages and intracellular growth of *M. tuberculosis* leads to serial killing of host cells via necrosis[60,82].

Macrophages engulf extracellular *M. tuberculosis* bacilli in the alveolar space and migrate them into deeper sites in the lung, where they incite granuloma formation[88]. Mycobacteria induce infected macrophage apoptosis and expression of host MMP9 in an ESX-1-dependent manner[89]. Newly recruited macrophages engulf infected cell debris, contributing to granuloma expansion[90]. Next, *M. tuberculosis* specific T cells arrive at the granuloma and produce IFN-γ to enhance the microbicidal activity of macrophages[91]. While TNF-α and IFN-γ stimulate inflammatory cell infiltration, they are not essential for granuloma initiation[92,93]. Recruitment of immune cells including macrophages within granuloma depends on their adhesion to the extracellular matrix (ECM). Macrophages use their integrins to adhere to fibronectin as a major ECM component[94]. The initial granuloma consists of a core of infected macrophages, surrounded by additional macrophages, and leukocytes (Figure 7)[81,95]. Several morphologically distinct forms have been described for granulomas i) solid, composed of dense aggregates of infected and uninfected macrophages and lymphocytes without central necrosis ii) neutrophilic with extensive granulocytic infiltration iii) caseous with central necrosis, which can progress to cavity wall, surrounded by a cuff of macrophages and lymphocytes.

Granulomas limit bacterial growth and distribution but serve as niches for persisting mycobacteria and a source for reactivation[96,97]. TNF excess and strong T-cell immunity can lead to macrophage necrosis and release of mycobacteria into the extracellular space[91].

Hidden in granulomas, *M. tuberculosis* can persist for a long period of time[75,82,98]. In unfavorable conditions inside the granuloma, such as nutrient limitation and low oxygen tension, the metabolic downshift of subpopulations of *M. tuberculosis* to dormancy is triggered. During this dormant period of *M. tuberculosis* bacterial replication is decreased and endurance to heat and drugs is increased[75,98].

Upon reactivation, hallmarks of active TB are necrotizing exacerbating granulomas, pathogenesis and neutrophil influx[61]. Orme *et al.* argue that occurring necrosis in granulomas can be considered to be associated with reactivation of TB. As central necrosis of granulomas induces inflammation, neutrophil influx occurs[82]. It is described that the bacterium itself can initiate necrosis, particularly in neutrophils, to break in the alveolar or bronchiolar space[60]. Here it can form biofilms, so called necrosis-associated extracellular clusters[82]. Now extracellular, the bacilli persist in the remaining necrosis waiting for cavitation and escape from the respiratory tract. In humans, this could be a rapid event or it could occupy much of the lifespan of the host. Orme even suggests that the bacterium will reside in those clusters for 60 – 80 % of its lifespan[82]. Break open of necrotic granulomas into the alveolar or bronchiolar space allows airborne transmission as bacteria can be coughed up[61]. However, the role of necrotic neutrophil necrosis in formation of mycobacterium-containing aerosols is still unknown.

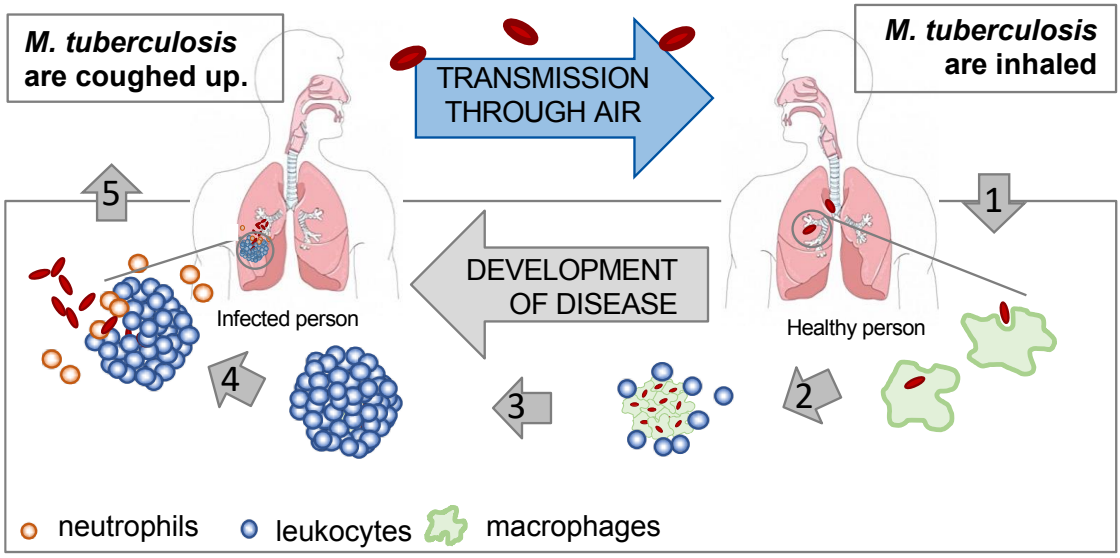

Figure 7: Pathogenesis of Tuberculosis. *M. tuberculosis* primary affects the respiratory tract, as mycobacterium-containing aerosols are inhaled and deposit onto the alveolar surface. **(1)** As a first line defense, the mycobacterium is taken up by an alveolar macrophage in an attempt to eliminate the bacterium. **(2)** But instead the mycobacterium employs phagocytosis and is transported by the macrophage to the interstitium and subsequently replicates intracellular. **(3)** Downstream of this initial infection step, onset of innate followed by acquired immunity leads to formation of granulomas, which limits mycobacterial growth but serves as niche for persisting mycobacteria and a source for reactivation. **(4)** Upon reactivation, hallmarks of active Tuberculosis are necrotizing granulomas, exacerbating pathogenesis and neutrophil influx. The bacterium itself can initiate necrosis, particularly in neutrophils, to break in the alveolar or bronchiolar space **(5)** Extracellular mycobacteria can be coughed up and exhaled, which allows airborne transmission.

1.5 Transmission of *Mycobacterium tuberculosis*

Tuberculosis is distinct among infectious diseases, in that it is almost exclusively transmitted through air. For TB, coughing is believed to be the main way in which *M. tuberculosis* is passed from a human host to the enviroment[99]. But recent studies showed that also tidal breathing induces increased aerosol formation in the size range of 0.1 to 5 μm, the range in which *M. tuberculosis* is believed to be transmitted[100].

Interestingly, the spread of tuberculosis is highly variable. While some patients infect all their household members, others infect none. This is caused by different factors, besides host susceptibility and environmental factors, also the frequency of expulsion of bacilli from the infected host matters.

Life outside the human host presents a number of potential challenges to the survival of *M. tuberculosis*. The time during which bacilli remain capable of causing infection after release into the environment is highly relevant for transmission. Once aerosolized bacilli are able to survive more than 10 minutes in air[101] and can be transported to a susceptible host. Environmental factors influence the transmissibility of *M. tuberculosis*-containing aerosols. Ambient conditions, including ultraviolet and ionizing radiation decrease the viability of *M. tuberculosis*[102,103]. RH has long been recognized as key factor in bioaerosol activity. Peccia *et al*. (2004) conducted a decay experiments in an aerosol reactor (0.8 m^3) to determine the impact of RH and UV on airborne bacteria and showed that a high RH is protective against UV light radiation for airborne bacteria such as *Mycobacterium bovis* BCG[104]. Depending on the RH of the environment water layers starts to evaporate and condensate around the bacterium[9,30].

Most important, the risk of developing disease is related less to the inhaled dose, but more specifically to the nature of the inhaled particle. If a single bacterium makes it through the tidal volume into the alveolus, the macrophages are well equipped to deal with it, and this might be indeed the actual reason why 75 % or more of exposed individuals never get the disease. But when the individual breathes in a small clump, the engulfing alveolar macrophages are overwhelmed by the accumulation of virulence factors and the bactericidal capacities of these cells is quickly exhausted[105].

2 Results

2.1 Mass density and Hygroscopicity of Mycobacteria

The ability of airborne particles to stay airborne, is highly dependent on different biophysical characteristics of the bacterium, including mass density and hygroscopicity of BCG. Mass density was determined indirectly by defining the volume of one bacterium at 65 % RH by AFM. It was calculated from 3D reconstructions of mycobacterial cell topography (Figure 8A) and found at (0.43 ± 0.08) μm^3. The weight of one bacterium was determined to be at ($7.66*10^{-15}$ ± $6.92*10^{-16}$) g. The mass density of one BCG bacterium is therefore at (1.79 ± 0.08) g/cm^3. When bacteria travel through air, they will meet different RHs, depending on the present ambient conditions. Therefore, the hygroscopicity of the mycobacterial cell, i.e. the ability to take up water from the environment, was analyzed by the change in volume of a single bacterial cell by AFM. Dimension of single bacteria were determined at different RHs and the volume was calculated from 3D reconstruction (Figure 8A). At 25 % RH, the volume of one mycobacterium was found at (0.26 ± 0.09) μm^3, which almost doubled to (0.47 ± 0.19) μm^3 at 80 % RH. At 65 % RH the volume was found at (0.43 ± 0.08) μm^3, suggesting a stage of saturation between 65 % and 80 % RH, in which the bacterium is not able to take up additional water from its surrounding (Figure 8B). Supporting the results, changes in mass were measured by a gravimetric method, where uptake of water was assessed by the increase in weight (Pfrommer *et al.* 2020).

2.2 Resilience of Mycobacteria to Air

As mycobacterium containing aerosols are faced with the risk of dehydration while traveling through air, the ability to withstand dehydration was analyzed. The cell membrane damage was determined by microscopical analysis upon life/dead staining and the viability by their ability to form colonies (CFU) of mycobacteria out of growth broth at different time points after being exposed to ambient air at room temperature (20 – 25 °C) and 60 – 70 % RH.

In the source suspension of mycobacterial in broth, (12.73 ± 0.74) % were not viable. Due to dehydration the percentage of dead bacteria increased from (12.73 ± 0.74) %, to (21.95 ± 1.53) % after 30 min, to (31.8 ± 1.51) % after 60 min, to (49.96 ± 2.02) % after 90 min to finally (98.23 ± 0.98) % after 300 min. Similar, the viability of mycobacteria determined by CFU decreased from $1.41*10^7$ ± $2.15*10^5$ (100%) already after 30 min

and 90 min in air to 65.5 % ($9.23*10^6 \pm 2.87*10^5$) and 49.9 % ($1.21*10^6 \pm 1.45*10^5$), respectively, and became further reduced after 300 min to 0.01 % ($3.2*10^2 \pm 317$) (Figure 8C and 8D).

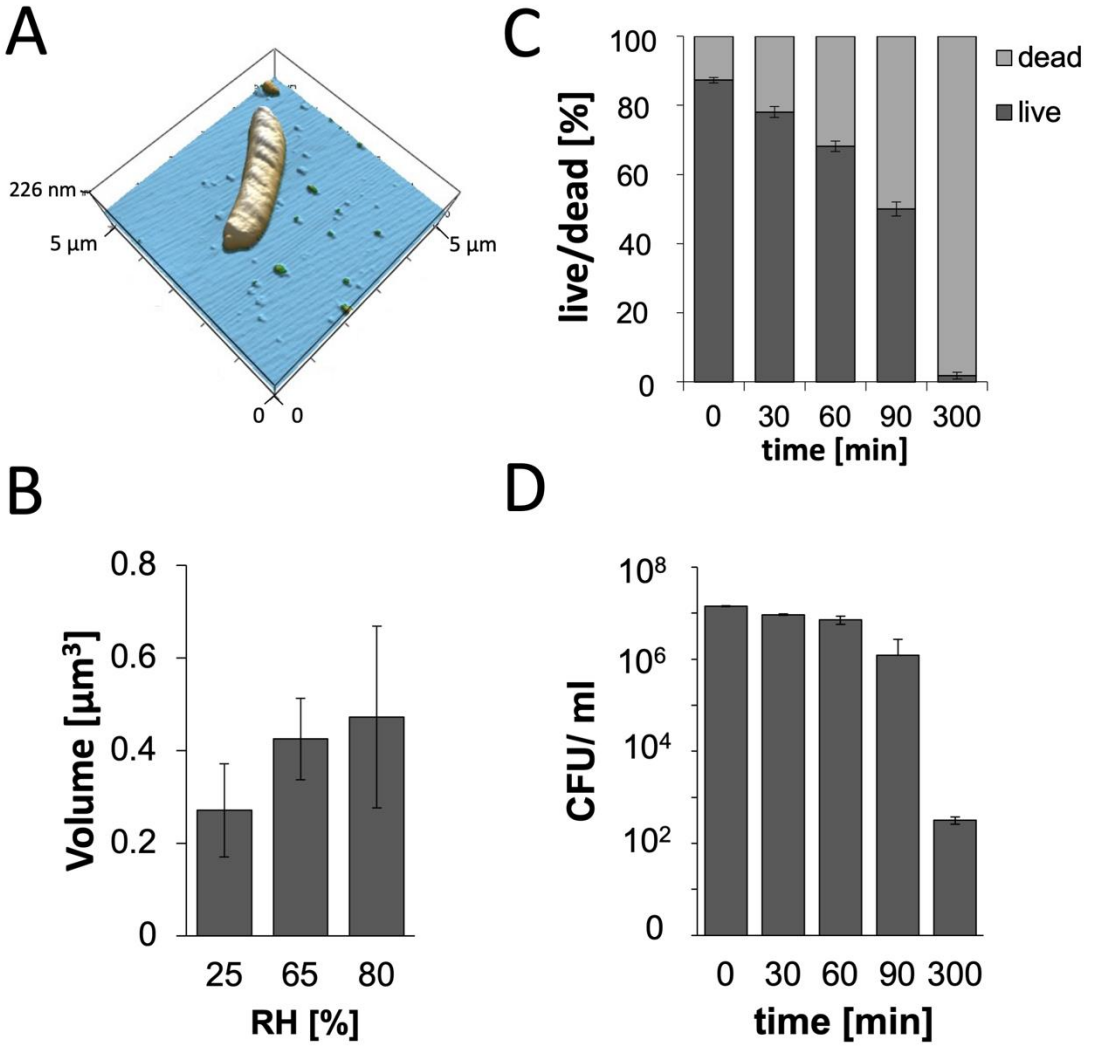

Figure 8: Biophysical Properties of Mycobacteria. (A) Representative 3D reconstruction of a mycobacterial cell using Igor Pro software to calculate the volume of a single mycobacterium in air. **(B)** Volume of a single mycobacterium in air under different RH's. The RH was adjusted by deliquescence salts inside a closed chamber (mean and standart deviation of three independent experiments are shown per humidity, p = 0.0008). **(C, D)** Ability of mycobacteria from broth cultures to survive drying conditions for different time periods. **(C)** Live/dead staining using the LIVE/DEAD BacLight Bacterial Viability Kit and depicted as the ratio between live vs. dead out of 100 mycobacteria analyzed (mean and standart deviation of three independent experiments are shown). **(D)** Independent determination of CFU counts in dehydrated mycobacteria ((mean and standart deviation of three independent experiments are shown).

2.3 Aerodynamic Size and Survial Rates of Airborne Mycobacteria

Successful airborne transmission of mycobacteria depends on their aerodynamic size and ability to survive environmental conditions in air. The ACI allowed simultaneous assessment of both, aerodynamic size as well as airborne pathogen viability as determined by CFU recovered and live/dead staining as a measure of membrane damage. Dependent on their velocity, particles with smaller aerodynamic diameters settled at lower and bigger ones at higher levels of the ACI. Aerosols were continuously generated during the sampling time of 10 min.

Viability testing by CFU revealed that 85 % of airborne viable mycobacteria can be found on level 6 – 8, corresponding to an aerodynamic diameter between 0.22 and 1.7 µm (Figure 9A, Table 3). Live/dead stain showed a significant loss of viability in airborne BCG when compared to control non-airborne mycobacteria directly transferred from culture medium into PBS (Figure 9B). Transfer into PBS already affected mycobacterial viability as (24.56 ± 3.1) % mycobacterial cells were already dead before aerosolization, as determined by live/dead staining (compare control in Figure 9B to timepoint 0 in Figure 8D).

Table 3: Relative Distribution of Airborne BCG on ACI Levels. Relative distribtion of BCG-containing aerosols in comparison to the diameter cut off at 28 l/min, provided by the manufacture.

Level	1	2	3	4	5	6	7	8
Diameter cut off [µm]	8.0	6.5	5.2	3.5	2.6	1.7	1.0	0.22
Rel. Distr. of mycobacteria [%]	0.4	0.8	1.4	2.9	9.4	27.3	40.6	17.1
Std. deviation	0.3	0.3	0.8	2.0	3.3	1.7	4.3	3.9

By applying different solid supports on the levels of the ACI we were able to simultaneously generate samples suitable to analyze the morphology as well as the viability of airborne mycobacteria. To analyze the morphology including potential aggregation of airborne mycobacterial particles, negative stain was used. Most airborne BCG (53 ± 2) % traveled as single, (32 ± 1) % as double and only 15 % as aggregates of more than 5 bacteria per clump (Figure 9C). The aerodynamic diameter of mycobacteria-containing particles was linked to the number of mycobacteria within the particle, as singlets were mainly found on levels 7 and 8 and doublets primarily on levels 6 and 7 whereas clumps of more than 5 mycobacteria were predominantly observed on levels 1

and 2. AFM analysis of unfixed mycobacterial aerosol particles further confirmed that most particles represented single cells, whereas only a small fraction of those was found as larger clumps (Figure 9D).

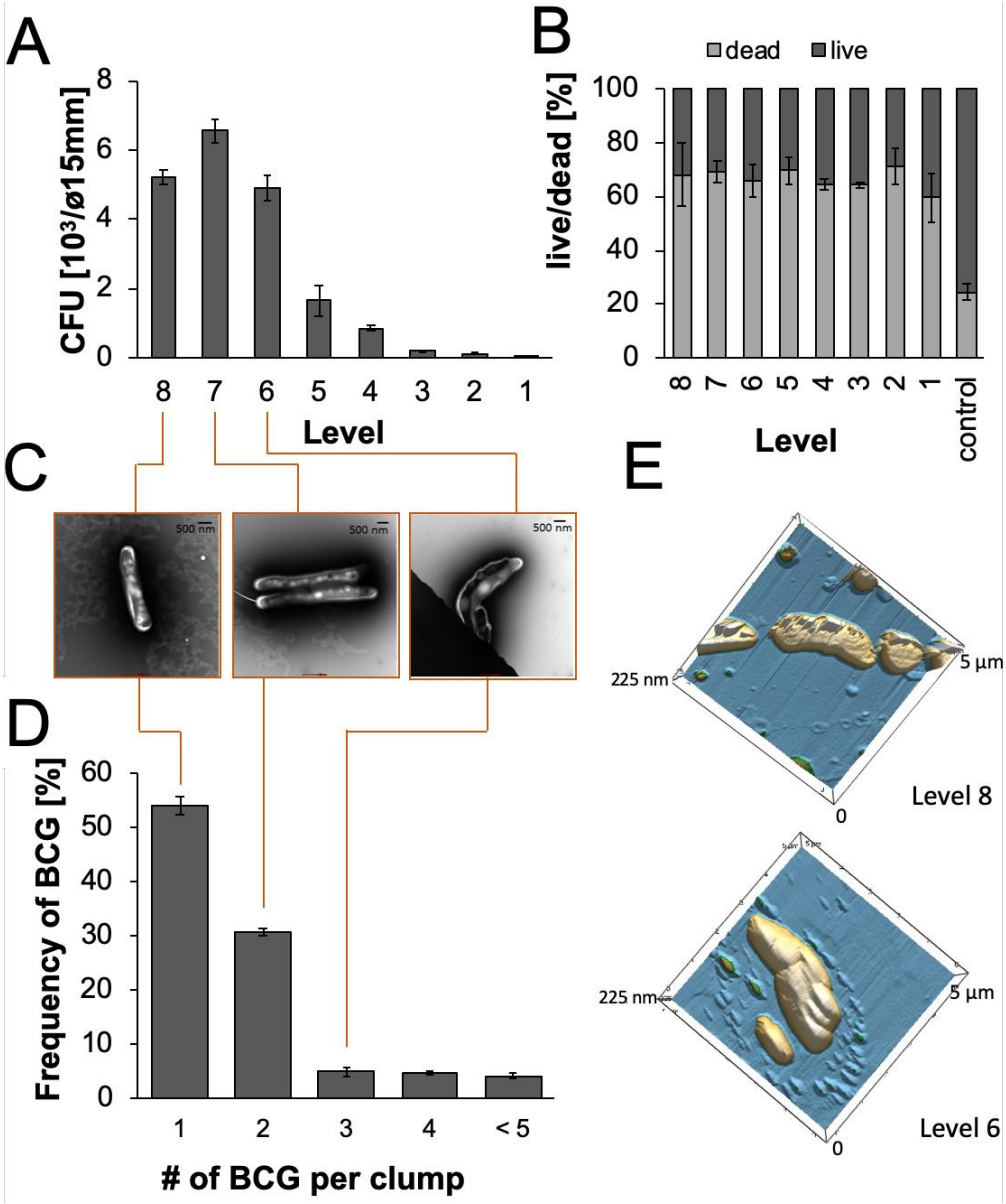

Figure 9: Properties of Mycobacteria-Containing Aerosols. (A) CFU of mycobacteria collected from the different levels of the ACI upon aerosolization in PBS at a 28 l/min airflow. (mean and standart deviation of five independent experiments are shown; p>0.001) **(B)** Percentages of live vs. dead mycobacteria as determined by LIVE/DEAD stain upon aerosolization in PBS assessed immediately after settling for 10 min at the different Impinger levels in comparison to control samples directly transferred from culture into PBS for viability stain before nebulization (mean and standart deviation of three independent experiments are shown/100 bacteria, p>0.0015). **(C)** Frequency of different mycobacterial cell numbers within aerosol particles as depicted by electron microscopy analysis counted on level 1 – 8 (mean and standart deviation of three independent experiments are shown, p>0.0001). **(D)** Representative 3D reconstruction of airborne mycobacteria collected at different levels and analysis by AFM (mean and standart deviation of three independent experiments are shown).

To confirm the aerodynamic diameter of BCG-containing aerosols as determined by the ACI, we measured the flight time of aerosol particles between two lasers in a certain distance in a fixed airflow of 1 l/min using an Aerosol Particle Spectrometer (APS). Simultaneously the optical diameter of each particle was determined, as the refraction of the laser light by the particle could be traced.

The main aerodynamic diameter of empty vs. mycobacteria-containing aerosols was almost twice as high when aerosols were generated by jet nebulizing, but not in a statistically significant manner ($p = 0.292$) (Figure 10A left and Figure 10B left). The aerodynamic diameters of mycobacteria-containing aerosols varied between 0.5 und 5 µm. Most aerosols showing an aerodynamic diameter of 0.89 µm whereas the main diameter of PBS aerosols was 1.38 µm. In contrast to the aerodynamic diameters, the optical diameters of mycobacteria-containing aerosols generated by jet nebulizing were larger than those of empty PBS aerosols, but not in a statistically significant manner ($p = 0.608$). Aerosols generated by the ultrawave (Piezo) nebulizer showed lower variability in the aerodynamic diameters measured (compare Figure 10A right with Figure 10B right) and the optical diameters between empty PBS and mycobacteria-containing aerosols was comparable (Figure 10B right).

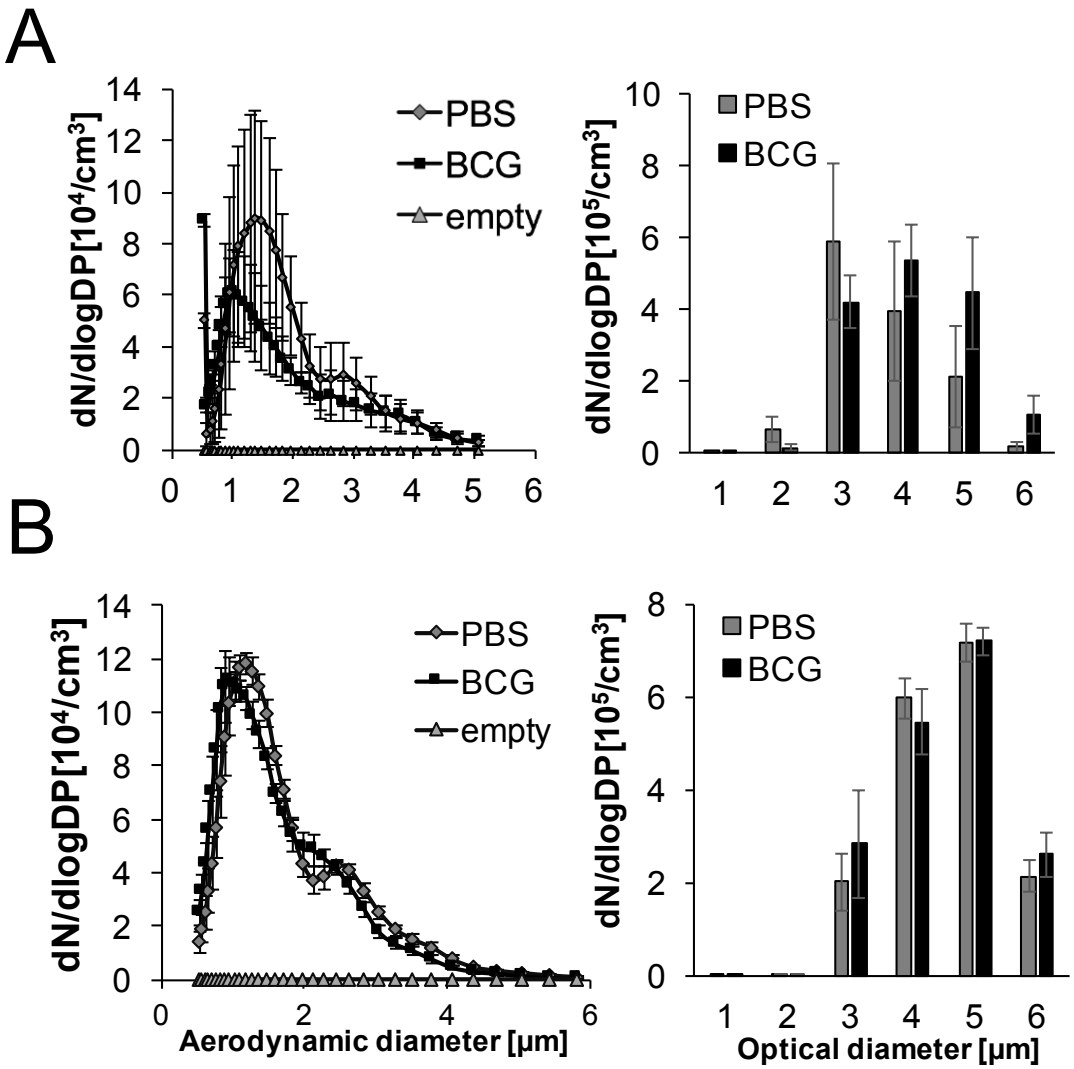

Figure 10: Aerodynamic and Optical Diameters of Airborne Mycobacterial Particles as Determined by APS. (A) Left: Distribution of aerodynamic diameters of jet nebulized buffer and mycobacterium-containing aerosols (OD 0.6, 580 nm) Right: Distribution of optical diameter of jet nebulized buffer and mycobacterium-containing aerosols (mean and standart deviation of three independent experiments are shown). **(B)** Left: Frequency of aerosol particles with a certain aerodynamic diameter upon ultrawave nebulizing. Right: Optical diameter of ultrawave nebulized buffer and mycobacterium-containing aerosols (mean and standart deviation of three independent experiments are shown).

To assess the tenacity of airborne mycobacteria, the length the aerosols stayed airborne and viable was measured. The aerodynamic diameter distribution at different time points after aerosolization did not differ, meaning that a certain aerosol particle size did not dropout of the air earlier than the others. However, the total number of detectable aerosols was drastically reduced already after 60 min (Figure 11A). Interestingly, even though both nebulizers produced a comparable number of aerosol particles and aerodynamic and

no differences in aerodynamic diameters of aerosols between jet and ultrawave nebulizer were observed, those from the piezo nebulizer dropped out of the air quicker (Figure 11B and Figure 10). Independent of the nebulizing device, we were able to detect, a large number of aerosol particles by APS 30 min after nebulizing. But those aerosols did not contain viable BCG (Figure 11).

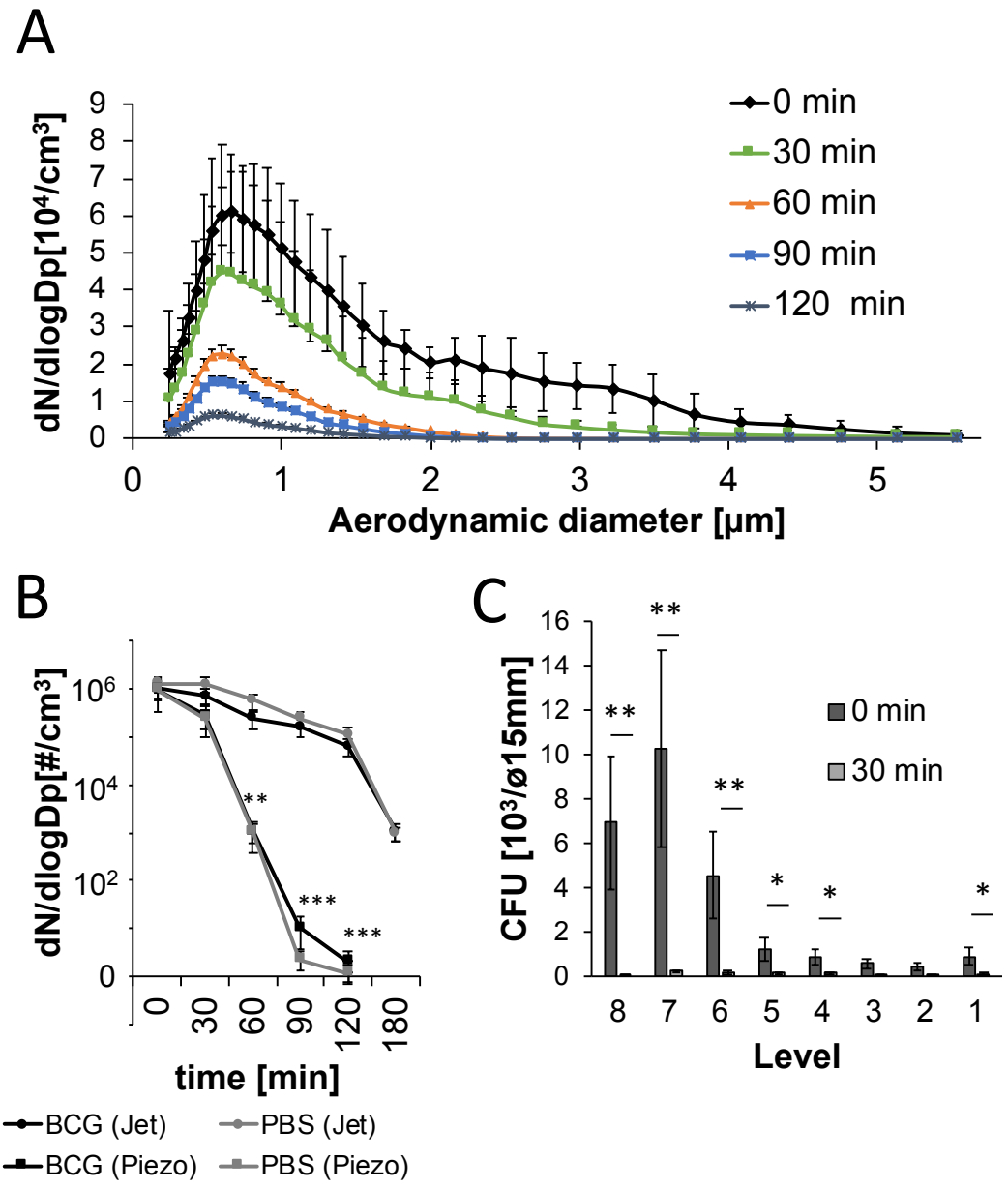

Figure 11: Tenacity of Airborne Mycobacteria. (A) Distribution of aerodynamic diameters of aerosols generated by jet nebulizing from either buffer (PBS) or mycobacterial suspensions in PBS in ACD air at different time points after aerosol generation (mean and standart deviation of three independent experiments are shown). **(B)** Settling time of jet nebulized aerosols vs ultrawave nebulized aerosols (mean and standart deviation of three independent experiments are shown, **p>0.001, ***p>0.0001). **(C)** CFU of airborne mycobacteria collected from the different levels of the ACI at the starting time point of jet nebulizing and 30 min later (mean and standart deviation of three independent experiments are shown, *p>0.01, **p>0.001).

2.4 The Role of Neutrophil Necrosis in the Formation of Mycobacteria-containing Aerosols

The role of neutrophils (PMN) in the pathogenesis of active Tuberculosis is still under discussion but more and more evidence recently was shown that neutrophils play a major role in breaking up granulomas and provide access of bacteria to the airways for expulsion and transmission by cough[62,106]. In order to mimic ROS induced necrotic cell death in BCG infected neutrophils, as described for virulent but not attenuated *M. tuberculosis* infected neutrophils[107], we used H_2O_2 to induce necrotic cell death. Necrosis is determined by measuring the activity of Lactate Dehydrogenase (LDH) in the cellular medium. LDH is a cellular enzyme that cannot be detected in the supernatant of intact cells. The induction of necrotic cell death was measured in culture supernatants of untreated neutrophils, H_2O_2 treated ones, BCG infected, and in neutrophils that were infected with BCG and treated with H_2O_2. The 100 % reference was determined by lysing neutrophils with Triton X, a chemical detergent that disintegrates the cellular membrane and thereby releases LDH out of all cells.

Untreated neutrophils or those infected with BCG showed an LDH concentration of (10 ± 8.6) %. H_2O_2-treatment of non-infected neutrophils already induced an LDH concentration rate of (40 ± 17.4) %. The LDH concentration was further increased when BCG infected neutrophils were treated with H_2O_2 to (>56 ± 9.6) % necrosis (Figure 12A). To study whether the passage of mycobacteria through neutrophils affect their viability upon exposure to air, we analyzed mycobacterial CFU from samples containing either free mycobacteria or BCG infected neutrophils, which were either non-treated or exposed to H_2O_2. Under all three conditions, mycobacterial loads were comparable with only a slight reduction in viability 0.5 h after exposure to ambient air. After 5 h of dehydration, viability of BCG alone and BCG from necrotic neutrophils became significantly reduced. Interestingly, mycobacteria from intact neutrophils were more resilient to exposure to air. After 5 h of exposure to ambient air, mycobacterial viability was not as drastically reduced in intact neutrophils compared to mycobacteria from H_2O_2-treated necrotic neutrophils or free mycobacteria with or w/o H_2O_2 treatment. Even after 18h of exposure to ambient air, still 269 ± 27 mycobacterial CFU were detectable, when they were shielded in intact neutrophils. Whereas, only 3.67 ± 0.5 CFU were recovered from mycobacteria in H_2O_2-treated neutrophils or free ones with or w/o H_2O_2 treatment (Figure 12B).

H_2O_2-induced cell death in BCG-infected neutrophils was also visualized by light microscopy or by SEM. Untreated neutrophils, isolated from human blood, showed a typical round morphology with a segmented nucleus. Infection with BCG, did not induce necrosis, but lead to the loss of neutrophils and promoted aggregate formation. Treatment of BCG-infected neutrophils with H_2O_2 led to neutrophil necrosis as characterized by membrane disintegration and appearance of filamentous cell remnants. SEM analysis revealed no differences between PMN alone and BCG infected BCG. When treating the BCG infected cells additionally with H_2O_2, the neutrophils membrane disintegrated and formed filamentous structures (Figure 12C).

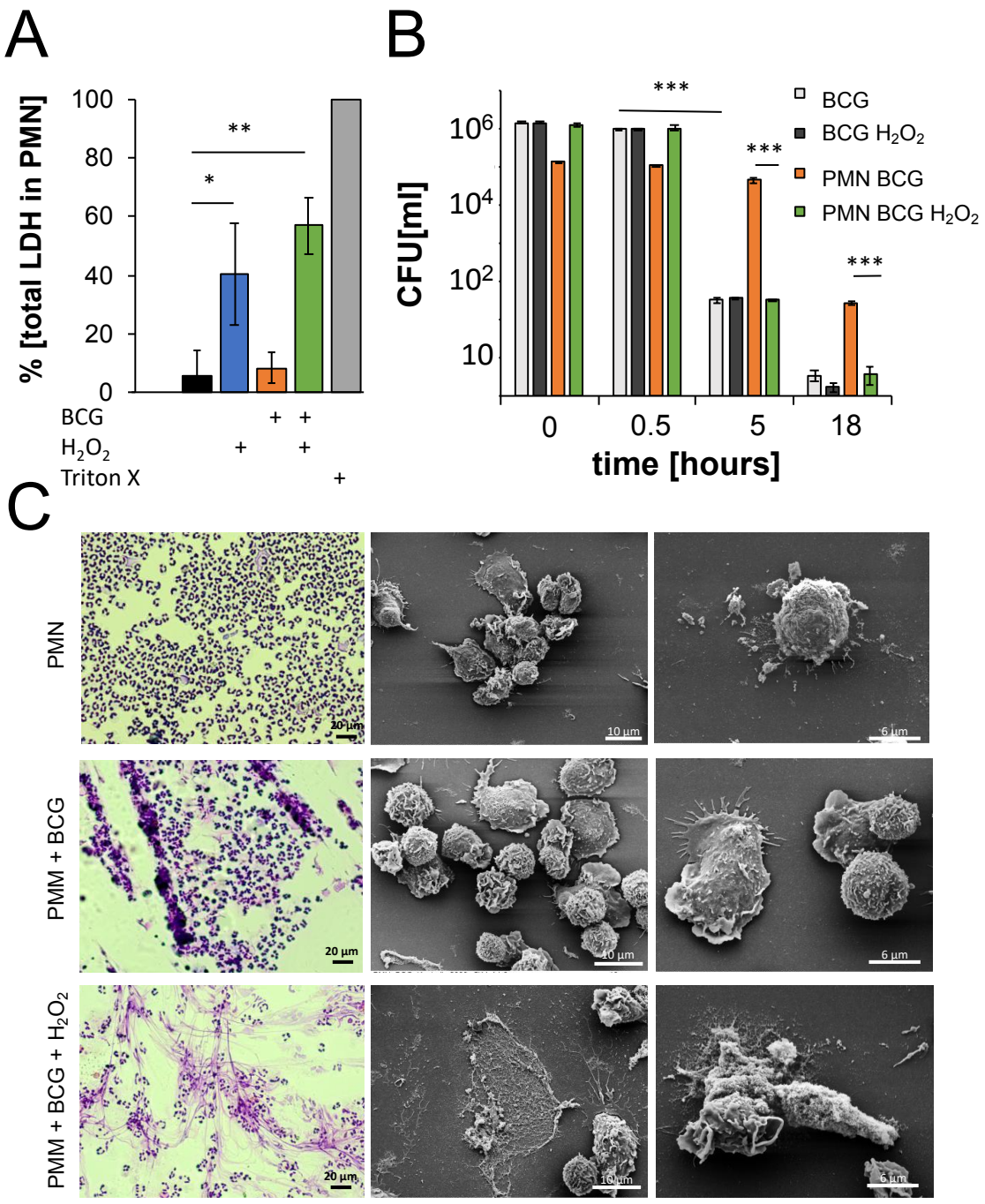

Figure 12: Mimicking Aerosols Expelled from Active TB Patient. (A) Human neutrophils isolated from peripheral blood were infected with *M. bovis* BCG and were either left untreated or treated with H_2O_2 to induce necrotic cell death. Necrotic cell death was assessed by measuring activity of the cytoplasmic enzyme, LDH, in culture supernatants (mean and standart deviation of three independent experiments are shown, *p>0.01**p>0.001). **(B)** Viability, as assessed by CFU, of mycobacteria recovered from *M. bovis* BCG infected neutrophils that were either treated with H_2O_2 to induce necrotic cell death or were left untreated and succumbed to default apoptotic cell death. CFUs were determined upon exposure to ambient air for the indicated time periods (mean and standart deviation of three independent experiments are shown, **p>0.001, ***p>0.0001). **(C)** Morphological analysis of human neutrophils either left uninfected or infected with *M. bovis* BCG w/o or w/ H_2O_2 treatment by H&E stain and SEM (mean and standart deviation of three independent experiments are shown).

To identify the effect of neutrophil infection on the aerodynamic diameter and optical diameter of mycobacterial aerosol particles, from intact neutrophils and necrotic neutrophils were analyzed by APS in comparison to RPMI media. As observed before (Figure 9) for PBS aerosols, empty RPMI aerosols were similar in their aerodynamic diameter size as those from free mycobacteria. Notably, less numbers of aerosol particles were generated from intact infected neutrophils (Figure 13A).

In contrast, we observed a shift in the optical diameter of BCG from necrotic neutrophils compared to the other samples. The higher optical diameter observed, however was not in a statistically significant manner ($p = 0.342$) (Figure 13B).

The aerodynamic diameter correlated with the distribution of particles containing viable mycobacteria as sampled by the ACI (Figure 13C). Notably, despite initial killing of the mycobacteria by H_2O_2 during induction of neutrophil necrosis (see Figure 12 for comparison), more viable mycobacteria were recovered from necrotic neutrophil derived aerosols, when compared to those from intact infected neutrophils. Aerosols from mycobacteria infected necrotic neutrophils contained a significant higher number of viable mycobacteria on levels 1 and 2 of the ACI corresponding to aerodynamic diameters between 6.5 and 8.0 μm. These aggregates were neither seen in aerosol particles from intact mycobacteria-infected neutrophils nor in those from mycobacterial suspensions. Additionally, to those aggregates of viable mycobacteria at levels 1 and 2, a shift in aerosol size distribution was observed at the lower ACI levels. While a great proportion of viable mycobacteria were found in aerosols from BCG suspension at levels 7 and 8, more viable mycobacteria were found on levels 4 to 6 in aerosols generated from BCG infected necrotic neutrophils (Figure 13B). This result suggests an overall shift in aerosol size proportion between mycobacterial aerosols generated from BCG suspensions in comparison to those from necrotic neutrophils. The compositions of mycobacterial aerosols generated from infected intact vs. necrotic neutrophils were analyzed by SEM. Mycobacteria from infected but intact neutrophils primarily appeared as singlets, and samples contained the occasional intact neutrophil (data not shown). In contrast, aerosols from mycobacteria infected but H_2O_2-treated necrotic neutrophils appeared as single bacterial cells or doublets at level 8, and as clumps at level 4. Aggregates associated with residual neutrophil material were found on level 1 and 2, containing higher numbers of viable mycobacteria (Figure 13C).

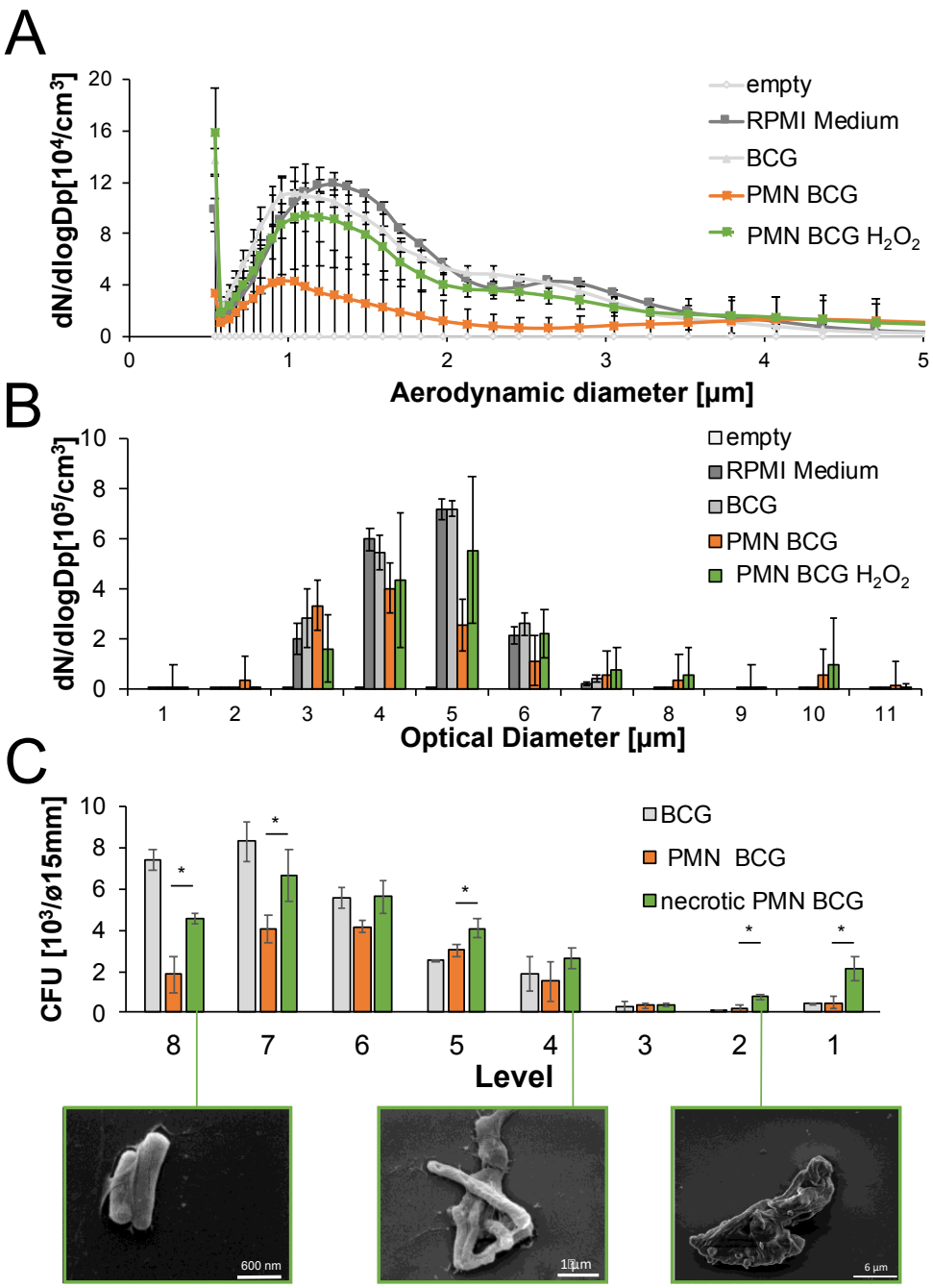

Figure 13: Aerosols of Mycobacteria-Infected Neutrophils. **(A)** Frequency of aerosol particles with certain aerodynamic diameters upon ultrawave nebulizing free mycobacterial cells in RPMI, RMPI alone, mycobacteria infected but untreated or H_2O_2-treated necrotic neutrophils (mean and standart deviation of three independent experiments are shown). **(B)** Distribution of optical diameters of aerosol particles generated by ultrawave nebulizing from either mycobacterial suspension in RPMI, RPMI alone, mycobacteria infected but untreated or H_2O_2-treated necrotic neutrophils (mean and standart deviation of three independent experiments are shown). **(C)** Mycobacterial viability was assessed by CFU in aerosols collected from different levels of the ACI after nebulizing using the ultrawave nebulizer either mycobacterial cells alone, or mycobacteria infected but untreated or H_2O_2-treated necrotic neutrophils. Selected fractions containing airborne mycobacteria from necrotic PMN were further analyzed by SEM (below), (mean and standart deviation of three independent experiments are shown as well as repesentative EM pictures, *p>0.001).

3 Discussion

It is well established that M. *tuberculosis* can be transmitted through air, but little is known about the biophysical properties of mycobacteria that allow successful transmission. This study on M. *bovis* BCG revealed that aerodynamic diameter as well as mass density of mycobacteria-containing aerosols could allow long distance transport, but airborne mycobacteria quickly lost their viability. However, by experimentally induced necrotic cell death in BCG infected PMN as has been recently described for *M. tuberculosis* infected cells[61], aerosolized mycobacteria from infected and necrotic neutrophils, maintained their viability when compared to those aerosols derived from intact neutrophils. Despite reduction of mycobacterial viability during necrosis induction by H_2O_2. Enhanced aggregate formation and association with necrotic neutrophil material likely contributed to mycobacterial viability as bigger aggregates are less likely to dehydrate. This study on *M. bovis* BCG suggests that the major portion of the living mycobacteria could be transmitted over short distances.

3.1 Airborne Transmission of Mycobacteria-Containing Aerosols

As mycobacteria are facultative intracellular pathogens in phagocytes, the formation of mycobacteria-containing aerosols is influenced by the host cell at the infectious site harboring the bacteria and mode of their release. After aerosolization by coughing, the airborne particles are exposed to different environmental factors, including varying RHs. Directly after the release of mycobacteria-containing aerosols from the respiratory tract, the bacteria are coated with water. During their airborne lifetime in air, water will condensate and evaporate from the bacterial surface, depending on ambient RH. On short distance transmission airborne bacteria remain coated with water and that water layer will mainly influence the airborne behavior of the bacteria-containing aerosol. In contrast on long distance transmission, the ability of the bacterium to endure dehydration and the biophysical characteristics of the bacterial particle, such as mass density and hygroscopicity will determine the success of airborne transmission.

3.1.1 Formation of Mycobacteria-Containing Aerosols

M. tuberculosis can initiate necrosis, particularly in neutrophils and break into the alveolar and bronchial space. Extracellular mycobacteria can be coughed up and/or exhaled[100,108]. Neutrophils represent the predominant mycobacteria infected cell population in pulmonary samples from active TB patients, such as broncho-alveolar

lavages or sputum, and succumb to necrotic cell death upon infection with virulent *M. tuberculosis* strains[62,106,109]. Until this study, the effects of mycobacterial infected neutrophil necrotic cell deaths on the composition of mycobacterium-containing aerosols was not known.

Necrotic cell death of infected neutrophils can lead to more mycobacterial clumps associated with neutrophilic remnants, which can be aerosolized from active TB patients during coughing (Figure 13). Although mycobacterial clumps fall out of air quicker due to their higher mass, their increased virulence bears an enhanced risk of short distance transmission of *M. tuberculosis* (Figure 12 and Figure 13).

In our experimental aerosol model, only a small fraction of mycobacteria were presented in clumps, they could still enhanced the chance of infection then single one. As observed by increased aerosol size and SEM in this study, induction of necrotic cell death in infected neutrophils promoted formation of mycobacterial clumps (Figure 13).

Besides the host cells involved in pathogenesis, the mode of released influences the airborne behavior of mycobacteria-containing aerosols (Figure 11). As reviewed before in Chapter 1.2, different ways of expelling infectious aerosol particles, i.e. by coughing, sneezing, speaking or singing influences the particles behavior drastically. In this study, aerosols were generated by two types of nebulizers and the aerosols produced showed different tenacities. Those produced by the ultrawave nebulizer felled out of air faster than those generated from jet nebulizing despite both aerosol types showed comparable aerodynamic diameter distributions (Figure 11B). So even though different modes of release may not alter the aerodynamic diameter, different modes of release by body functions will influence drastically the tenacity of particles. It is therefore important not only to study the aerodynamic size and number of released particles but also to compare the tenacity of airborne particles released by coughing, talking or singing, as this will allow to assess a more realistic risk of infection.

3.1.2 Short Distance Transmission

The aerodynamic diameter of mycobacterium-containing aerosols, were measured using APS (Figure 10 and Figure 13A/B) as well as the ACI (Figure 9A and Figure 13C). Since the aerodynamic diameter did not differ between empty and mycobacterium-containing aerosols, the aerodynamic diameter is likely defined by the surface tension of the buffer used, in this case PBS (Figure 10). Interestingly, the optical diameter, which can be analyzed simultaneously to the aerodynamic one, revealed a difference between empty

and mycobacterium-containing aerosols upon jet nebulization. This difference was particularly pronounced in mycobacteria from necrotic neutrophils (Figure 13B). As mycobacteria are rod-shaped, they can show a smaller aerodynamic than optical diameter as they can turn into the air flow during travel. Notably, the difference between optical and aerodynamic diameter was not observed in aerosols generated by ultrawave nebulizing (Figure 10B).

The aerodynamic diameter was determined by the tension force of the buffer and was independent on the aerosol nuclei. Most mycobacteria-containing aerosols consist of one or two bacterial cells and rarely a clump of bacteria with a layer of buffer around the bacterial nuclei (Figure 9C). However, clumps were considered more infectious than single bacteria, since airway defense cell, alveolar macrophage, are better equipped to handle single mycobacteria[88,105]. Macrophage that engulf groups over five bacilli or more in a single phagocytic vesicle have to deal with more of bacterial virulence factors. The accumulation of these virulence factors could overwhelm the bactericidal capabilities of these cells[105]. It should be noted that the settling velocities of aerosols in the 1 – 5 μm size range are prone to reach the lower respiratory tract independent of whether they consist of single bacteria or clumps of bacteria (Figure 11A).

It should be noted that, airborne mycobacteria lost their viability after a short period of exposure to ambient air in the aerosol chamber. Death of airborne bacteria has been described as a two-step process[110]. In our experiments, most bacteria died within the first few minutes after becoming airborne, which was likely due to the sheering stresses during the vaporizing processes. Second stage death affected bacteria that are airborne for longer time periods are caused, for example, by deprivation of nutrients and UV light[29,30,110]. As we continuously produced aerosols, while we sampled the ambient air from our experimental box, we excluded second stage death affects, other than dehydration and nutrients deprivation that occur inside the ACI.

3.1.3 Long Distance Transmission

The success of airborne transmission depends on the mycobacteria's ability to remain viable for prolonged time period while airborne, which depends on different factors including environmental cues, such as ambient humidity. A relationship between efficacy of airborne transmission of *M. tuberculosis* and relative environmental humidity was described before[34,111]. Higher transmission rates were observed at a higher RH. Thus, it was hypothesized that high humidity can protect mycobacteria against UV light and

drying out[30]. Experimental studies revealed that only humidity´s between 60 and 80 % RH were supportive of transmission. At higher humidity´s (> 85 % RH) the effect was reversed and lower transmission rates were observed[30,34,111]. By measuring the volumes of single mycobacterial cells, the hygroscopicity of mycobacteria became saturated at 80 % RH, (Figure 8B) indicating that an excess of water in air cannot be further adsorbed by mycobacteria but is likely condensing around bacterial nuclei. Interestingly, even though we observe such a drastic change in mass and volume of the mycobacterium, in previous studies performed by *Peccia et al.* (2001) no change in aerodynamic sizes of airborne bacteria were observed at different RH ranging from 20% to 90%[112]. This can also be seen in Figure 11, were the measured aerodynamic diameter of aerosol did not vary, even though the ambient air of the chamber lost humidity during the experiment. As nebulization inside the chamber increased the RH up to 90 %, the ambient air of the chamber quickly returned to the room RH of 60 – 75 % by air exchange after nebulization. At a lower RH of 65 %, mycobacteria became sensitive to dehydration, which reduced their viability already 30 min after exposure to air by more than 30 %. As water evaporates from the bacterial culture, the salt content increases in the sample and therefor the bacterial dehydration occured more rapidly. This can be seen in the increased rate of viability loss 60 min after. Since it is not far off to measure the effects of dehydration in a salt solution, also body fluids contain salt.

We also need to keep in mind, that this loss of viability in air occured even quicker (Figure 11), as bacteria are already stressed by the process of aerosolization (Figure 9B). The same was described for the release of aerosols from the respiratory tract, where high sheer forces are needed to release bacteria from cavities and bronchial obstruction and to overcome mucus viscosity[99,113].

When environmental influences are excluded, the Archimedes' principle, which describes the interplay between gravity force on a particle as defined by its mass density and buoyancy depending on its volume, characterizes an aerosol particle's properties. The mass density of a single mycobacterium was determined as (1.79 ± 0.08) g/cm3 at 65% RH (Figure 8B). Thereby we were able to calculate the settling velocity of mycobacterial particles using the Stokes law depending on their size and mass density. Notably, the difference in mass density between PBS (1 g/cm^3) and a mycobacterial cell (1.79 ± 0.08 g/cm^3) did not affect the aerosol velocity, especially when the size ranged between 1 and 5 μm, the range of mycobacterial aerosol sizes measured in these experiments.

Successful infection may therefore be determined by the distance a particle can travel through air and the time before viability and thus infectivity is reduced. Therefore, single mycobacteria are able to cover larger distances whereas clumping preserves both mycobacterial infectivity and virulence[30,88,105]. Computer simulating of airborne transmission taking into consideration the different aerosol sizes determined in this study, will help to solve the question, which aerosol composition bears a higher risk of infection.

3.2 Conclusion

This study provides insights on the biophysical properties of airborne mycobacterial transmission indicating that transmission of TB happens more likely over short distances. Mimicking the situation in active TB patients, aerosols from mycobacteria infected necrotic neutrophils showed enhanced clumping by association with neutrophil remnants, which can limit the transmission radius but at the same time increase infectivity upon inhalation by a naïve host. The quick loss of viability after exposure to ambient air is likely reducing the chance of successful infection upon transmission over longer distances[114]. Depending on the ambient RH, mycobacteria containing aerosols will shrink or grow as water condensate and evaporates around the particle. RH above 75 % have been described as protective for the airborne mycobacteria[104], supporting the idea, that short distance transmission is the prominent form of transmission as the negative effects of higher RH and thus bigger particles are not overweighing the positive effects of RH such as UV light protection. Association with neutrophils can prolong viability during air transmission. However, the minimal infectious dose of *M. tuberculosis* has been suggested to be rather low, i.e. less than 10 bacterial cells. Therefore, *M. tuberculosis* transmission is mainly occurring between close contacts as it is happening between house hold members, people in narrow occupational facilities as well as between closely interacting patients and health workers.

3.3 Critic and Outlook

An independent experimental study revealed that the viability of the wildtype *M. bovis* strain 61/4086/ 00 spoligotype 21 remained at 80 % right after nebulization[115]. These results are in striking contrast to our ones shown herein using *M. bovis* BCG, which revealed a drop in viability by > 90 % as a result of first stage death upon aerosolization. Gannon *et al.* used a 135 l containment to collect aerosols and a slow air drought of 14 l/min at a relative humidity of 75 % RH, which was in contrast to our set up of a 27 l box and an airflow of 28 l/min. Our findings however, are comparable to studies in structurally

unrelated Gram-negative *E. coli* cells[32]. Thus, the faster air exchange of one complete ambient air volume per min could have reduced the viability of airborne mycobacteria. Furthermore, we used a commercial nebulizer usually employed for therapeutic medication, which generated aerosols by air drought, the shear forces could additionally have affected mycobacterial viability.

The small size of the chamber used in here only allows to mimic a situation in which donor and acceptor person are in close contact. The major aim of our study was the generation of reproducible aerosols containing a sufficient high number of life bacteria and not to investigate the influence of the properties of the ambient air (RH, wind, UV-light, velocity) on the tenacity of the mycobacteria. This should be the topic of a future study.

CHAPTER 2: Airborne Influenza A Virus is Definded by its Origin

1 Introduction

Every year, seasonal influenza A viruses (IAV) epidemics result in 3 to 5 million severe cases and account for approximately 290,000 - 650,000 deaths worldwide[116]. Two main modes of transmission, which are not mutually exclusive, have been shown to support the spread of influenza between humans: contact and airborne transmission. Airborne transmission can occur via two modes. Respiratory droplets, larger than 5 μm, do not remain suspended in air and deposit at distance of less than 1 meter. Small aerosols (< 5 μm) have a slower settling velocity and can remain suspended in the air for up to hours. The importance of airborne transmission in the overall transmission of influenza is still discussed. In resent papers it was shown that the highest viral RNA copies can be found in fine particles[20] which would prolong the time virus particles could stay airborne. Thus, airborne transmission is involved in rapid spread of influenza and understanding airborne transmission may help to control influenza transmission.

1.1 Clinical Aspects and Pathogenisis of Influenza

Upon infection, influenza is characterized by a sudden onset of disease, following a short incubation time of approximately one to two days[116]. Patients usually present with a number of symptoms that can vary and are depended on the strain, infection dose, route of inoculation, and the presence of preexisting immunity. Symptoms include fever, cough, malaise, myalgia and joint paint[116]. In most cases, seasonal IAV causes relatively mild upper respiratory tract infections and progresses sub-clinically but in some cases seasonal IAV can cause severe lower respiratory tract infections. The influenza virus, as it spreads via aerosols and droplets (for more details see Chapter 2; 1.7) first comes in contact with the oral mucosa, nasal mucous membrane and the ocular conjunctivae where it can infect epithelial cells[117]. Acute symptoms and fever can often persist for 7 to 10 days, whereas the feelings of weakness and fatigue may remain for several weeks[118]. Virus replication peaks approximately 48 hours after infection and viral particles are usually shed for about six days[118]. Even when the infectious viruses can no longer be recovered, viral antigens can be detected in host cells and secretions of infected

individuals for several days[118]. Influenza can be diagnosed by viral culture, detection of viral antigens or genetic material of viruses and antibody titers against IAV.

IAV transmission can be reduced by changes in behavior, like regular hand washing, vaccination or administration of antiviral drugs. Studies of healthy young adults have shown influenza vaccine to be 70 % to 90 % effective in preventing influenza A disease[116]. Re-vaccination is necessary as constant genetic changes of influenza virus strains facilitates evasion from preexisting immunity. Genetic changes occur by i) antigenic drift in which acquired mutations limit antibody binding to the virus or ii) antigenic shift, where RNA segments from another influenza subtype is acquired recombined into the IAV genome (also see Chapter 2; 1.4).

1.2 Classification of Influenza

IAV is a negative-sense, single-stranded, segmented RNA virus, belonging to the family of *Orthomyxoviridae*[119]. The *Orthomyxoviridae* can be divided into several genera, including influenza A, B, C and the recently discovered influenza D[120] viruses as well as tick-transmitted Thogoto and Dhori viruses[121], Isavirus and Quaranjavirus[122].

IAV are distinguished by serological and molecular biological differences in their nuclear protein (NP), matrix protein 1 (M1) and matrix protein 2 (M2). Further subtypes are defined by their surface proteins the hemagglutinin (H) and neuraminidase (N). To date 18 hemagglutinin (H1 to H18) and 11 different neuraminidase (N1 to N11) subtypes have been described. Except H17N10 and H18N11 which have only been found in bats so far, all other known subtypes of IAV have been isolated from birds[123]. The convention how influenza A and B virus strains are named is as follows: genus (type), species from which the virus was isolated (if isolated from humans, human is not mentioned), location of isolation, isolate number, isolation year and for IAV – the hemagglutinin (H) and neuraminidase (N) subtypes in brackets (A/Hamburg/05/09 (H1N1)) [119].

1.3 Virion Structure

The viral particles of influenza viruses are pleomorphic and differ in size and shape. The main configuration is a spherical shape with 80-120 nm diameter in size but also filamentous virions with a size of 300 nm can be found, especially in fresh clinical isolates[124,125]. Even though filamentous IAV particles play are crucial role in transmission of influenza , they are understudied as laboratory adapted strains usually used in these studies do not form those filaments[126]. Each virion consists of three major sub-viral components, namely i) a viral envelope decorated with three transmembrane proteins HA, NA and M2, an ion channel. HA and NA, glycoproteins on the surface , protrude as spikes from the viral envelope in a 4:1 HA to NA ratio[119] ii) an intermediate layer of matrix protein (M1), and iii) an innermost helical viral ribonucleocapsid [vRNP] core, formed by nucleoprotein (NP) and negative strand viral RNA (vRNA)[119,127]. The vRNP associates with the three subunits of the viral polymerase PA, PB1 and PB2 (Figure 14).

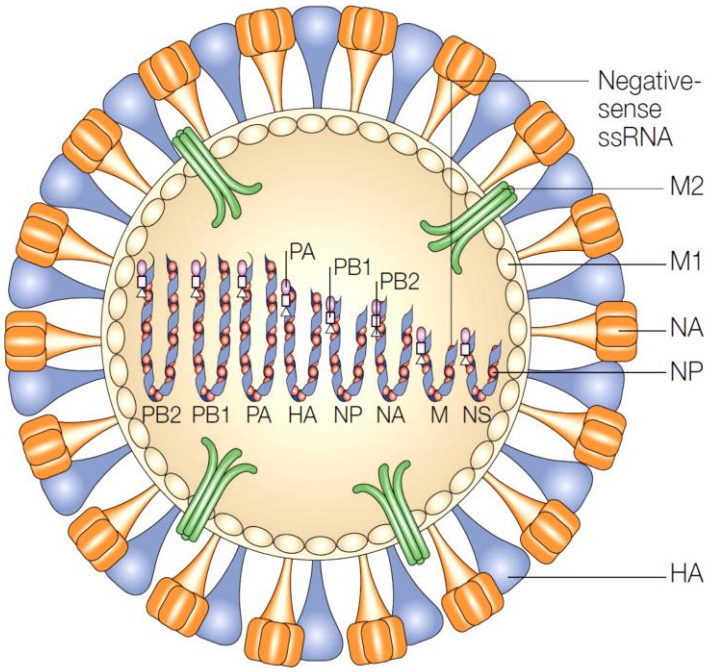

Figure 14: Schematic Representation of an Influenza Virus Particle. The lipid bilayer of the virion which forms the envelope, contains the HA, NA and M2 proteins. The M1 protein can be found inside the virion. The vRNP complex contains a vRNA segment encapsidated by the viral NP and associated with the three subunits of the viral polymerase (PB1, PB2 and PA). Modified from Horimoto *et al.*[128].

1.4 Genome Structure

IAV genome consists of eight negative-sense, single-stranded RNA (vRNA) segments of different length. In total the genome size is approximately 13.6 kb. The eight RNA segments are numbered in order of decreasing length and encode for at least 18 proteins**.** The HA, NP and NA gene segments encode for the corresponding protein. PB2-S1, M2, M42, NS2/NEP and NS3 proteins are encoded by spliced mRNAs, whereas the PB1-F2 results from a second open reading frame (ORF). PB1-N40, PA-X, PA-N155 and PA-N182 are also encoded via alternative ORFs. Additionally, each influenza segment entails noncoding regions of varying lengths at both the 3′- and 5′- ends. These untranslated regions of all segments are highly conserved among all IAV genome segments and regulate transcription and replication as they include promoter sequences[129]. The HA, NP and NA gene segments encode for the corresponding protein. PB2-S1, M2, M42, NS2/NEP and NS3 proteins are encoded by spliced mRNAs, whereas the PB1-F2 results from a second open reading frame (ORF). PB1-N40, PA-X, PA-N155 and PA-N182 are also encoded via alternative ORFs[119,127,130–136].

1.5 Viral Replication Cycle

The IAV properties and thus their ability to transmit airborne, is dependent on the membrane properties of the host cell, it is of pivotal interest to understand the viral replication cycle.

Viruses do not have their own metabolism and therefor require a host cell for replication. Viral replication consists of several steps including virus attachment (1), virus entry (2), synthesis of viral RNA (3), synthesis of viral proteins (4), packaging of RNA (5), assembly of virus (6), virus budding and release (7) (Figure 15).

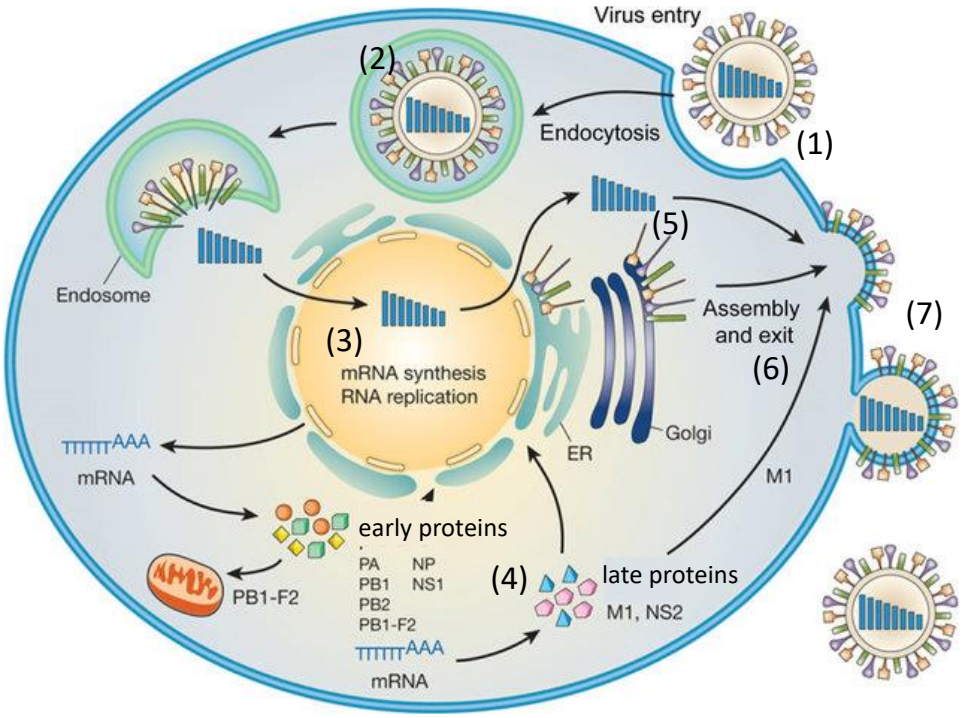

Figure 15: Viral Replication Cycle of Influenza A Virus. After receptor-mediated endocytosis, the viral ribonucleoprotein (vRNP) complexes are released into the cytoplasm and subsequently transported to the nucleus where replication and transcription take place. Messenger RNAs are exported to the cytoplasm for translation. Early viral proteins, that is, those required for replication and transcription, are transported back to the nucleus. Late in the infection cycle, the M1 and NS2 proteins facilitate the nuclear export of newly synthesized vRNPs. PB1-F2 associates with mitochondria. The assembly and budding of progeny virions occurs at the plasma membrane (modified from Neumann *et. al*[137])

In order to initiate infection and replication, IAV binds to the sialic acids (SA) expressed on the host´s cells surface, effected by the viral surface protein HA[138,139]. SA are found ubiquitously on many cell types and is the determinant of host cell tropism of influenza[140]. The SA appear in two configurations which are preferentially recognized by influenza viruses: α-2,3- or α-2,6-linked SA. In the human upper respiratory tract, α-2,6-linked SA are predominant, while α-2,3-linked SA are more common in human lower respiratory tract and in the avian gastrointestinal tract[140]. In general, human adapted IAV strains prefer α-2,6-linked SA, whereas avian influenza prefer α-2,3-linked SA[140]. Thus, seasonal IAV replicates mainly in the upper respiratory tract.

Once the IAV HA protein attaches to SA on the host cell, the virus is internalized via receptor-mediated endocytosis and is uncoated in the endosome. For this, a low pH of the endosomal compartment is crucial, i) the acidic environment triggers a conformational change in the HA and induces fusion of the viral envelope with the endosomal membrane; ii) protons enter the virus particle by passing the M2 proton channel and disrupt internal protein-protein interactions, releasing the viral RNPs from the viral matrix. As a result viral RNPs are discharged into the host cell cytoplasm[141,142]. After the release of RNPs into the cytosol, they are transported to the nucleus via nuclear localization signals (NLSs) encoded by the viral RNPs. Transcription and replication of the influenza virus genome takes place in the nucleus. Translocation from cytosol to nucleus is active and cytoplasmic vRNPs use the importin-α - importin-β nuclear import pathway to gain entry to the host cell nucleoplasm. On site, the viral messenger RNA (mRNA) is translated by the host cell machinery into viral proteins, including the viral RNA dependent RNA polymerase (vRNP). The vRNP uses the negative-sense vRNA as a template to synthesize two positive-sense RNAs i.) viral mRNA for viral protein synthesis; ii.) complementary RNA (cRNA), that is then transcribed by the vRNP into more copies of negative-sense, genomic vRNA. Viral mRNA can be exported out of the nucleus and translated like host mRNA, after it is polyadenylated and capped. Freshly produced viral proteins M1 and NEP/NS2 mediate the nuclear export of vRNA segments[143]. M1 interacts with both, vRNA and NP, and is thought to conjoin these two components within the RNP complex. M1 is additionally associated with the nuclear export protein NEP, which mediates the M1-vRNP export via nucleoporins into the cytoplasm[141,142].

The envelope proteins HA, NA and M2 are translated from viral mRNA in ribosomes on the rough endoplasmic reticulum. They are folded in the endoplasmic reticulum and are trafficked to the Golgi apparatus for post-translational modifications. The three proteins

show apical sorting signals that direct them to the cell membrane for virion assembly. Although little is known regarding the translation and sorting of the non-envelope proteins, M1 is thought to play a role in bringing the vRNP-NEP complex into contact with the envelope-bound HA, NA, and M2 proteins for packaging at the host cell membrane[144]. For a fully infectious influenza virus particle, one particle must contain all eight vRNA segments. Packaging appears to be a selective process, by which discrete packaging signals on all vRNA segments assure that a complete genome is incorporated into virus particles[144].

Initiated by the accumulation of M1 protein at the cytosolic face of the lipid bilayer, the influenza virus budding process takes place at the cell membrane. Following the budding process, the HA molecules continue to tether the virions via sialic acid moieties on the cell surface. They are actively released by the sialidase activity of viral NA. If NA is inactive or absent, or if neuraminidase inhibitors are present, virus particles aggregate at the cell surface and as a result, the infectivity is reduced[144].

1.6 The Evolution of Influenza A Virus

The natural reservoir of IAV are wild waterfowl but infections in hosts outside the main reservoirs occur periodically and avian IAV was isolated from humans and other mammals (Figure 16). Avian influenza outbreaks were recorded in pigs[145], seals[146], whales[147], horses[148] and mink[149].

In birds, influenza viruses are transmitted via the fecal oral pathway. In feces high concentrations of virus can be found, as influenza preferentially replicate in the epithelial cells of the gastrointestinal tract. After deposition of infected fecal material in the water, waterfowl can efficiently transmit influenza viruses to other animals. The asymptomatic appearance of influenza infection in waterfowl is most likely the result of a successful viral adaptation to its host and allows the influenza viruses to circulate without selective pressure. While avian influenza viruses in humans and animals appear to be primarily poorly transmissible, the genetic pool of influenza viruses provides the genetic variability needed to allow the emergence of pandemic influenza viruses in humans and animals.

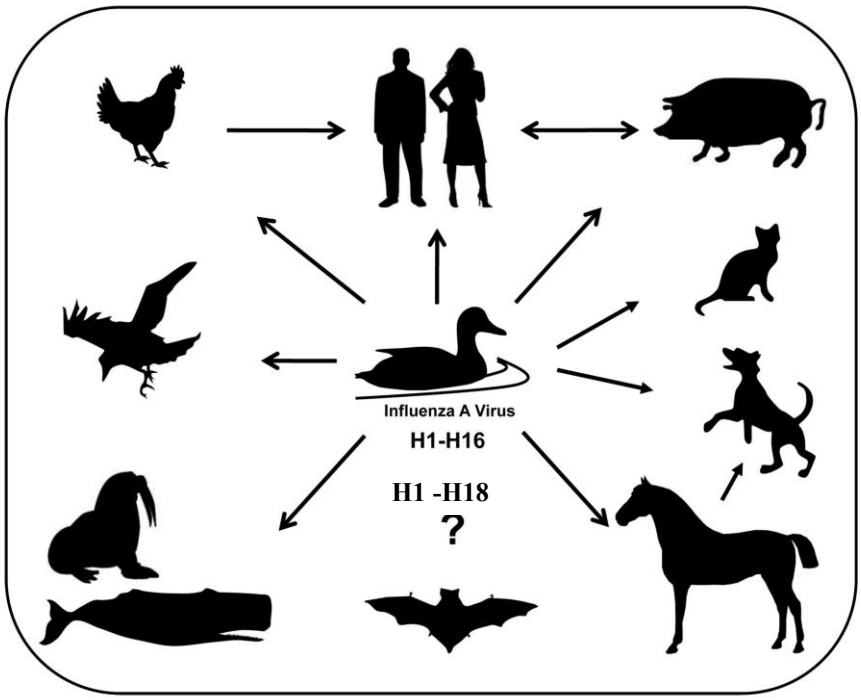

Figure 16: Host Range of Influenza Viruses. The natural reservoir of influenza A viruses are wild waterfowl. Usually, in order to enter the mammalian hosts, avian influenza A viruses are transmitted to domestic birds – such as chickens and ducks – or swine, which serve as a "mixing vessel" as they are susceptible to both avian and human influenza viruses. Both domestic birds and swine can spread influenza A viruses to humans which occasionally causes pandemics, depending on the population´s existing immunity and the virus characteristics. Up to date, no actively replicating viruses have been isolated from bats and it is unclear if bats can transmit influenza viruses to other species (modified from[150]).

Continuous viral evolution is mainly observed in the surface glycoproteins of influenza viruses but occurs in all eight gene segments[151]. The variability results from following known mechanisms: i.) antigenic drift including point mutation including substitution, deletion, insertion in the HA and NA protein; ii.) antigenic shift, driven by the genetic re-assortment of gene segments.

The antigenic drift is mainly facilitated by the RNA polymerase. The lack of a proof-reading function allows for fast adaption to a new host and environment. With an error rate of 10^{-4} bases per replication, each viral replication cycle leads to a mixed virus population also referred to as viral quasispecies[152,153]. Most of those are not viable but some have potentially advantageous mutations which can become dominant under a certain selective pressure. Airborne transmission is an evolutionary bottleneck, allowing the selection of highly transmissible virus species[152].

Genetic re-assortment is an important mechanism for influenza viruses to guarantee rapid diversity. Since the influenza virus genome is segmented, gene segments can be

exchanged arbitrarily if a cell is infected simultaneously by two or more influenza virus subtypes. Examples for successful re-assortments, that increased human adaptation are the emergence of the pandemic H2N2 virus (with new HA, NA and PB1 gene segments) and H3N2 virus (with new HA and PB1 gene segments) in 1957 and 1968[154,155]. Some mammals like domestic birds and pigs may function as intermediate hosts and 'mixing vessels' as they are easily infected with several influenza strains[156].

This high genetic diversity allows for the emergence of antigenically new virus subtypes which can, when introduced to an immunologically naïve population, cause an outbreak eventually leading to a pandemic.

1.7 Transmission and Persitance of Influenza A Virus

Transmission between humans and influenza virus may occur by three routes: i) direct or indirect contact between an infected and a susceptible person, usually resulting in contamination of a susceptible person's hands followed by hand to respiratory mucosa contact; ii) large droplet spray wherein droplets of respiratory fluid greater than approximately 100 nm in diameter are expelled with sufficient momentum to deliver a direct hit on the respiratory mucosa; and iii) aerosols generated by release of smaller, virus-containing droplets, as may occur during tidal breathing and coughing that rapidly evaporate into residual particles (droplet nuclei), which are inhaled and deposited in the respiratory tract. There is evidence for each of these routes[20,23,157–161] but their relative importance is not known.

Successful airborne transmission depends on the ability of the virus to endure environmental conditions. The persistence and infectivity of IAV in open air is promoted by low humidity[38]. Aerosols containing IAV may remain infective for up to 24 hours or more at humidity lower than 50 % RH but only for an hour at RH higher than 85 % RH[35,162]. Other limiting factors in open air are ambient temperature, UV-radiation, and wind[38,39,160]. Transmission of IAV is also increased at colder temperatures[38] (also see Chapter 3 1.4 Seasonality of Influenza incidence).

In experimental settings guinea pigs were used to generate IAV containing aerosols, aerosols sizes were mostly between 1.1 and 2.1 μm[159]. These findings were comparable to these with aerosols found in humans. Increasing evidence makes out breathing as an important mode of airborne transmission. Fabian *et al*. showed that 60 % of patients with influenza A and 14 % of patients with influenza B had detectable levels of viral RNA in their exhaled breath; they also reported that over 87 % of the exhaled particles were less

than 1 µm in diameter[23]. Milton *et al.* collected aerosol particles exhaled by influenza patients and found that patients shed about 33 viral copies/minute in aerosol particles > 5 µm and simultaneously 187 viral copies/minute in particles < 5 µm[20]. And thus, showed that aerosols (ø < 5 µm) contained 8.8 - fold more viral copies than did droplets (ø >5 µm). But also coughing may produces IAV-containing aerosols. Lindsley *et al.* collected coughed-up particles and found that 81 % patients within their cohort studied were positive for influenza RNA. In difference to breathing, coughing produced bigger IAV positive particles. As 35 % of particles were bigger than 4 µm and 23 % were sized between 1 to 4 µm and 42 % were smaller than 1 µm, 2 -fold more viral copies were found in aerosols (ø < 5 µm) [21].

2 Result

2.1 Hygroscopicity of IAV particles

Airborne IAV encounter different environmental factors including varying RH. The hygroscopicity of IAV was measured in a closed chamber with varying RH. The volume of one IAV particle was calculated from 3D reconstruction by AFM obtained topography measurements (Figure 17A). At 25 % RH one IAV particle had a measured volume of (20 ± 5) nm^3, which increased to (60 ± 18) nm^3 at 65 % RH and even further to (80 ± 6) nm^3 at 85 % RH, showing no hygroscopic saturation of IAV particles (Figure 17B).

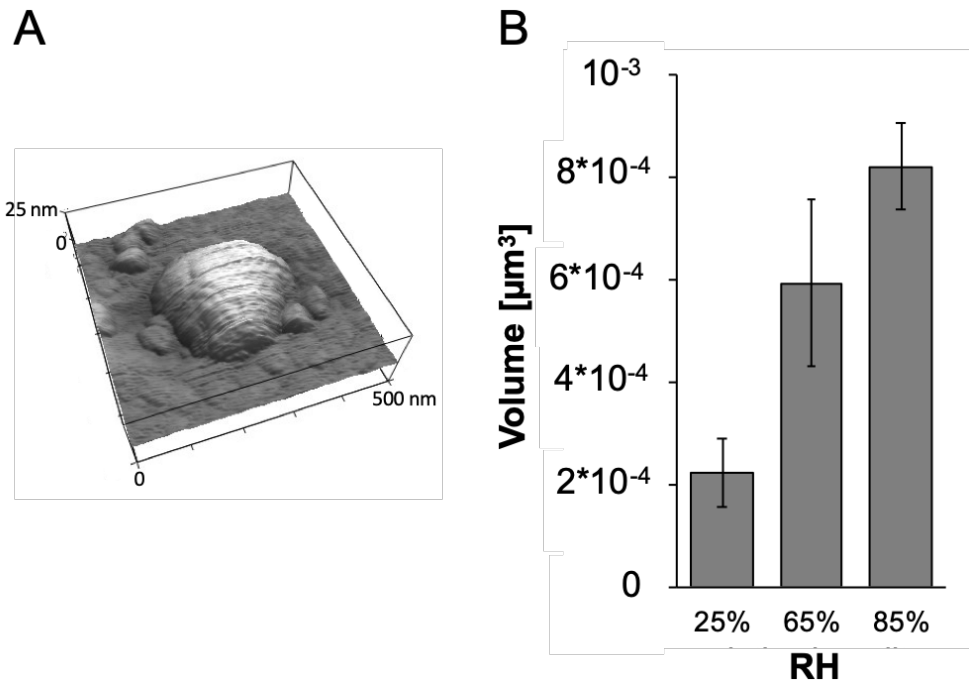

Figure 17: Hygroscopicity of IAV Particles. (A) Representative 3D reconstruction of an influenza particle using Igor Pro software to calculate the volume of a single virus particle **(B)** Measurment of hygroscopicity of single viral particles. Different RHs were adjusted by deliquence salts inside a closed fluid chamber (mean and standart deviation of three independent experiments are shown).

2.2 Nasopharyngeal Tissue Culture Model from Adult Stem Cells

IAV, dependent on the strain, can be grown in different host systems. The strain used in our study, A/Hamburg/2009/05, is usually grown in Madin Darby Canine Kidney (MDCK) cells, a dog kidney cell line. Virus particles isolated from MDCK cells, lack a prominent mucus corona when compared to virus particles isolated from Guinea pigs (Figure 18A). The lack of a mucus corona may reduce viral resistance to environmental influences. Thus, it was necessary to find a system that mimics generation of influenza particles similar to *in vivo* generated virus from naturally infected cells. A/Hamburg/2009/05 predominantly replicates in the upper respiratory tract. Thus, it was feasible to use adult stem cells from the nasopharynx to differentiate into primary epithelial cells. These primary cell cultures were established and performed together with Wilhelm Ching.

Adult stem cells can be found throughout the body, even after embryogenesis, they multiply by cell division to replenish dying and regenerate damaged cells. Wilhelm Ching established a method that allowed (a) the isolation of adult stem cells from patient material, as characterized by the stem cell marker p56 (red), (b) the expansion of these stem cells in culture and formation of colonies and (c) re-differentiation of tissue like structures on air liquid interface cultures (ALI) (Figure 19). *In vitro* re-differentiated tissue was comparable to the original tissue and expresses epithelial markers such as Krt5 and was multilayered with adult stem cells in the basal layer as depicted in Figure 18.

Like all biological systems, also the isolated adult stem cells and their corresponding re-differentiated tissue have different properties. In order to provide a ‘patient cohort’ collection of stem cells, they were isolated from 4 different patients. The patients vary in age and gender (Table 2).

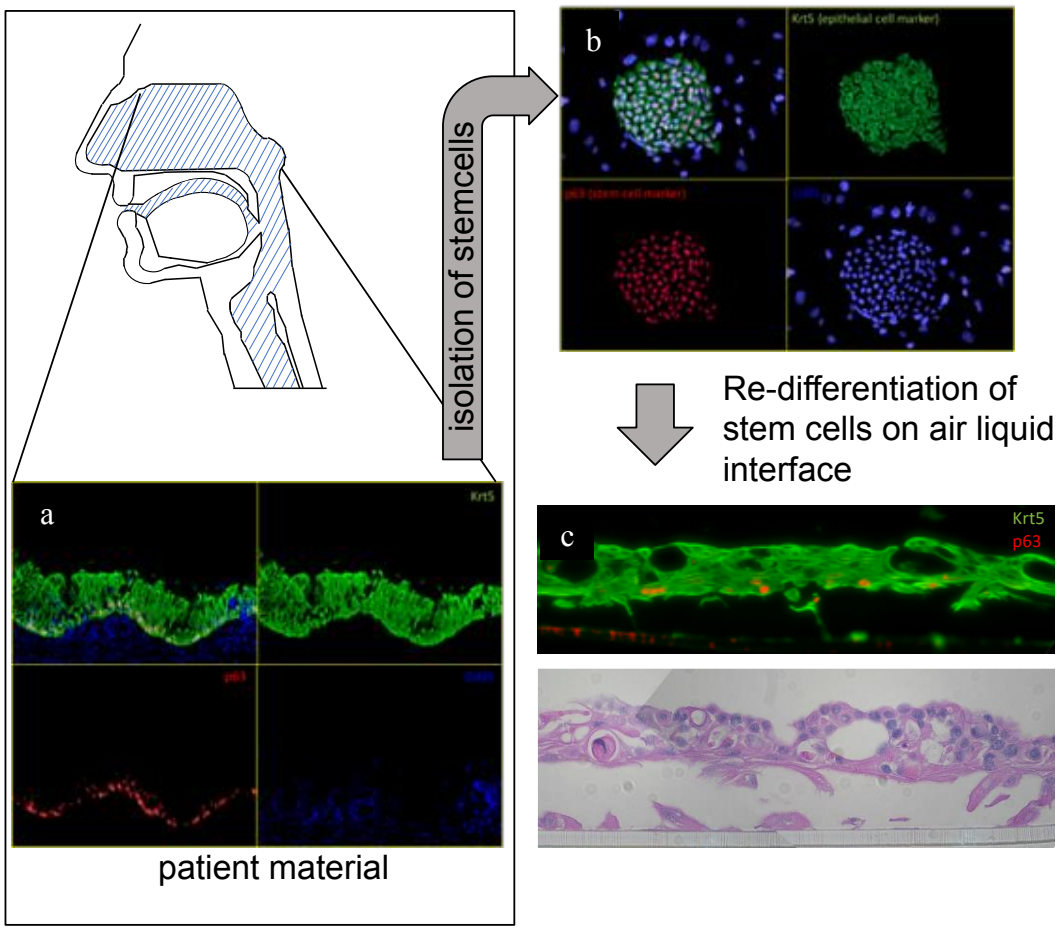

Figure 18: Workflow of Isolation and Redifferentiation of Nasopharyngeal Tissue Culture Model. Workflow of isolation and differentiation of nasopharyngeal adult stem cells. The nasopharynx is part of the upper respiratory tract. Pictures above are representative for all patients but come from patient 6. Pictures were taken from 3 independent experiments (a) Fluorescent analysis in paraffin slides of primary patient tissue (b) isolated adult stem cells (c) nasopharyngeal tissue culture model analyzed in paraffin slides both fuorescent and with H&E staining.

The differences and similarities between the re-differentiated uninfected cell models of 4 different patients (Table 2) can be seen in Figure 19. Analysis by Scanning Electron Microscopy (SEM), revealed that the cell surfaces showed distinct cell borders and different cell phenotypes. Some of them being ciliated while others are unciliated (Figure 19). Also, the length and width of cilia differed between the cell types. Distinct differential morphologies were also seen between cells from different patients. For example, cells from “patient 14” had extreme long cilia. Epithelial tissue cultures from patient 6 and 14 appeared far more elevated then patient 13 and 7. The cells from patient 7 appeared quite flat. But besides those differences, all nasal epithelial features were present from all patient’s tissue cultures. Interestingly, all samples, except those from patient 7, showed a net like structures between cilia. Since the probe was dehydrated upon preparation, the net is likely a residue of a mucus, similar to structures found in bacterial biofilms that contain mucus (Figure 19). Differences between patient samples can be explained by both individual differences between patients as well as different isolation areas in the respiratory tract, where samples were obtained from.

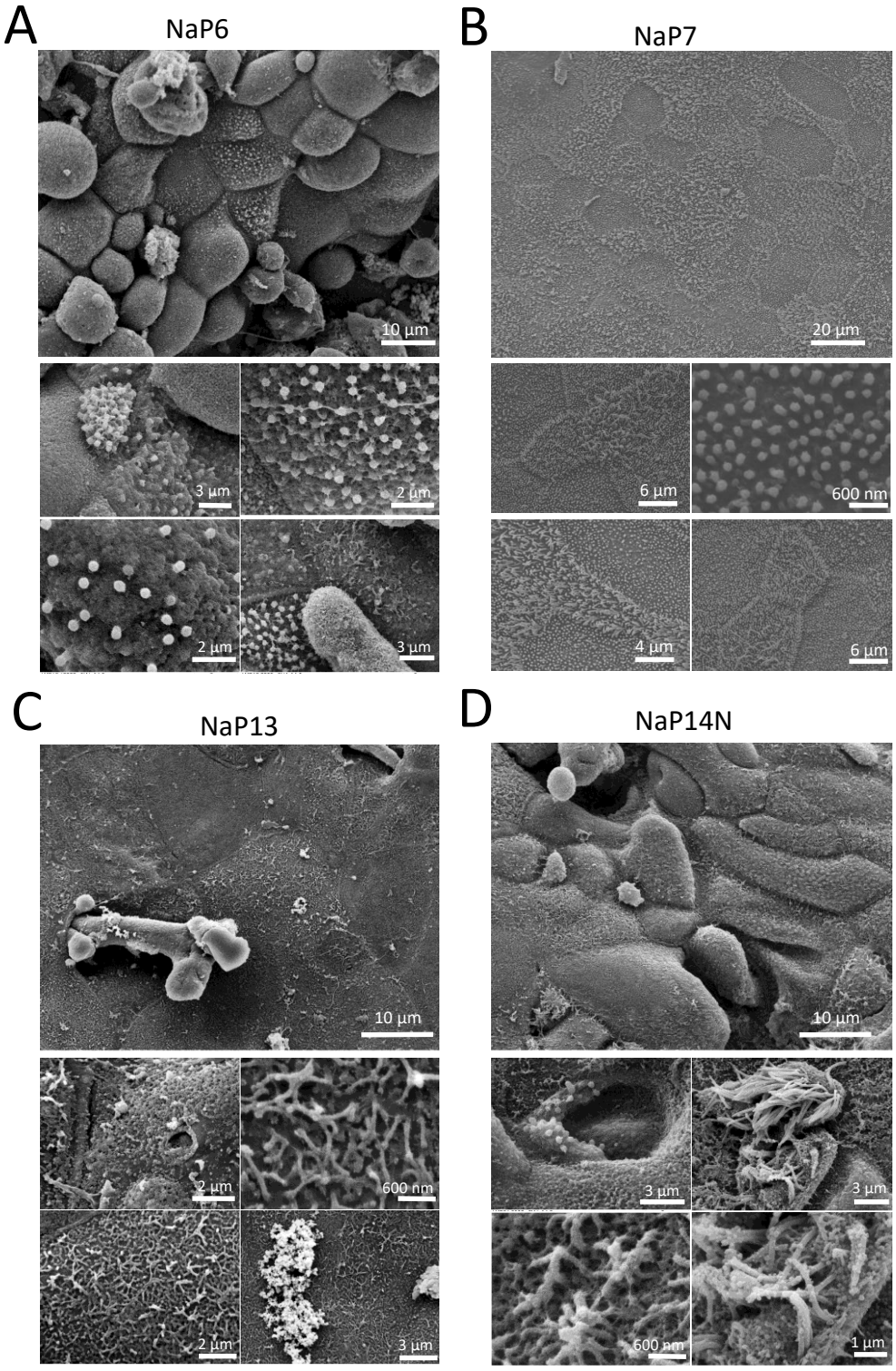

Figure 19: SEM Analysis Nasopharyngeal Tissue Culture Model. Representative selection of scanning electron microscopy analysis of nasopharyngeal tissue culture model from 4 different patients. For each patient 3 independent experiemts were performed. **(A)** Selection of SEM images of redifferentiated nasopharyngeal tissue culture model originating from patient NaP6 **(B)** Selection of SEM images of redifferentiated nasopharyngeal tissue culture model originating from patient NaP7 **(C)** Selection of SEM images of redifferentiated nasopharyngeal tissue culture model originating from patient NaP13 **(D)** Selection of SEM images of redifferentiated nasopharyngeal tissue culture model originating from patient NaP14N.

To compare different influenza strains in their ability to infect the established nasopharyngeal tissue culture model, *in vitro* cultures were infected by 3 different influenza strains. A/Hamburg/05/09 (HH05) and A/Netherland/213/03 (H3N2) are fully human adapted isolates but have different Hemagglutinins (HA). Additionally, we infected the system with an avian control (H5N1-HA_{mono}). For comparison, we also used a non-respiratory tract virus, a Zika virus (ZIKVFB GWUH-2016). First the reproduction of influenza viruses in the nasopharyngeal tissue culture model from patient 6, 13 and 14 was checked and results were merged. All samples were infected with the same titer of $1.8x10^5$ PFU. The re-differentiated tissue was most effectively infected by HH05 and even though we also observed replication of H5N1 and ZIKV, the H3N2 virus strain replicated significantly better in the *in vitro* regenerated tissue (Figure 20A, experiments performed by Carola Dreier). When staining for viral nuclear protein in HH05 infected cells, a good signal located in the nucleus of infected cells was detected, though not all cells were infected (Figure 19B).

SEM analysis showed no difference between infected and non-infected samples (Figure 20C). Differences could easily be missed though, as not all cells were evenly infected. Viral particles buded from the tip from the cilia of infected cells and revealed a mucus corona (Figure 20D), similar to what we observed in virus particles derived from guinea pig nasal washes (compare to Figure 21D).

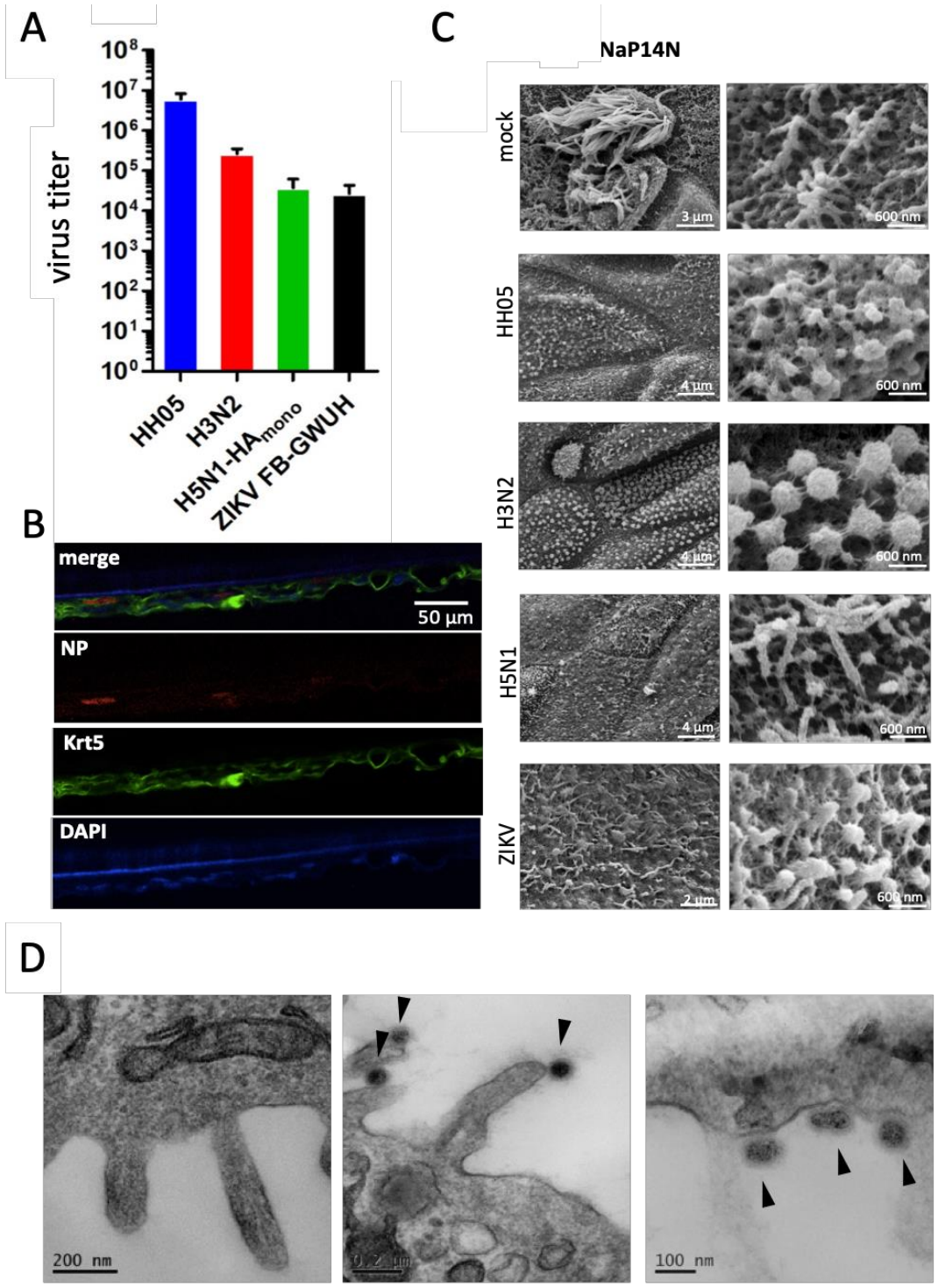

Figure 20: A New Nasopharyngeal Tissue Culture Model for Viral Infections. (A) Measurment of virus titer by plaque forming unit assay (mean of virustiter observed in 3 different patients, experiement was perfomed ones) **(B)** Histology of cell staining for NP proteins (IAV marker), Krt5 (epithelial marker) and DAPI (cell nuclears). Representative pictures of histology analysis in 3 different patients, experiment was perfomed ones. **(C)** Representatives of scanning electrone microscopy analysis in patient NaP14N. Analysis was also performed in patient 6 and 13, but carried out only ones. **(D)** Representatives of transmission electron microscopy analysis of all 3 patients. Images were obtained from patient NaP14N. (left) mock infected sampe (middle and right) HH05 infected nasopharyngeal tissue culture model. IAV particles bud from both the ciliae (middle) and the basal epithelium (right).

2.3 IAV Particle-Containing Aerosols

Different factors, like aerodynamic size and ability to survive environmental condition, determine the success of airborne transmission. The ACI allows simultaneous assessment of aerodynamic size, by testing for viral RNA as well as airborne pathogen viability measured by PFU. Additionally, the composition and morphology of airborne particles can be observed. Dependent on their velocity, particles with smaller aerodynamic diameters settle at lower and bigger ones at higher levels. During the sampling time of 10 min, aerosols were continuously generated by the ultrawave nebulizer. Analysis of IAV containing aerosols by PFU revealed that no viable virus particles could be found in the ambient air samples (Figure 21A). To ensure, that IAV particles were collected in the ACI and were not missed because of their size, we demonstrated the presence of IAV particles by detecting the presence of viral RNA through amplification of the nuclear protein (NP) sequence by polymerase chain reaction (PCR) (Figure 21B). The expected size for the NP fragment is at 1565 base pairs, as seen here. Most copies of virus RNA were found on level 7 and 8 correlating to an aerodynamic diameter of 0.22 to 1 µm. Using negative stain transmission electron microscopy (TEM) analysis, different compositions of airborne IAV particles were observed (Figure 21C). Such as spherical (Figure 21Ca), filamentous (Figure 21Cc) and intermediate phenotypes (Figure 21Cb).
Comparing virus particles from different infected tissues, clear differences concerning the mucus corona were observed. While virus particles isolated from nasal washes from infected guinea pigs showed a prominent mucus corona were coated with a prominent thickness of 30 nm, virus particles isolated from MDCK cells did not show a corona or if at all that is at most 20 nm thick. In virus particles isolated from nasopharyngeal tissue culture model, a corona of 25 nm was observed (Figure 21D). As only a limited number of particles were analyzed, statistically analysis was not possible.
Aerosols containing IAV particles, obtained in the following presented nasopharyngeal tissue culture model showed a corona of mucus around the virus particles. It was still not possible to detect viable airborne IAV particles, but interestingly when testing for viral RNA by PCR, we could also detect viral RNA on level 6, indicating that the corona enhanced the aerosol size from 1.0 µm to 1.7 µm (Figure 21E).

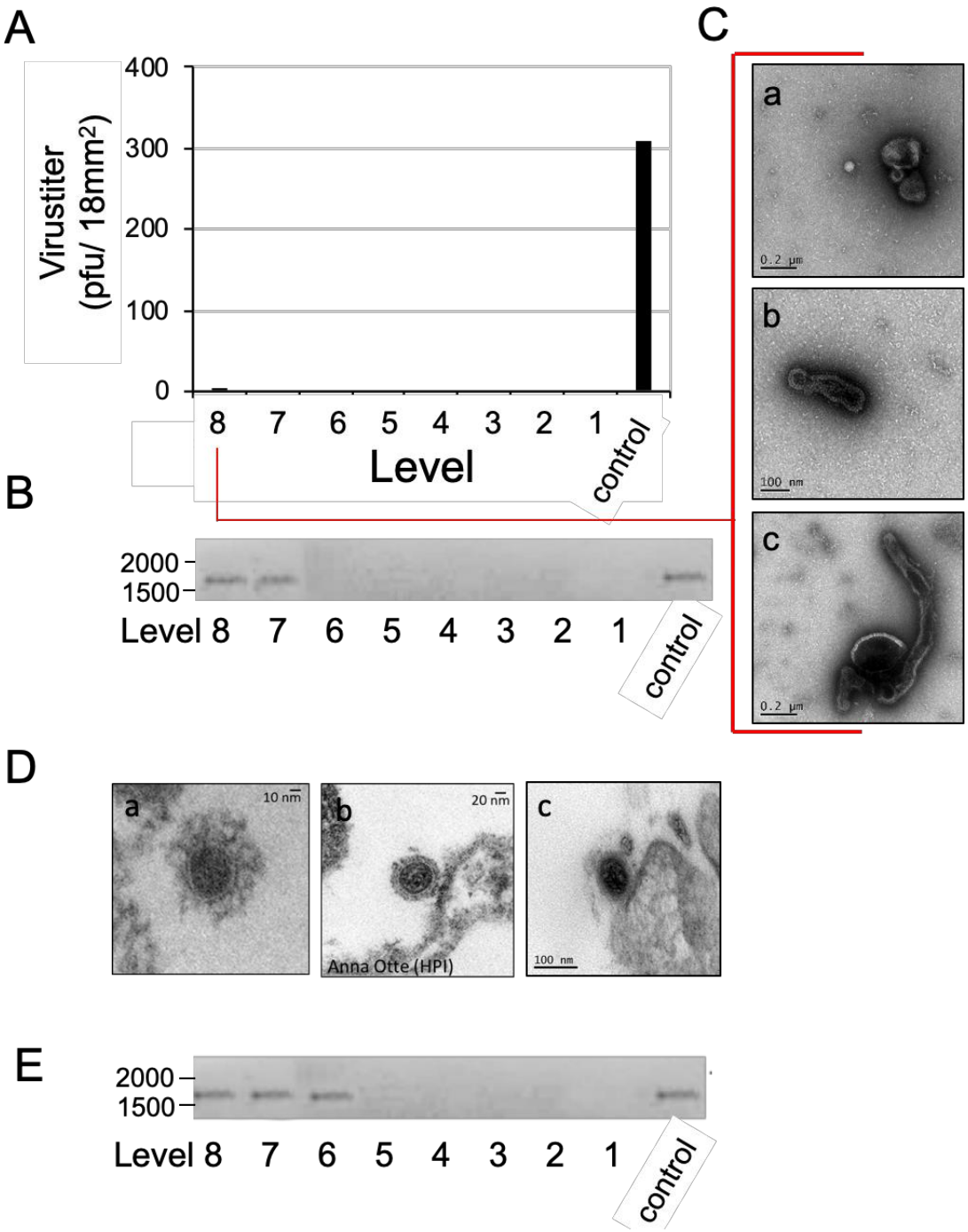

Figure 21: Airborne IAV Particles Originating from Different Cell Cultures. (A) Measurement of viable IAV particles within the ambient air of the Aerosol Collecting Device (ACD) after particle production by ultrawave nebulizer and collecting for 10 min on glass plates inside the ACI and measurement of plaque forming units. **(B)** Detection of IAV RNA by PCR after collection of airborne particles on glass plates inside the ACI **(C)** Analysis of particle formation of airborne IAV particles by negative stains by transmission electron microscopy. **(D)** Comparison of IAV particles isolated from different cells with TEM a) Isolate from nasal washes from with an IAV H5N3 infected guinea pig b) IAV particle of A/Hamburg/15/09 infected MDCK cell culture c) virus particle isolated from A/Hamburg/05/09 (H1N1) *in vitro* infected nasopharyngeal tissue culture model **(E)** Detection of IAV RNA, coming from nasopharyngeal tissue culture model by PCR after collection of airborne particles on glass plates inside the ACI.

3 Discussion

The mode of airborne transmission is a well-established concept for IAV spread. But limited information is available on the composition and physicochemical properties of airborne IAV particles. This study introduced a good performing nasopharyngeal tissue culture model that can be infected by influenza A virus, and even models the tissue tropism of different IAV strains. This model has been validated successfully as cell culture system mimicking natural viral infection. Seasonal human IAV is usually grown in MDCK cells, but lacks important characteristics in comparison to nasopharyngeal tissue derived virus which cannot be dismissed, especially in the context of viral aerosol formation. IAV particles from nasopharyngeal tissue culture model were comparable to naturally occurring IAV particles, as seen in nasal washes from infected guinea pigs. The increased mucus corona around IAV particles increased the aerodynamic diameter.

3.1 Airborne Transmission of Influenza

Two main modes of transmission, which are not mutually exclusive, have been shown to promote the spread of influenza between humans: contact and airborne transmission. Airborne transmission can occur via two modes. Respiratory droplets, larger than 5 µm, do not remain suspended in air and deposit at distance of less than 1 meter[163]. Aerosols, smaller than 5 µm have a slow settling velocity and can remain suspended in the air for more than 3 hours[164]. Settling deposition of IAV particles is highly dependent on the ambient RH[164]. The importance of airborne transmission in the overall transmission of influenza is still discussed, though in resent publications it was shown that the highest viral RNA copies can be found in smallest particles[20]. While breathing produces not high enough sheer forces to overcome the viscosity of mucus, the contagious aerosols may mainly consist of the viral particle itself. Thus, the aerodynamic diameter of IAV particle-containing aerosols is defined by the natural occurring mucus corona, emphasizing the importance of natural epithelial cell source as origin tissue for airborne transmission. As IAV particles are highly hygroscopic, this study indicated the relevance of ambient RH for IAV, which is further analyzed in *Chapter 3*.

Comparable to mycobacteria-containing aerosols, also IAV-containing aerosols can be transmitted long and short distances, as the presence or absence of the water coat will define the airborne properties of IAV-containing aerosols.

3.1.1 Formation of IAV Particle-Containing Aerosols

The influenza strain A/Hamburg/05/09, a H1N1 subtype, causes a spectrum of diseases ranging from milder upper respiratory tract infections to severe lower respiratory tract infections. Already upon breathing, a high yield of influenza RNA was detected, emphasizing the importance of upper respiratory tract infections in the context of airborne transmission[20,23,165]. Using a nasopharyngeal tissue culture model, the H1N1 strain showed strong virulence and viral replication (Figure 20A). The effect of the origin of IAV particles on the aerosols has not been shown before, but defines the aerodynamic diameter of airborne IAV particles (compare Figure 21B to 21D). It is plausible to suggest that the mucus corona, composed of epithelia derived glycoproteins, can lead to increased hygroscopicity and therefore increased aerodynamic diameter. This enlarged water layer may on the one hand protect the IAV particles against environmental influences like dehydration and UV light exposure, but on the other hand leading to a higher velocity of the particle as it gets heavier.

Even though it is well established that IAV can travel through ambient air[38,166], there is little evidence in the literature, that IAV particles remain viable when travelling over longer distances. This is mainly caused by the lack of good measurement equipment so far that only allows the detection of viral RNA but not viability of the viruses[167].

3.1.2 Short Distance Transmission

Over short distance transmission the aerodynamic diameter, defined by the aerosol composition and the ability of the particle to retain water, determines the success of IAV-containing particles to spread. For influenza it was shown, that depending on the tissue of origin the aerodynamic diameter shifted from 0.22 – 1 µm in MDCK grown IAV particles (Figure 21B), to 0.22 – 1.7 µm of IAV grown in nasopharyngeal tissue culture model (Figure 21D). The aerodynamic diameter of IAV was described before in the literature with a diameter up to 2.1 µm[159]. This difference in size can be explained by the difference in mucus corona around the particle. There is a correlation between the thickness of the mucus corona and the aerodynamic diameter. The mucus corona and the aerodynamic diameter of IAV particles grown in the nasopharyngeal tissue culture model were still smaller than particles found in guinea pig nasal washes.

Airborne MDCK based IAV particles display a wide variety in aerodynamic diameter sizes ranging from 0.22 to 1 µm (Figure 21B). When analyzing the composition of airborne IAV particles, it becomes clear that this is based on the differences in the IAV

morphologies. Different viral morphologies, from spherical to filamentous, have been described in the literature, but their contribution to airborne transmission is not known. As most IAV particles seem to travel as singlets (Figure 21C), the different IAV morphologies may determine the aerodynamic diameter.

Besides the aerodynamic diameter also the ability to stay viable while airborne will determine the success of airborne transmission. We were not able to detect any viable airborne IAV particles upon aerosolization, but this was probably caused by the rather harsh nebulizer and sampling method. For future studies improved sampling methods could allow detection of viable IAV virus and determination of IAV tenacity.

3.1.3 Long Distance Transmission

After release from the human respiratory tract, IAV is in theory able to be transported over long distance. During that transport, IAV will encounter different ambient RH, temperatures and UV light stressors. In solution and on surfaces IAV is able to resist many different physical factors. UV light was not able to inactivate IAV even after 60 min exposure[31]. The temperature on the other hand has a strong influence on the viability, changing survival from less than 30 min at 56 °C to 24 hours at 28 °C and more than 100 days at 4 °C[31]. Interestingly, airborne transmission between guinea pigs revealed that cold and dry conditions were most favorable for airborne transmission[38]. With increasing ambient RH, the transmission rate of IAV was quickly reduced. Besides the previously described hygroscopic mucus corona, also the IAV particle itself is highly hygroscopic. The volume of one IAV particle increased 4-fold from 25 % to 85 % RH (Figure 17B). This could explain why the ambient RH is one of the key drivers of influenza transmission. This aspect of IAV transmission will be further investigated in *Chapter 3*.

Not taking environmental factors into account, the mass density will mainly decide the ability of the IAV-containing aerosol to stay airborne. The mass density of one IAV particle is at 1.19 kg/l[168], which would allow a long distance transport. In the literature there is no report for long distance transport (> 1 meter) of viable IAV particle, which is corroborated with our failure to detect viable IAV after nebulization. Therefore, IAV is not very likely transported over longer distances.

3.2 Evaluation of Nasopharyngeal Tissue Culture Model

The nasopharynx is, by definition, the upper part of the throat behind the nose. It is a part of the pharynx, which comprises three separate segments: the nasopharynx, oropharynx, and the hypopharynx. Beside the mechanical barrier, a high concentration of lymphatic

tissue in the pharynx emphasizes the importance of the pharynx as defense barrier against pathogens. The nasopharynx is lined by an epithelium, that contains ciliated columnar cells, goblet cells and basal cells. The nasopharyngeal tissue culture model displayed a strong similarity to the original tissue and was also ciliated and multilayered (Figure 18). The differences observed between various patient samples can be explained by individual characteristics of cells from patients, differing in age and gender (Table 2). Additionally, the area the stem cells were isolated from can differ between patients, as the removal of the tissues was medically indicated and not standardized (Figure 19). IAV does infect the upper respiratory tract including the nasopharynx. As this part is critical in the production of IAV-containing aerosols, the nasopharynx is of interest for this study.

3.2.1 IAV Infection of Nasopharyngeal Tissue Culture Model

The nasopharyngeal tissue culture model was successfully infected by IAV subtypes (Figure 20A). Interestingly, HH05 displayed the highest virus yield, even though in human's avian strains can induce a higher mortality than human IAV subtypes.

Influenza is a zoonotic pathogen, with a broad host range and the reservoir in water fowl (Figure 16). Wolfe *et al.* (2007) described five intergrading stages through which a pathogen that exclusively infected animals (Stage 1) may become transformed into a pathogen exclusively infects humans (Stage 5)[169]. It was described before, that different influenza strains, predominantly infect different areas of the respiratory tract and have a distinct tropism[170]. This is based on differential binding of IAV hemagglutinins (HA) to certain sialic acids[170]. While HA type 1, exclusively found on human influenza, prefers the α-2,6 sialic acid link, the avian HA type 3 and 5, prefer the α-2,3 sialic acid link[170]. Differently linked sialic acids are differently expressed in the human respiratory tract. While α-2,6 linked sialic acid is mainly expressed in the upper respiratory tract, the α-2,3 sialic acid link is absent in the upper respiratory tract, but highly expressed in the lower respiratory tract[171]. This explains the high morbidity and mortality of humans of avian influenza infections but reduced transmissibility, in contrast to high transmissibility of fully human adapted strains.

This notion is corroborated by our nasopharyngeal tissue culture model study, showing that H1N1 and H3N2 subtypes more efficiently infected the tissue model than the H5N1-HA_{mono} subtype (Figure 20A).

3.3 Conclusion

This study provides insights on the biophysical properties of airborne influenza transmission. Even though those properties indicate a possible long-distance transmission, the viability of airborne IAV particles is drastically reduced. Mimicking the upper respiratory tract with the *in vitro* nasopharyngeal tissue culture model, revealed the importance of host cells for viral generation. The absence or presence of mucus corona directly influenced aerodynamic diameter of airborne IAV.

3.4 Critic and Outlook

Unfortunately, it was not possible to determine the viability of IAV-containing aerosols. One study showed the massive effect of aerosolization and sampling of IAV on the ability of IAV to maintain the viability[167]. A more sensitive sampling method needs to be developed, as all studies about IAV airborne transmission lack the viability test and instead focus on the sampling of viral RNA which is not a pivotal proof of viability and infectivity.

CHAPTER 3: Weather Shapes the Influenza A Seasonality

1 Introduction

Influenza virus circulate in annual epidemics and recurrent, yet irregular, pandemics. Seasonality of influenza occurrence peaks during winter in temperate regions while in tropical regions influenza occurs throughout the year[172–174]. Theories that try to explain this seasonality include seasonal modifications in melatonin and vitamin D levels, both influencing the host susceptibility; behavioral changes such as indoor crowding, limited ventilation due to closed windows or lack of windows and environmental factors such as low temperature, low humidity and UV irradiation[173]. More recent analysis could demonstrate that ambient humidity strongly modulates the airborne survival and transmission of influenza viruses[164,175]. The onset of intensity of IAV season in winter influenza-related mortality was found to be associated with low absolute humidity levels throughout the USA[36,37].

1.1 Biological Causes for Seasonality

During the winter months, the changed light/dark cycle hours may impact the immune system, leaving the host more susceptible for infections. Two possible intermediaries between photoperiod and immunity are melatonin and vitamin D (25-hydroxy-vitamin D)[173,176]. Melatonin appears to work partly by regulating the host immune response via interleukin-1β (IL-1β) levels, which rises when melatonin is present and can exhibit a protective effect in some viral infections[176]. Vitamin D levels have a strong effect on immunity by promoting CD^{4+} T cells and mucosal antibody responses[173]. In both cases, there is a direct link between availability of sun light and the host immune system status. Thus, one theory is that seasonality is not caused by sweeping waves of influenza traveling the globe, but rather that there is a constant level of pathogens present all year around but with altered susceptible populations[177].

Besides seasonal changes in the host's immunity, also the influenza strains change antigenetically and therefore can evade existing herd immunity. This ability of IAV is caused by the high rate of mutations in the HA and NA antigenic epitopes of IAV (estimated 6.7×10^{-3} nucleotide substitutions per site per year for HA) and the resulting occurrence of quasi-species[152,153]. This limits the ability of preexisting antibodies to bind to the mutant and thus allowing the transmission within the population. Models

incorporating this limited cross-protection driven by viral adaptation and immune responses have been shown to generate cyclical patterns closely resembling the seasonal patterns observed with influenza virus infection[178].

1.2 Social Causes for Seasonality

One common explanation for seasonality in infectious diseases is seasonal crowding of susceptible persons. Seasonal fluctuations in host behavior might give influenza a greater opportunity to spread and maintain itself at epidemic levels during the winter. Interestingly, there has been no study to really link crowding to seasonality and Dowell *et al.* addressed critically the plausibility of this theory, and argued that crowding might not be the driving cause of seasonal incidence but rather an amplifying factor, as there are no frequent epidemics at international summer conventions[173,177].

Besides crowding, also indoor heating can increase transmission of influenza. Indoor heating results in a continuously recirculated body of air with a very low humidity. On the one hand, the dry air harms barrier function of the respiratory epithelium leaving the host more susceptible to infectious diseases. On the other hand, as most heating equipment is unable to filter virus particles, the recirculated air leads to a high persistence of viral particles in breathed in air[173].

It is still discussed whether the population density can explain the observed synchronized seasonal pattern in the northern hemisphere. Iceland, with a fairly isolated population in the North Atlantic, exhibited an irregular cycle including late-spring and summer peaks in the early 20 century but only after population density increased, showed a strong winter-season with annual periodicity[179]. Bjørnstad *et al.* (2018) correlated urbanization with the intensity of influenza season and found that urban centers were in contrast to what was expected less affected by season intensity. They conclude that there is a higher basic herd immunity in urban centers as there are more off seasonal cases and thus, the spread epidemic intensity is diminished compared to more rural areas[36].

1.3 Environmental Causes for Seasonality

Transmission rate of IAV was found to increase at lower ambient humidity and lower temperatures[38,180]. Virus stability varies in dependency of the ambient RH. IAV was consistently found to be stable at low RH, relatively unstable at intermediate RH and again stable at high RH[38,181]. This can be explained by the salt content of the mucus in the IAV containing aerosols. While at a high RH the salt of the mucus is maintained at a physiological concentration, at intermediate RH (50 – 70 %) the containing salt interferes

with the virus stability[182]. At lower RH the salt starts to crystalize out of the solution leaving the solution yielding a low salt concentration[182]. Shaman and Kohn (2009) found that absolute humidity (AH), a measure for ambient humidity independent of the temperature, correlated with both the IAV survival and transmission properties[175]. They proposed two hypotheses to explain the relationship between humidity and transmission: i) due to the lower AH, more water evaporates from the expelled droplet, increasing the probability of the droplet to stay airborne as the velocity of the particle decreases, as the aerodynamic diameter differs[164]. Additionally, the ability to penetrate different areas of the respiratory tract differs at different AH[164]. ii) IAV survival increases at a lower AH, thereby increasing the tenacity of airborne IAV particles[175]. They also analyzed the correlation between lower temperatures (0 – 10 °C) and increased transmission and concluded that a cooler temperature may increase the stability of IAV during the airborne period[35,38].

1.4 Transport of IAV Particles through the Atmosphere

The transport of influenza particles through the atmosphere is determined by different factors: i) emission and biophysical characteristics of the virus particle that defines the ability of the particle to stay airborne; ii) influences of environmental factors, such as atmospheric turbulences, wind, temperatures and ambient humidity, that determine the transport and deposition of the particle[183].

Biophysical characteristics of IAV particles, such as aerodynamic diameter, mass density and surface area do, in theory, allow for long-distance transmission of influenza (for details see Chapter 2). In the lower atmosphere airborne microorganisms need to cope with different harmful conditions including meteorological ones like varying temperature, RH, and wind velocities[183]. Additionally, deprivation of nutrients, presence of oxidants and solar radiation can stress the organism. Some microorganisms have developed mechanisms that cope with those stressors, including pigmentation, sporulation and attachment to other particles. Viruses do neither have a metabolism and thus are not able to respond actively to stressors nor do they require nutrients. As for that, they must rely on passive mechanisms. For influenza these mechanisms are not known. Probably the mucus corona around the virus formed upon aerosolization can provide a protective shield against environmental hazards.

Particle dispersal in the atmosphere occurs at a range of length scales from millimeters to thousands of kilometers[183]. IAV emitted at the surface by the infected hosts respiratory

tract epithelium are released into the surface boundary layer (SBL) of the atmosphere[183]. The SBL forms the lowest part of the planetary boundary layer (PBL)[183]. The SBL increase during the day, under the influence of surface heating and collapses during the night. The typical depth of the SBL layer is between 50 to 100 meters. The PBL has a typical height of this layer is from 500 m to 2 km and is well mixed because of convection[183]. The PBL is usually capped by an inversion layer that limits further ascent of airborne particles[183].

To determine the emission and dispersion of a specific bioaerosol, it is necessary to consider wind, temperature, and relative humidity in the planetary boundary layer as they can display rapid fluctuation and change the particle transport dramatically[183]. Those parameters control whether the emitted particle stays at a particular height above ground, is mixed horizontally or vertically within the layer[183]. In general, three different scenarios for potential airborne infection are possible: i) bioaerosols released from the source are vertical mixed and transported to a higher level of the planetary boundary layer. They may even disperse through the inversion layer into free troposphere. Once in the free atmosphere, particles are no longer submitted to the intense mixing of the PBL and have the potential to travel for very long distances but cannot be breathed in by potential host; ii) frequent vertical turbulences will disperse the released aerosol quite quickly inside the SBL. The risk of infection is given, if the airborne pathogen is highly virulent and only a small dose is needed; iii) In the transfer between scenario one and two, the air movement oscillates and can transport released aerosols in a rather condensed manner. Infectious particles are trapped in this layer and dependent on the distance to the source the risk of inhaling a high dose of pathogens is given (Figure 22).

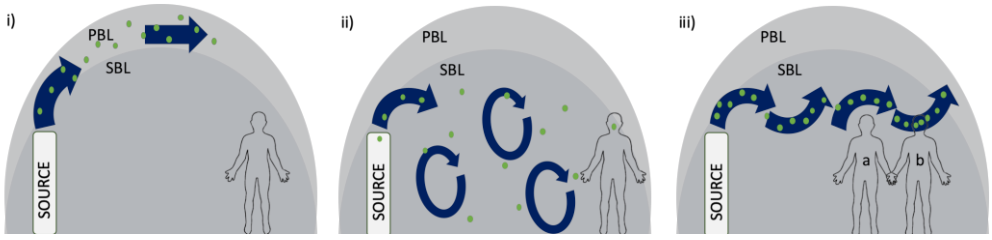

Figure 22: Pathogen Transmission Outdoors. After the infectious particle is released from the source, it can be transported through the atmosphere. Three different scenarios have been discribed (i-iii). The blue arrows represent the air movement (laminar to turbulent), while the green dots represent the pathogen containing aerosols i) in a stratified atmosphere, the particle will be transported upwarts and hold no infection risk. ii) through frequent vertical turbulences, the air movement will disperse the infectious particles. iii) in the transfer between scenario i) and ii) air can move in a oscillating manner, trapping the infectious particles inside a layer. Depending on the location of the susceptible host, the person will either breath in “clean” air (a) or air with a high amount of infectious particles (b).

Thus, successful transmission of IAV requires the presence of infectious particles in the SBL so that particles can be inhaled. Different mechanisms for particle deposition are described[183]. But the settling of IAV particle in the human respiratory tract is mainly driven by dry deposition. Dry deposition of particles involves three major processes acting in parallel: gravitational settling, inertial impaction on individual elements and Brownian diffusion through the boundary layer of the atmosphere[183]. For sub-micrometer particles (<10 µm), the dominant force is Brownian diffusion[183].

1.5 Influence of Weather on Influenza Transmission

While the influence of ambient temperature and humidity on the airborne transmission of IAV have been studied previously the spatial distribution of influenza in dependence of low humidity (< 65 %) and cold temperature (-5 – 5 °C) has not been assessed so fare. In this study we analyzed the influence of weather, including temperature, ambient humidity and wind, on influenza season in Germany. Understanding the spatial distribution of IAV in dependence of weather would provide vital information to improve public health measures, as prediction of arriving influenza season would allow a timely response. In this study we focused on Germany in particular on Cologne, Berlin, Hamburg and Munich and their surrounding counties. First, we analyzed the effects of temperature and humidity, on IAV season progression and intensity. Secondly, we involve the particle transport of airborne IAV in dependence of wind direction, to explain spatial distribution of IAV incidence (Figure 23).

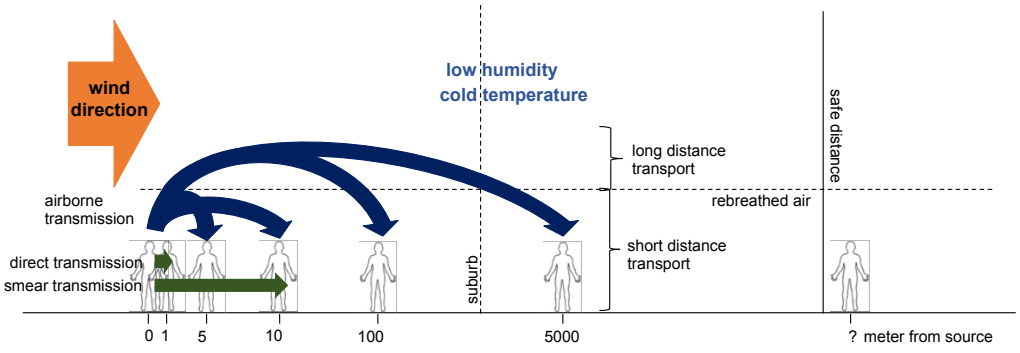

Figure 23: Schematic of IAV Transport. IAV can transmit via different routes from infected to sentinel host. When donor and sentinel host are in close proxemity, the virus can be transmitted both via direct transmission and smear transmission (green arrows). The virus is also able to transmit via air. Here, it is important to differentiate between short distance transmission (< 1 m), where the air containing the virus is rebreathed by the sentinel host and long distance transmission (> 1m), where the virus is transported for a prolonged period of time.

2 Methods and Data

2.1 Data

To analyze the effect of weather conditions on the influenza seasonality, datasets from the Deutsche Wetter Dienst (DWD)[184] for weather related data, and the Robert Koch Institute (RKI)[185] for influenza related epidemiological data were used. All data covered whole Germany on city and county resolution and the time period from the 01.01.2010 till 31.12.2018.

2.1.2 Temperature, Relative Humidity Wind Direction and Wind Velocity

The datasets used on temperature, relative humidity, wind direction and wind speed were provided by the DWD through the climate data center (CDC). Data records were obtained from and controlled by the measurement stations maintained by the DWD. While temperature and humidity are assessed at 2 m above ground, wind direction and wind speed measurements were taken at 10 m above ground level. The datasets were generated on hourly temporal resolution. All data records used, corresponded to the inherent quality check provided by the measurement equipment.

2.1.3 Epidemiological Data on Influenza A

The epidemiological data in influenza A incidence and spreading in Germany for the here analyzed seasons were based on the analysis and assessment of data collected by the Robert Koch Institute (RKI). In this study we focused on 8 consecutive influenza seasons from 2010/2011 till 2017/2018. Data were collected in various surveillance systems for the monitoring of acute respiratory infections in Germany. It is mandatory to report laboratory confirmed influenza cases to German local health authorities. They submitted notifications via state health authorities to the RKI. The dataset used in this study, started with season week 1 (SW1) in calendar week 40 (CW40) and reported both the incidence of influenza A, an extrapolated value, and the case numbers. In this study, only data on influenza A was used, excluding influenza B and other acute respiratory diseases. The term ‘wave of influenza’ referred to the entire period of increased influenza activity. The wave of influenza began when in two consecutive calendar weeks the incidence exceeded 10 % of that period and ended when the positive rate felt below 10 % for two consecutive weeks. Thus, it was only possible to retroactive define the wave of influenza season.
RKI data on vaccine coverage in people older than 65 in Germany, in particular against influenza, were also used in this analysis

2.1.3 Sociological Data on Germany

For analyzing sociological factors that could influence the influenza season, datasets concerning population numbers, population density, and the number of people that were older than 65 years in each city or county were used. All datasets concerning the population in Germany were provided by the Statistisches Bundesamt[186].

2.2 Methods

Patterns of influenza spread are shaped by interacting ecological, evolutionary and sociological processes. Even though Germany is a comparably homogenous country in regarding to climate and socioeconomical factors, influenza incidence rates do not evenly occur in all German cities and counties (Figure 21B). We addressed this spatial difference of influenza A incidences using 8 years (2010/2011 to 2017/2018) of data on weekly incidences of influenza A virus cases in all counties of Germany, provided by the RKI (Figure 21A). As the provided incidence data is an extrapolation of reported case numbers, in this study the provided reports on case numbers per county in relation to its population for each county was used.

2.2.1 Epidemic Intensity

The incidences distribution (p_{ij}) over the weeks of one season year can be described by the epidemic intensity as introduced by Bjørnstad *et al.* (2018)[36]. They defined the epidemic intensity (v_j), as the inverse of the Shannon entropy of incidence distribution (p_{ij}) in a given year and city or county.

$$v_j = \left(-\sum_i p_{ij} \, log \, p_{ij} \right)^{-1}$$

Incidence distribution represented the fraction of influenza incidence rates of a given influenza year in a given week (i) in a given city. The epidemic intensity was normalized to be between 0 and 1 by subtracting the global minimum and then dividing the data by the global maximum across all cities. Following their definition of epidemic intensity, epidemic intensity was minimized when the incidence rate is spread evenly across weeks and increased as the incidence became more intensively focused in particular weeks.

2.2.2 Calcutation of Influenza Cases/Population

The reported influenza incidence rate is extrapolated, as for that we calculated the cases/population value. For that we divided the reported influenza cases per county by the number of inhabitants of that county. Through that we obtained a data set with comparable values that are not extrapolated. As we weren't correcting the population numbers each year, but used numbers of 2017, we tolerated the inherent error of this data set (modified after[186]). See supplementary figure 1 for comparison between incidence and cases/population.

2.2.3 Regression Analysis of Influenza Cases/Population vs. Weather

Temperature and humidity are linked closely, as the ability of air to hold water increases with increased temperature. This relationship is best described by relative humidity [%] (RH), which gives the ratio of absolute humidity to maximum humidity at a given temperature. Absolute humidity (AH) describes the presence of water vapor in a given air parcel volume and is expressed in g/m^3. AH was better suitable in comparing the effect of ambient humidity at different temperatures. The AH was calculated from the provided RH datasets, following the equation below, if ideal gas behavior was assumed:

$$AH\left[\frac{g}{m^3}\right] = C * \frac{Pw}{T[K]}$$

The equation for AH was derived from the ideal gas equation and includes the vapor pressure (Pw), the gas constant (C = 2.16679 gK/J) and temperature in Kelvin. The gas constant is given in one joule per kilogram per Kelvin (J / kg · K). It is a derived SI unit for the specific heat capacity. Thus, a material has the thermal capacity of 1 J / kg · K when the thermal energy of one joule is required to raise the temperature of one kilogram of this material by one Kelvin.

The dependency between temperature and ambient humidity is well described. Thus, certain combinations of temperature and ambient humidity will occur more frequently than others. As the amount of water vapor is temperature depended we observed a saturation curve when relating AH to temperature. Colder air can hold less water vapor than warmer air (Figure 27). Binning temperature and humidity combinations and counting the occurrence of those combination in four major German cities (Berlin, Hamburg, Munich and Cologne), allowed to describe that dependency.

By correlating the occurrence of influenza cases/population to those previously defined temperature-humidity combinations, we can describe a dependency between the probability of influenza and temperature - humidity combination values. All influenza cases were distributed throughout the whole week by dividing them by the numbers of hours occurring in one week. We did that to overcome the differences in time resolution of the data sets, for temperature and relative humidity, which were measured on an hourly basis, and the data for influenza incidence which was reported weekly. Following that, categories were defined as can be seen in Figure 31A. The temperature [°C] and absolute humidity [kg/m^3] felt into four categories: temperature into ≤ 0 °C, between 0 – 10 °C, between 10 – 20 °C and ≥ 20 °C and the absolute humidity into ≤ 0.005 kg/m^3, between 0.005 – 0.0075 kg/m^3, between 0.0075 – 0.01 kg/m^3 and ≥ 0.01 kg/m^3.

As many factors can modulate the wave of influenza incidence, it is difficult to compare different seasons. Thus, for each season the season maximum, when the overall highest number of cases/population in that year was reached, and the season start, when at least 10 % of influenza cases/population were recorded. Either the season maximum or season start were set to week 0. Then the average for each week between the 5 previous and 5 following weeks was calculated.

2.2.3 Spatial Analysis of Influenza Incidence

The counties surrounding each city were categorized in 8 predefined sectors orientated to a cardinal direction. Only counties with at least one mutual border to the city were analyzed. In cases where one county was in more than one cardinal direction, the sector covering most of the county area was chosen. In cases that two counties were equivalent to one cardinal direction, the influenza cases/population was summed up. To allow the comparison between the city and their surrounding counties, the cases/population of the county was divided by the maximum of influenza cases/population occurring in the city. Additionally, season start and maximum were defined for the city and assumed to be similar in the surrounding counties. Some counties endured more IAV cases/population than others. Interestingly, in some years abnormal distribution patterns of influenza were observed. To analyze the possible transport of IAV particles by wind and its correlation with distribution patterns of influenza observed, we also had to overcome the difference between the wind data, that is provided hourly and the IAV cases/population data that is provided weekly. As the temporal scale of weather changes are inevitable to capture when comparing different influenza seasons, it was necessary to extrapolate the IAV

cases/population data to fit to the wind data. To allow the comparison between all seasons, the season maximum of influenza cases/population for each season was defined in each city and set as week 0. Then the average of cases/population starting 10 weeks before the season maximum of influenza cases/population until 10 weeks after the calculated season maximum. The extrapolated averages cases/population data of all seasons were plotted with the hourly wind direction.

3 Results

During winter month influenza A incidence peaks in temperate regions[172,173]. The causes of this pronounced seasonality are not understood so far. Previous studies indicated that relative humidity (RH) and temperature affects both influenza virus transmission and influenza virus survival[35–38,187]. In this study the dependency between local IAV transmission and given weather conditions was investigated by simulating the spatial and temporal distribution pattern of IAV incidence in dependence of local ambient humidity, temperature and wind.

3.1 Influenza Season in Germany (2010-2018)

The influenza season in Germany can be categorized in three phases: i) season start which was in average at calender week 2 (± 4 weeks); ii) ascent phase and season maximum of influenza incidence rate , which differed significantly between seasons; iii) the decay of influenza incidence rate, which is comparable between seasons and occured in the time span of 2 – 3 weeks (Figure 24A).

The epidemic intensity of an influenza season describes the distribution of influenza A incidence among one season year. The intensity of the analyzed seasons did not differ significantly between the different years. Eventhough, we observed different time spans from season start to season end (Figure 24B in comparison to Figure 24A). Interstingly, the influenza incidence as well as the season intensity are not equally distributed in Germany (Figure 24C and D). The average of influenza incidence in all cities and counties showed a distinct east-west gradient (Figure 24C). This gradient becomes even more distincted when plotting the average of the epidemic intensity (Figure 24D).

The season intensity was partly determined by the transmission potential of influenza, meaning the propensity for two randomly selected hosts in a population to attain spatiotemporal proximity sufficient for influenza transmission. Bjørnsted *et al.* (2018) observed a higher intensity in smaller towns. They explained this paradox with an increased basic level influenza incidence that promoted the herd immunity training the populations immunity throughout the year[36].

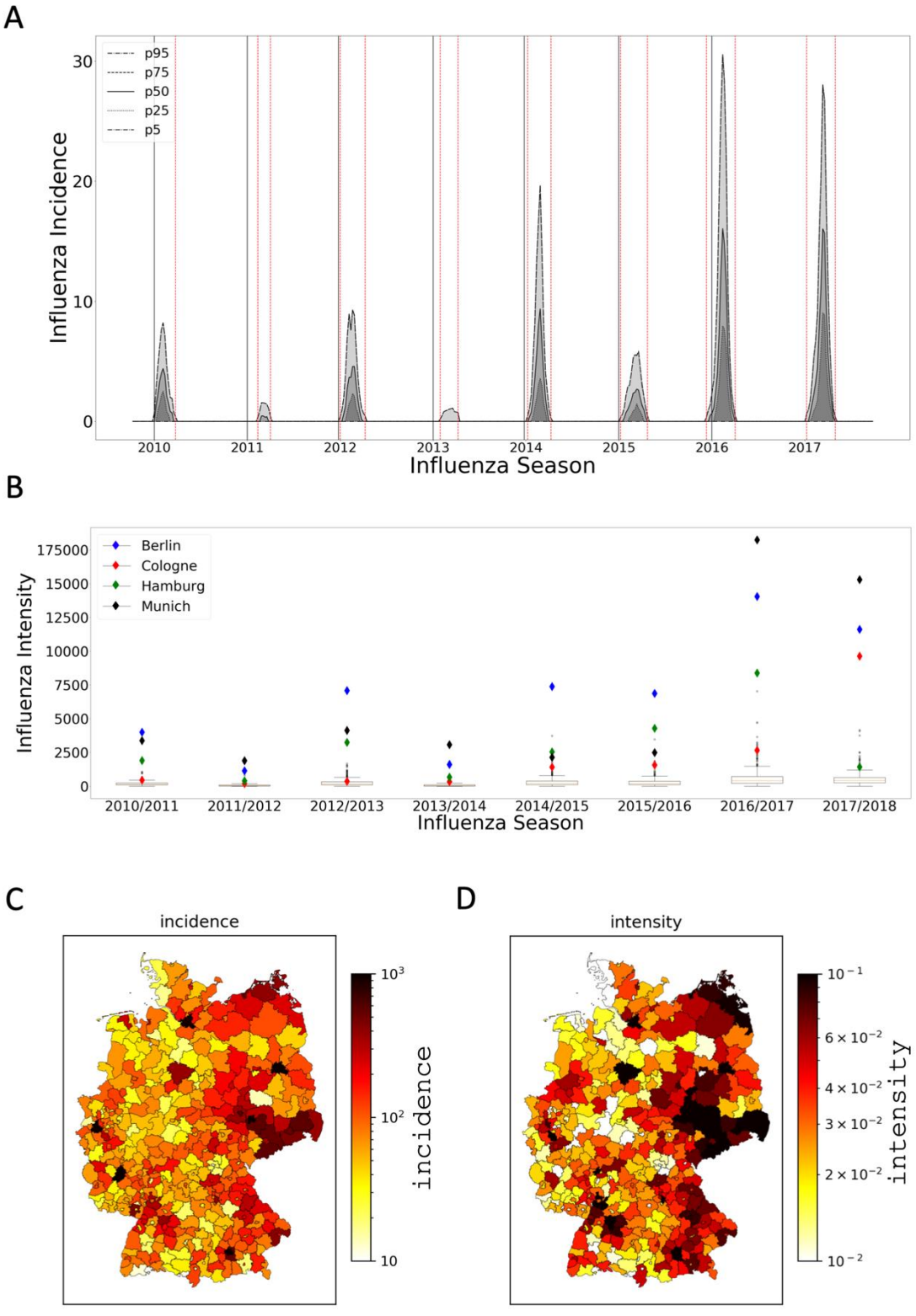

Figure 24: Influenza Season in Germany. (A) Yearly incidence of influenza during the years 2010 until 2018 in Germany. The first of January is marked with a black line, while in the red lines mark the start and end of one season. **(B)** Comparison of epidemic intensity between different influenza seasons in Germany, in all cities and counties in Germany. **(C)** Average incidence of all seasons analyzed shown across all German counties. **(D)** Average epidemic intensity of all analyzed seasons shown across all German counties.

The seasonal pattern of influenza incidence is driven by a complex network of different factors. In the following, different aspects of this network were analyzed, focusing on the role of outdoor environmental factors such as humidity, temperature and outdoor particle transport. Additionally, sociological aspects that are specific for Germany, like population density and demography, were also analyzed.

The current population of Germany was around 83 million people and was distributed relatively even across the different counties (Figure 25A). The average population density was at 240 people per km^2 but varied significantly between different parts in Germany: the west part of Germany has an evenly high population density of 528 people per km^2; in contrast the eastern part has only 85 people per km^2 (Figure 25B).

The population size does not correlate with the population density. As for that, even though two cities may have similar population size, due to local conditions, one city can have a higher population density (Figure 25). Also, the average intensity of an influenza season was independent of both population size and population density (Figure 25C). Interestingly, the main driving factor for the intensity of influenza season seemed to be the geographical location of the city (Figure 25D). We plotted the 20 highest and lowest intensity values and observed, with exception of the larger cities, that low intensity values were found exclusively in the north-western part of Germany. The high values were in the east-southern part (Figure 25D).

Advanced age is a well described risk factor for influenza infection[188]. Thus, we analyzed the distribution of people older than 65 years and whether it correlated with influenza incidence rates and intensity. A strong gradient between eastern and western Germany was seen. In the eastern part more than 30 % of the population were older than 65 years, while in the western part less than 20 % were that age (Figure 25E). We also observed an east-west gradient of anti-influenza vaccine coverage with a better vaccine coverage against influenza in the new federal states of Germany (Figure 25F). In western and southern Germany an average of 33 % of the population older than 65 years got vaccinated against influenza, whereas in eastern Germany in average more than 54 % were vaccinated (RKI).

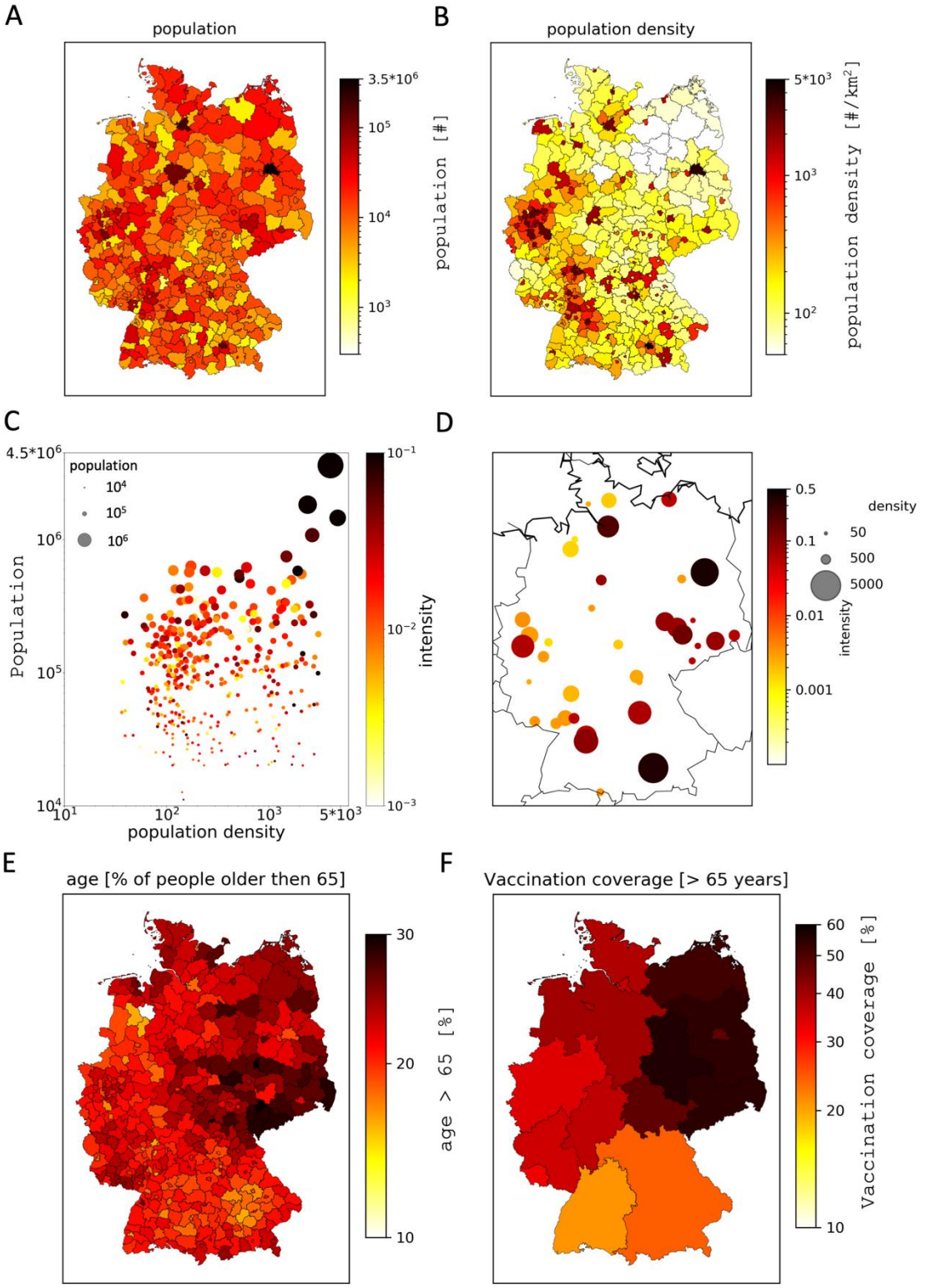

Figure 25: Sociological Factors Influencing Influenza Distribution. (A) Population of Germany for each city and county (updated 2017) **(B)** Population density in each county and city (Germany) **(C)** Dependency between population, population density and average intensity of influenza in all analyzed seasons. **(D)** 20 lowest and 20 highest cities and counties, shown geograhically in correlation to the population density and average intensity of infuenza season. **(E)** Demographics of people older than age 65 in Germany (source: Statistisches Bundesamt; Bundesinstitut für Bevölkerungsforschung) **(F)** Vaccination coverage against influenza in people older than age 65 in Germany (source: RKI)

3.2 The Role of Environmental Factors on Influenza Season

Germany is part of the warm temperate and moderate rain climate of the middle latitudes. It lies in the transition area between the oceanic climate of Western Europe, where western air currents ensure precipitation and a subdued temperature change all year round and the continental climate of Eastern Europe, which is characterized by strong seasonal temperature fluctuations[189]. From the influences of the Mediterranean climate of southern Europe, is Germany protected by the Alps. Northern European influences are dampened by the oceans in between[189].

The climate of Germany was thus shaped predominantly by western winds, whose moist air masses ensure precipitation, relatively mild winters and not too hot summers all year round. This oceanic influence decreased from northwest to southeast[189]. Consequently, in the Northwest and the North the climate is maritime with moderate winters and summers, influenced by warm water provided by the northern extension of the Gulf Stream and the North Atlantic Drift[189]. The climate in the North is Central and Southern Germany are transition regions which vary from moderately maritime to continental. The East is dominated by continental climate, leading to winters with very cold and long-lasting dry periods.

The meteorological winter includes December, January and February. The spatial variability in the average relative humidity and temperature can be seen in Figure 26. By calculating the average value for the winter months from 2010 until 2018, it was possible to reaffirm the difference in climatic conditions in Germany. As described above, the North of Germany was characterized by maritime climate with in average high RH and warmth (Figure 26A and B). In contrast the eastern and southern parts of Germany were characterized by a continental climate and thus can be described as rather dry and cold (Figure 26A and B).

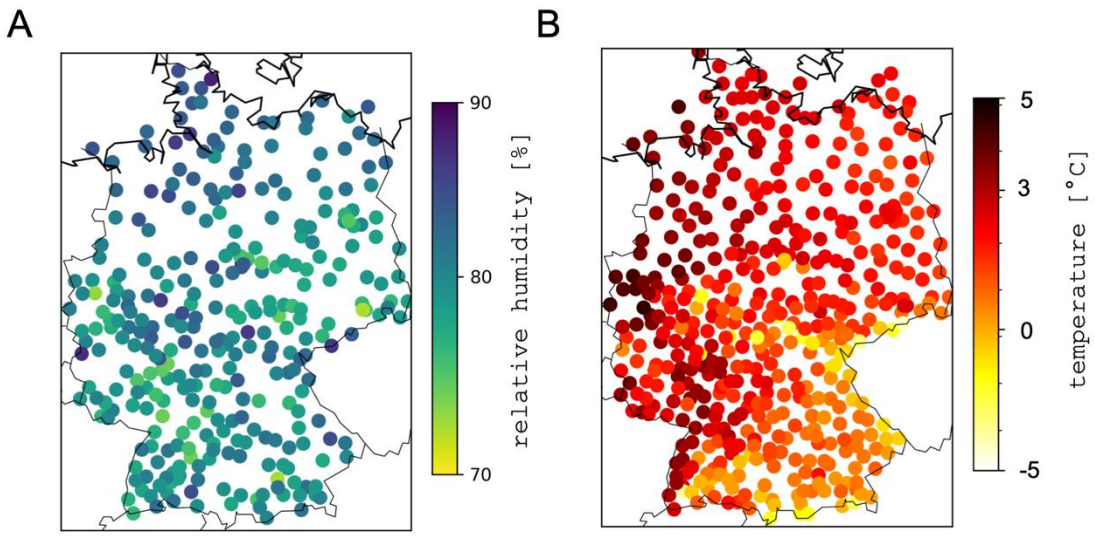

Figure 26: Climatic Conditions during Winter Month in Germany. Every point represents a DWD controlled measuring station **(A)** Average relative humidity in Germany during winter month from 2010 until 2018 **(B)** Average temperature in Germany during winter month from 2010 until 2018. (Source: DWD)

3.3 Influenza Season in Selected Cities

In order to analyze the influence of environmental factors on the influenza season in urban areas, four different cities and their surrounding counties were selected: Hamburg for the North (Figure 27Aa), Berlin for the East (Figure 27Ab), Munich for the South (Figure 27Ac), and Cologne for the West (Figure 27Ad).

Those cities are population wise the four largest cities in Germany with distinctly different population structures. For example, the contrast between the city and its surrounding counties in Berlin was quite profound, as the population in each county was equal to only (4.75 ± 1.1) % of the population of Berlin. Even when the population numbers of all surrounding counties were summed up, only half as many people (47 %) live in the surrounding areas compared to Berlin (Figure 27Ab). In contrast, three times as many people lived in the surrounding counties of Cologne as in Cologne itself (Figure 27Ad).

The four cities also represented the previously described different climate zones of Germany. In Germany three different Köppen climate classification can be observed. Hamburg had an oceanic climate (Köppen: *Cfb*), with average RH during winter of (87.95 ± 4.38) % and a temperature of (0.68 ± 1.65) °C. The proximity to the coast and maritime influences drived the weather in Hamburg. Interestingly, due to its transitional climate zones, frosts are common in winter and there are larger temperature differences between seasons than typical for many oceanic climates. The average RH, of all analyzed years, is the highest and the temperature the lowest compared to the other cities (Figure 27B).

Berlin felt in the continental category (Köppen: *Dfb*). Average humidity was at (84.33 ± 4.14) % RH and average temperature at (1.67 ± 1.73) °C. This type of climate has cold but not rigorous winters. Munich felt by Köppen's classification in the *Dfb* category but had the lowest average of RH ((79.28 ± 7.01) % RH) during winter and average temperature of (2.07 ± 1.7) °C (Figure 27Ba). Cologne has a mild continental climate, with an average RH of (83.3 ± 4.63) % and temperature of (4.01 ± 1.58) °C and falls into the *Cfb* Köppen classification. As the climate is influenced by the Atlantic Ocean and the North Sea this region is one of the mildest in Germany during winter (Figure 27Bb).

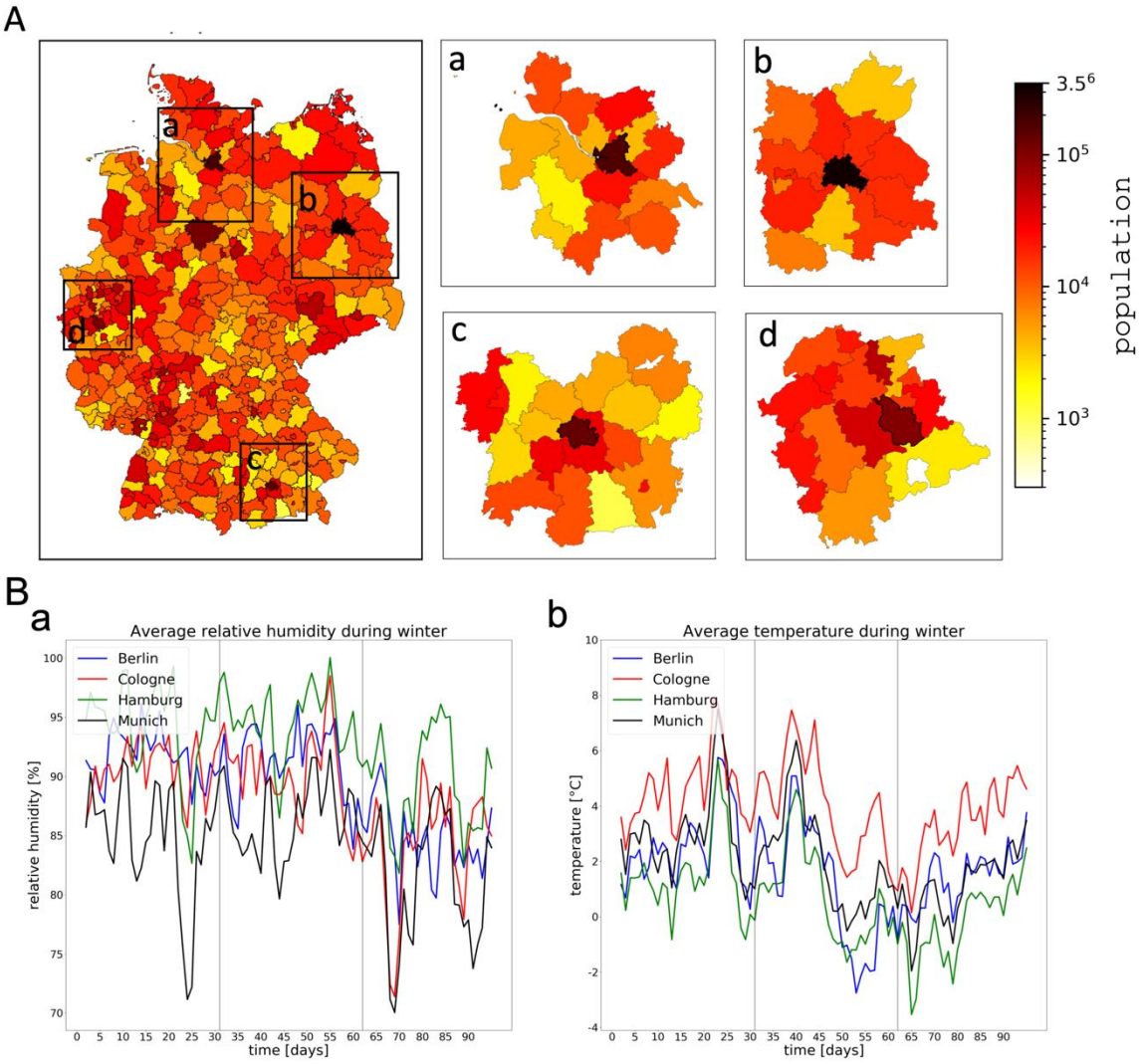

Figure 27: Selection of Four Major Cities and their Surrounding Counties. (A) Population of the four chosen cities and their surrounding counties in 2018 (source Statistisches Bundesamt[186]). **(B)** Average RH [%] and temperature [°C] during meterological winter (December, Januar and Februar of the years 2010 – 2018) in the four selected cities (source: DWD[184]).

The ratio of influenza cases per population (cases/population) differed between the cities and their surrounding counties. Especially among the counties are drastic differences, with some having a 100fold higher cases/population value than others (Figure 28A, Suppl. Figure 3). In the following we compared the burden of influenza season in the four cities with each other and to their surrounding counties.

The average intensity in the four cities, compared to their surrounding was significantly higher than in the surrounding counties. Interestingly, in the Hamburg area, a difference between the South-West (0.0199 ± 0.001) and the North-East (0.0282 ± 0.003) can be observed with a significant higher intensity in the North-East (Figure 28Ba). A comparable difference in intensity can be seen in Berlin where in the South-East a significantly higher intensity can be observed (0.039 ± 0.014) compared to for example the North-East (0.014 ± 0.00065) (Figure 28Bb). Such a distinct geographical difference in intensity cannot be observed in Cologne and Munich, even though different counties differed significantly in their intensity (Figure 28Bc and Bd)

When comparing the average value of intensities between the four cities, we observed the highest intensity in Berlin, followed by Munich and Hamburg and the lowest in Cologne (Figure 28C). Interestingly, the degree of intensity did not reflect in the overall number of cases/populations. Despite the fact that Berlin showed the highest intensity, its cases/population value was lower than that found in Munich and Hamburg (Figure 28D).

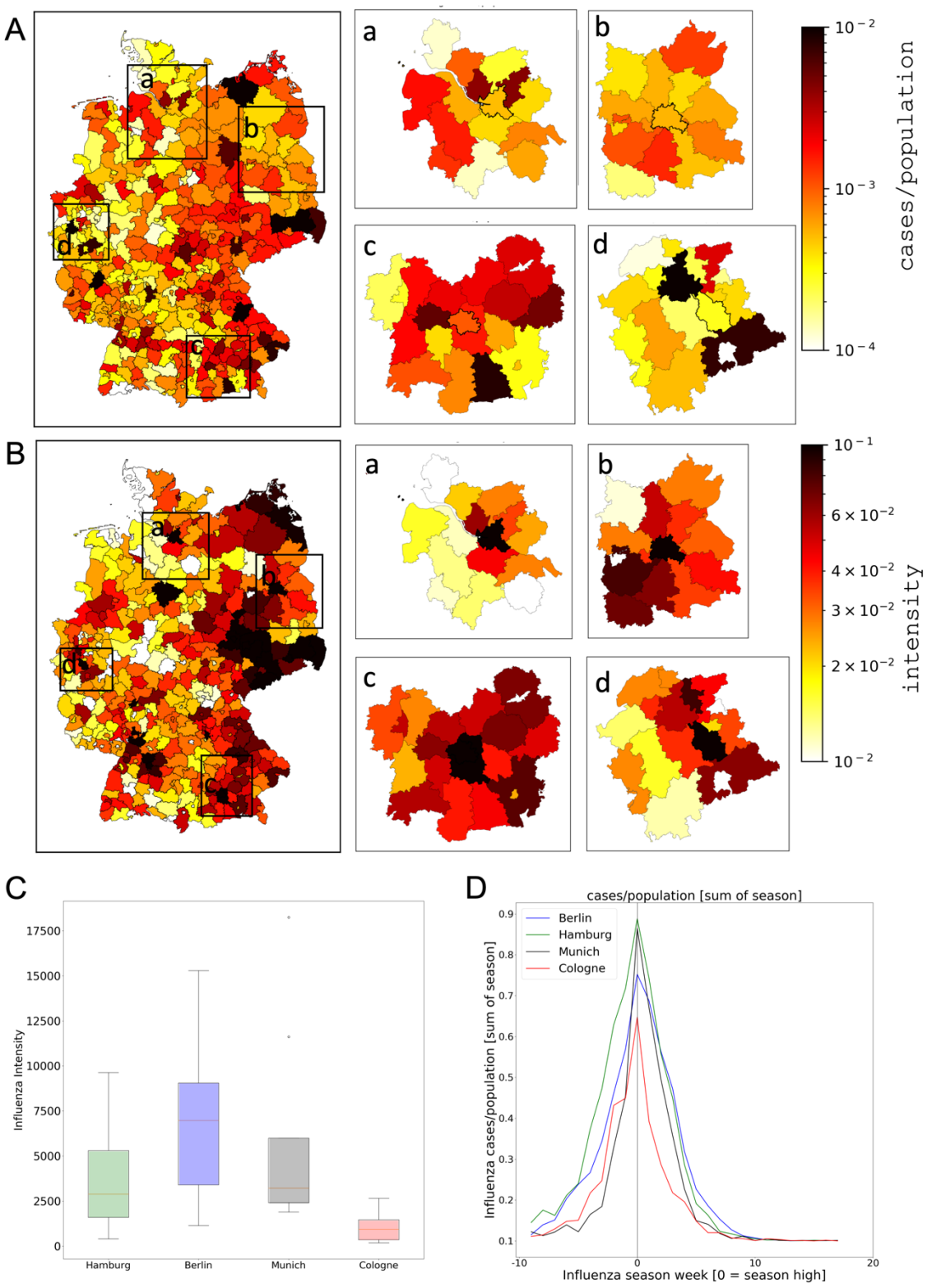

Figure 28: Influenza Season in the Four Selected Cities and their Surrounding. **(A)** Average influenza cases/population over the analyzed seasons. **(B)** Geographicla distribution of average intensity during the analyzed seasons. **(C)** Intensity values during season 2010/2011 till 2017/2018. **(D)** Sum of cases/population over a time line. Season high was determined in each season and set to 0. Then the average for each week 10 weeks before and after the season high was formed. The standart deviation is not shown.

The RH is highly dependent on the given temperature. The regression analysis of temperature and humidity showed that certain combinations of temperature and RH were more frequently found than others. Between the four cities no remarkable difference was seen (Figure 29A). The prevalence of influenza cases depended on specific combinations of RH and temperature. Increased cases/population values correlated with low RH and temperatures (Figure 29B). As the absolute humidity (AH) allowed the comparison of water vapor, independent of the temperature, it was of interest to analyze the impact of AH on influenza spread. The ability of air to hold water vapor was dependent on the actual temperature, as for that a saturation level of water vapor in air was seen (Figure 29C). Absolute humidity and temperature clearly influenced the transmission of influenza viruses, as only at certain combinations of absolute humidity and temperature, higher influenza A cases/population values were recorded (Figure 29D).

Consequently, categories were defined, representing certain combinations of temperature and absolute humidity (Figure 30A). Applying those categories on the temperatures and humidity's measured over one year in all four cities, it was possible to compare the influence of weather on cases/population and epidemic intensity for each year in one city (Figure 30) and one season (Suppl. Figure 4). The literature suggests that low AH and low temperatures are most favorable for IAV transmission, we thus expected that an increased abundance of category 1 and 2 with higher cases/population values and epidemic intensities.

Overall influenza cases/population values and epidemic intensities seemed to be independent of the abundance of category 1 or 2 during the season year analyzed and varied distinctively between season years (Hamburg: 0.00062 ± 0.0005, Berlin: 0.00053 ± 0.00032, Munich: 0.00039 ± 0.00034, Cologne: 0.00031 ± 0.00029) (Figure 30B). Also, the epidemic intensity varied in Hamburg (0.0251 ± 0.008), Munich (0.0467 ± 0.025) and Cologne (0.0077 ± 0.0029), independently of the abundance category 1 and 2 (Figure 30C). Interestingly, the epidemic intensity in Berlin was relatively stable, and showed a value of 0.051 ± 0.006 throughout all seasons in comparison to the other analyzed cities (Figure 30C). Each year both influenza cases/population as well as intensity varied within one city.

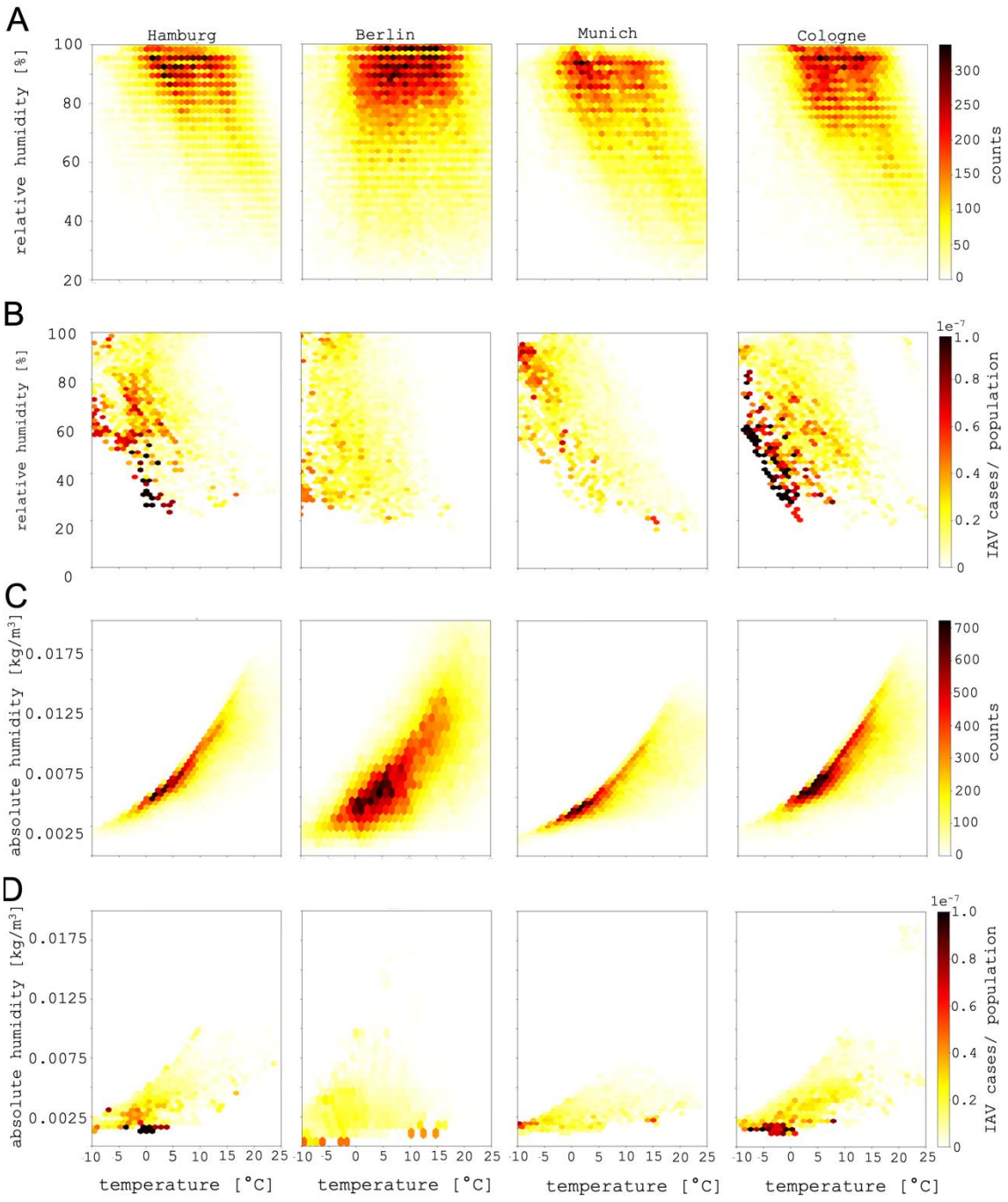

Figure 29: Regression Analysis between Temperature and Humidity in Correlation to IAV cases/population. IAV incidence was increased at certain temperature and humidity combinations. **(A)** Counts of occurrence of certain RH and temperature combinations in predefined bins (source: DWD[184]) **(B)** Occurrence of influenza A cases/population in previous described RH and temperature bins (source: DWD[184] and RKI[185]). **(C)** Counts of occurrence of certain AH and temperature combinations in predefined bins (source: DWD[184]). **(D)** Occurrence of influenza A cases/population in previous AH and temperature bins (source: DWD[184] and RKI[185]).

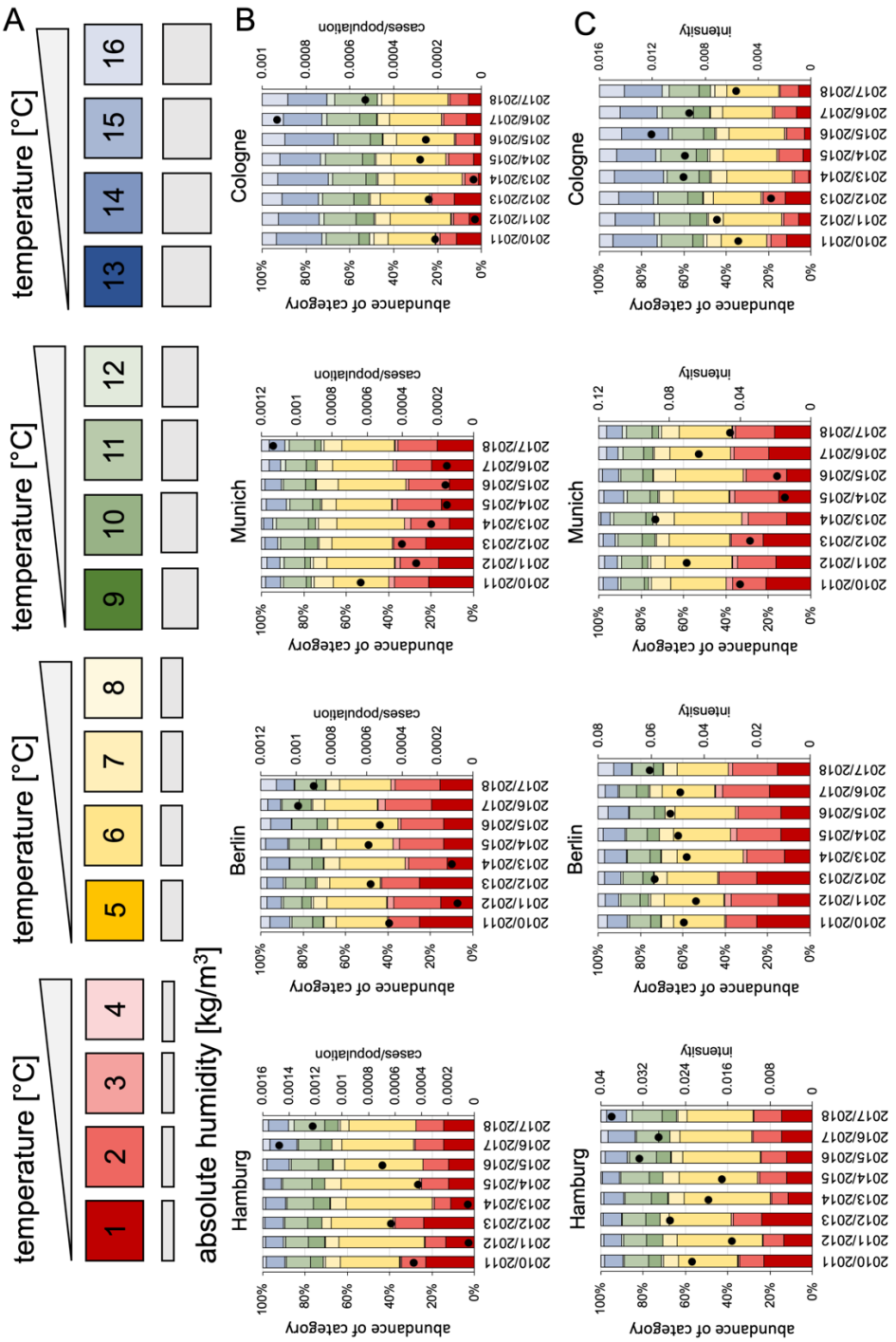

Figure 30: Influenza Season is Independent of the Overall Temperature und Humidity. (A) Development of categories that can combine temperature and absolute humidity values. Absolute humidity increased from category 1 - 4 (< 0.005 kg/m3) over category 5 - 8 (0.005 – 0.0075 kg/m3) , category 9 - 12 (0.0075 - 0.01 kg/m3) till category 13 - 16 (> 0.01 kg/m3), while temperature increased in smaller intervals and was increasing from < 0 °C (category 1, 5, 9 and 13), over 0 - 10 °C (category 2, 6, 10 and 14), 10 - 20 °C (category 3, 7, 11 and 15) to > 20 °C (category 4, 8, 12 and 16). **(B)** Sum of observed categories and proportion of certain categories over one season year in Cologne, Hamburg, Munich and Berlin, in relation to the annual season sum of cases/population. **(C)** Sum of observed categories and proportion of certain categories over one season year in Cologne, Hamburg, Munich and Berlin, in relation to the annual season sum of epidemic intensity.

Analysis of the influence of temperature and air humidity on the progression of the IAV season each city. For that we fitted influenza cases/population to the season high, defined as the week and number with the highest value in cases/ population (Figure 31). In comparison two neighboring councils, the one with the highest and lowest overall cases/population value, were analyzed and also normalized to the city season high. In general, it seemed that before season peaks, weather conditions were classified predominantly as category 1 and 2. They seemed to amplify the progression of IAV transmission (Figure 31A). Interestingly, even though it can be assumed that in the neighboring councils similar weather conditions were present, the neighboring councils analyzed had a belated season high, with the IAV season mainly originating in major cities (Figure 31A, Supp. Figure 3). Similar results were seen when fitting the season start to 0. We observed a simultaneous increase of cases/population to an increased abundance of category 1 and 2. As influenza has a short incubation period of less than 24 hours, the weather condition during each week appeared to influence the progression of influenza season (Figure 31B).

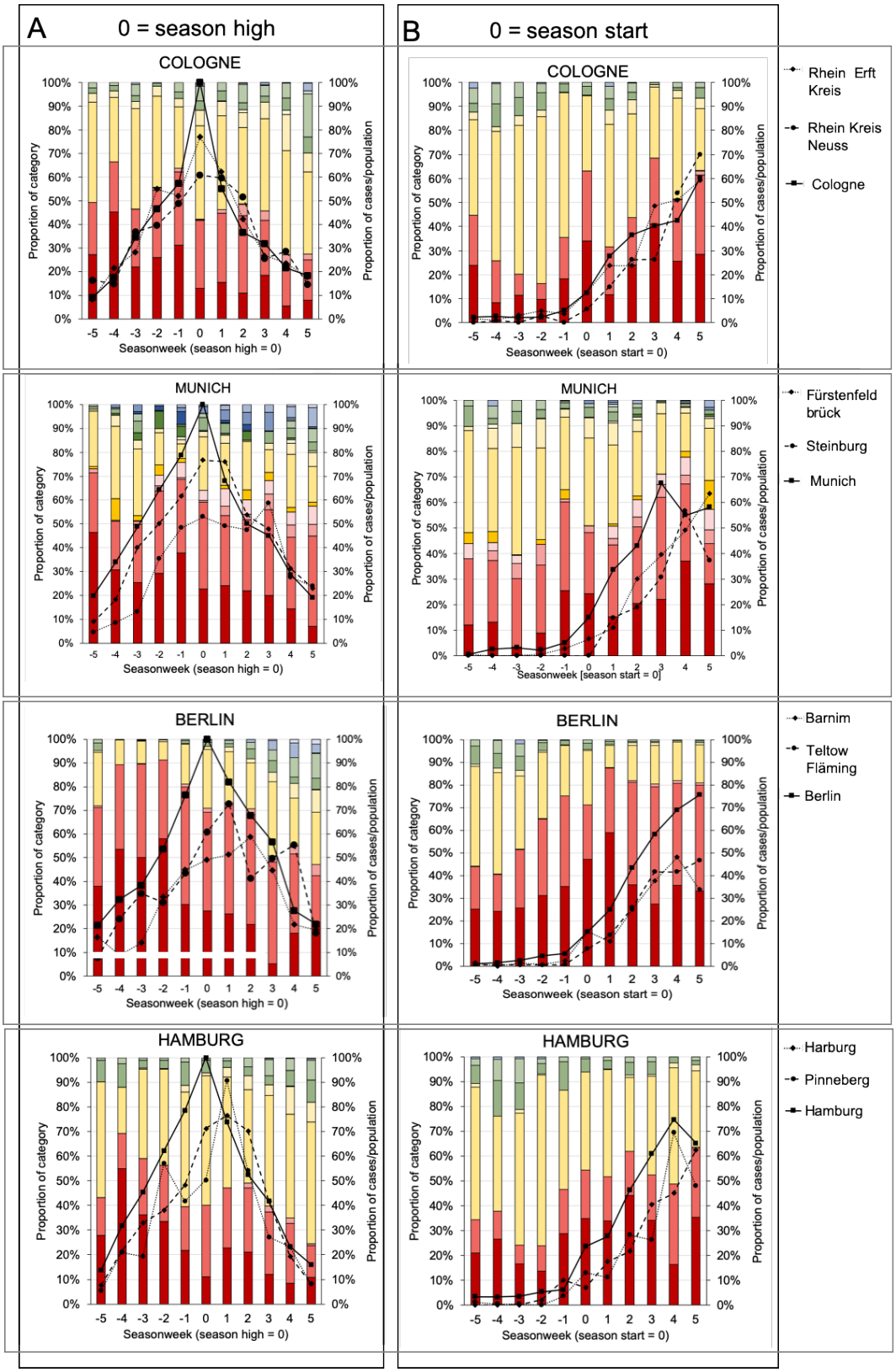

Figure 31: Cold and Dry Weather Supports Influenza Season Progression. (A) Proportion of categories five weeks before and after season high. Season high was defined as maximal value of cases/population per season year. All values were normalized to the season high, therefor season high equals one. **(B)** Proportion of categories five weeks before and after season start. Season start was defined, when 10 % of maximum IAV cases/population was reached.

3.4 Spatial Analysis of Progression of Influenza Season

To analyze the spatial distribution and progression of influenza in the neighboring counties, we also normalized the cases/population to the maximum of cases/population observed in the city and fitted week 0 to the season high. This allowed the direct comparison of the different neighboring counties in relation to their geographical position. Marked in green was season week -10 and in red the defined season max (Figure 32). In Berlin all surrounding counties were comparably hit by the IAV season, with exception of the county west and west-north of the city. In contrast, Hamburg showed a distinct increase in cases/population value in the western and west-northern counties (Figure 32A and 32B). Also, in Cologne and Munich influenza cases/population were not equally distributed over the neighboring counties (Figure 32C and 32D). Those differences are most likely caused by inherent factors, like population structure and commuting as well as geographical and environmental conditions, which could favor some counties over others with regards of IAV spread. Interestingly, we observed a delay in the season maximum (red line) for all four areas in the counties. This suggested, that the influenza season started in the cities (Figure 32).

To test if the wind was coherent with influenza distribution, we correlated the main wind direction with the average influenza cases/population (Figure 33). For that we calculated the average of cases/population between all seasons with season maximum equaled zero and plotted the wind record for all seasons during week -10 till 10. During the timespan analyzed, which was predominantly at winter time, the wind comes in Hamburg mainly from the South and West and just in rare cases from the North (Figure 33A left). Considering wind as the main factor in the geographical distribution of influenza, we correlated the influenza cases/population observed with wind directions and found that according to the wind direction most cases would be found in the northern and north-eastern counties (Figure 33A middle). However, in all four cities, it was not possible to correlate the overall wind direction with the overall influenza cases/population distribution (compare Figure 33 middle to Figure 33 right).

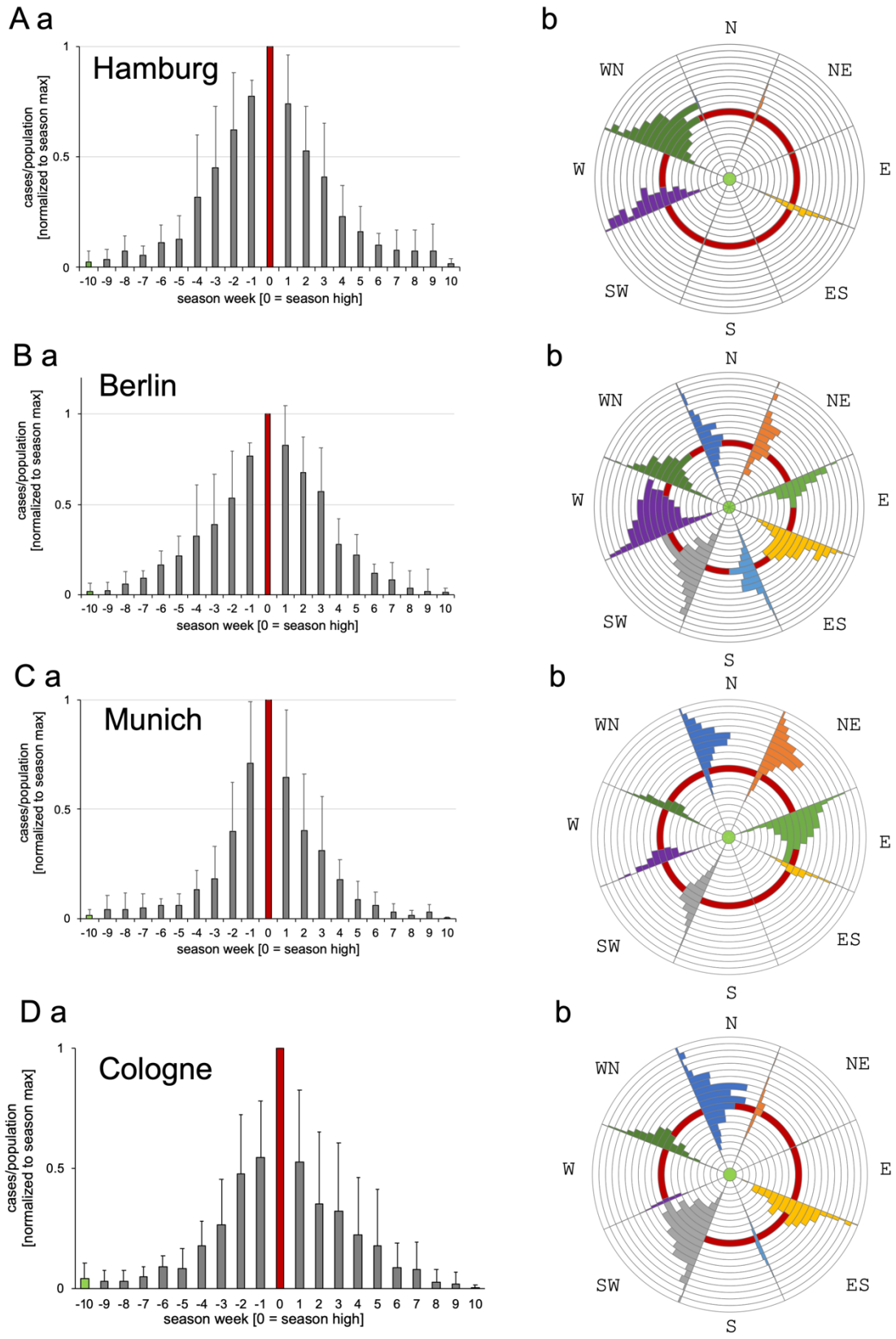

Figure 32: Spatial Analysis of Influenza cases/population. (a) Season progression in the city normalized to the season maximum in the city **(b)** Season progression in the surrounding counties of the city, normalized to the season maximum (marked as red) in the city. Each line represents one week, starting with week -10 in the middle (marked as green).

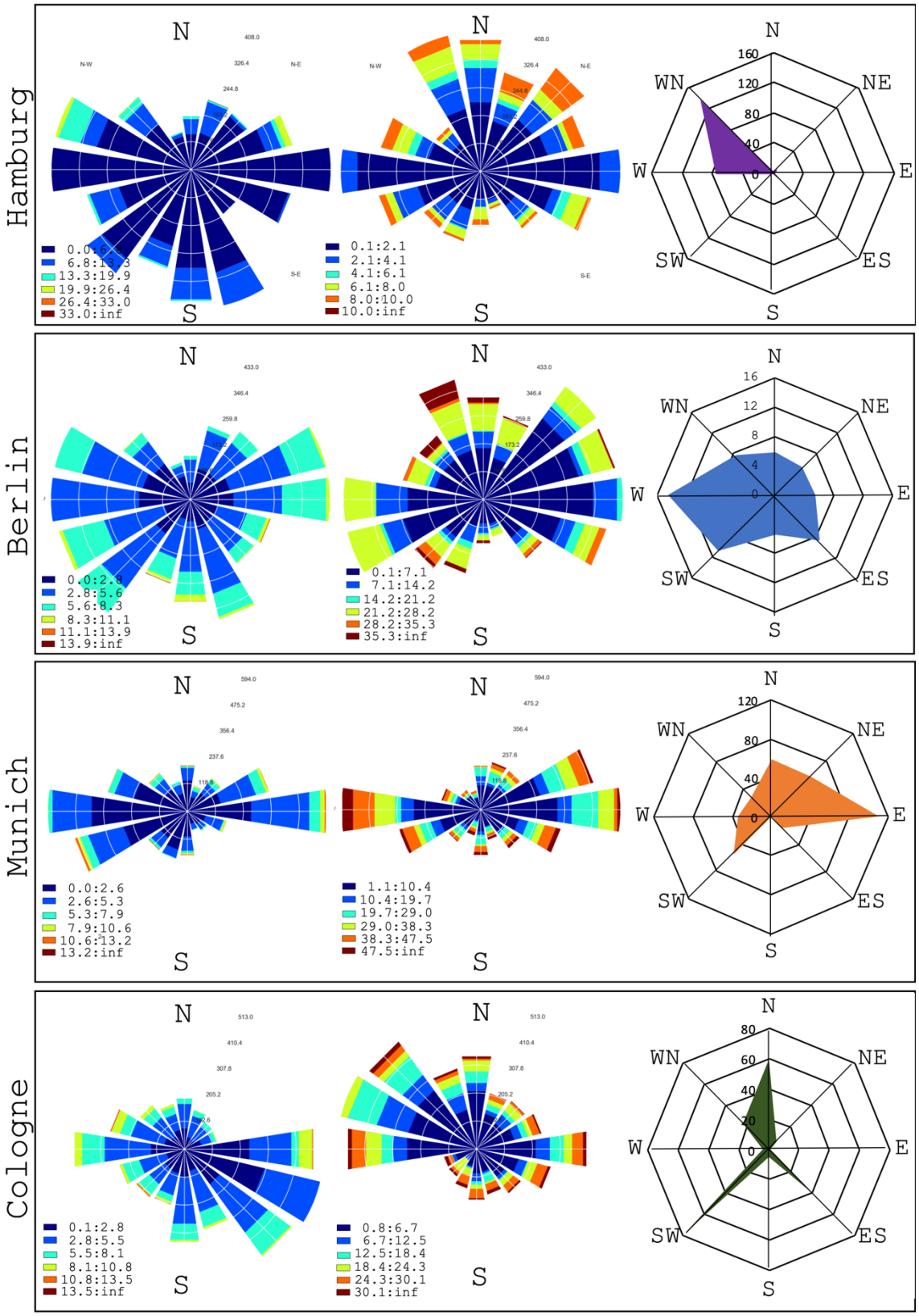

Figure 33: Influence of Wind on the Distribution Pattern of Influenza. (left) wind rose for each city, recognizing the wind direction and wind speed recorded during the influenza season **(middle)** theoretical IAV particle distribution. The colors show the different bin for influenza cases/population. **(right)** actuall observed influenza cases/population in the different surrounding counties.

4 Discussion

Influenza seasonality is a well observed but poorly understood concept. With many different factors interacting with each other, it is very difficult to consider all factors that might modulate influenza season. In our study we analyzed the effects of geographical factors including environmental and demographical one on transmission rate of influenza. We identified favorable temperature/humidity combinations for influenza transmission and were able to correlate the observed gradient in influenza cases/population values to predominant weather conditions in Germany. We thus identified low humidity as main driver of influenza season progression.

With increased global urbanization, the city as transmission hot spot for infectious diseases becomes the focus of attention. In Germany already 77 % of the population lives in urban areas (Statistisches Bundesamt). Close proximity of susceptible hosts in cities make them the principal location for influenza transmission and form the primary context where drivers of transmission (Figure 25A). Among those drivers for seasonality are general ones such as biological, sociological and environmental drivers. Those include varying susceptibility of hosts throughout the year, changed host behavior during winter and increased virus stability caused by low humidity and temperature.

The role of city size and structure in shaping transmission patterns of seasonal influenza in cities in the USA was recently analyzed by Bjørnsted *et al.* (2018). Their data suggested that endogenous differences among cities may interact with climatic and drivers of antigenic evolution and thus caused divergent epidemic dynamics at the individual city level[36]. In Germany, the overall observed epidemiological intensity did not differ between high incidence years and low incidence years (Figure 25B) but showed a clear geographical distribution pattern (Figure 25D). Interestingly, we observed reduced epidemic intensities with increased population densities when we compared the geographical distribution pattern, suggesting that the population density can influence the influenza transmission (compare Figure 25C and 25D with Figure 26B). By increased proximity of susceptible hosts, the background infection rate was increased, which in turn could lead to increased levels of herd immunity[36]. Interestingly, in contrast to this observation, cities that have the highest population size in Germany were strongly impacted by influenza incidence and epidemiological intensity (Figure 25B, 25C and 25D). Analysis of the correlation between population sizes, population densities and influenza intensities did not reveal a direct correlation as suggested by Bjørnsted *et al.*

(2018) (Figure 26C). Instead, we were able to show that the geographical position of the cities and counties were crucial for the observed pattern of incidence and epidemiological intensities (Figure 26D). Even though sociological factors like demography and anti-influenza vaccination coverage are believed to also partly drive influenza seasons, we were not able to identify a correlation between those drivers and patterns (Figure 26E and 26F). However, this was not surprising, despite the fact that to the older population influenza had an increased morbidity. Cases in people older than 65 make up only a small part of the overall number of influenza cases (Suppl. Figure 1B).

In the framework of this study we suggested that the climate in Germany is one of the drivers for the geographical distribution of influenza cases/population and epidemiological intensities (Figure 27). To further analyze this, we selected four cities in Germany (Figure 28A). These areas and their surrounding counties differed from each other in several characteristics that could potentially influence influenza transmission. They differed in population size, population density, and spatial structure but also in their climatic conditions. As a result, we observed different epidemiological intensities as well as overall burdens of influenza cases/population (Figure 28).

As we were not able to connect the overall progression of influenza season to either the temperature - humidity category (Figure 30B) nor the wind direction (Figure 33), IAV transmission may have not occurred outdoors and other factors may have led to increased IAV transmission. The indoors are considered as main transmission place, as here crowding provides susceptible hosts in close proximity, and air was easily rebreathed. Heating, which is probably increased during cold temperatures, reduces RH in the indoor environment to levels as low as 40 % RH[190,191]. Low RHs not only help to preserve the viability of IAV but also enable IAV carrier aerosols to persist longer in air because of their smaller size and lower settling velocities that result from more vigorous evaporation[163]. Ambient humidity also affected the IAV particles directly as they were highly hygroscopic (Figure 17B). Interestingly, we observed a higher variability of the volume at 65 % RH, the RH where virus particles were described as unstable[182]. The observed mucus corona in IAV particles derived from nasopharyngeal tissue culture model may enhance the effects of ambient humidity (Figure 18D) and thus explained the significant influence of ambient humidity on IAV particle transmission.

4.1 Limitations and Outlook

Main limitation of this study was the different time resolutions of the data sets concerning the weather and the epidemiological information on influenza A incidence. While the weather is a fast-changing parameter it was difficult to correlate the hourly information provided by the measuring stations of the DWD to the weekly output of influenza epidemiology information from the RKI. Thus, in future, it is of essence to monitor the influenza season in a shorter time resolution but also to develop equipment that allows for the measurement of viable IAV in an outdoor environment. To link different factors such as humidity's, temperature and particle transport, additional laboratory experiments will be needed, even though first steps considering the influenza transmission in guinea pigs under different environmental conditions have been undertaken by Lowen *et al.* (2007)[38].

3 CONCLUSION

Pathogen containing aerosols are a complex mixture of various components including the pathogen and other organic matter, like salt, mucus and cellular material, it is essential to realize that the size of the pathogen particle itself does not solely determine the airborne particle size[192]. This becomes obvious by comparing aerosols from viruses and bacteria, where the aerodynamic diameter of both pathogens is fairly comparable (compare Figure 9 and to Figure 18) even though the volume of one mycobacterium is 10.000-fold larger in volume than of one virus (compare Figure 7B to Figure 17B). Interestingly, the aerodynamic diameter of pathogen-containing aerosols was strongly influenced by the origin of the pathogen (Figure 13 and Figure 18), highlighting the importance of using relevant infection models to study airborne pathogens (Figure 12 and Figure 20). The importance of ambient humidity on airborne transmission has been discussed before[34,38,112,187,193]. Both, BCG particles as well as IAV particles are very hygroscopic (Figure 8B and Figure 17B), emphasizing the influence of variations in humidity on airborne transmission through alterations in the volumes of pathogen particles and thus changed airborne behavior.

The influence of ambient humidity on airborne transmission has been described for both, TB and influenza. For TB, it was proposed that a higher RH will increase the transmission rate of *M. tuberculosis*[30,34]. Consequently, lower humidity's and colder temperatures can protect household contacts from infection[34]. In contrast, for influenza, higher transmission rates were observed at lower humidity's and colder temperatures. Despite the effects of humidity on transmission of both pathogens, increased transmission rates during winter season were observed for IAV. By modelling the effect of the ambient humidity on the infection dynamic during influenza seasons we observed, in support to other studies, the importance of weather conditions on IAV seasonality and confirmed that ambient humidity was main driver of IAV transmission (*Chapter 3*). Influenza incidence increased during winter months of 2010 till 2018 in Germany (Figure 24). In our study we were able to link increased influenza cases/population with the occurrence of certain combinations of ambient humidity's and temperatures (Figure 29 and Figure 31).

In contrast to Influenza, the number of TB cases increases during summer[194]. This seasonal variation was suggested to be due to more recent transmission than tuberculosis reactivation[195,196]. Transmission likely occurred during winter time, possibly in

association with increased viral catarrh. Coinfection of *M. tuberculosis* and IAV does not only increases coughing frequency in patients and thus increases the release of *M. tuberculosis* from the respiratory tract but viral infection also impairs the immune system on several levels and may favor tuberculosis reactivation[197].

To gain more detailed data on conditions for pathogen transmission under various in- and outdoor conditions is highly relevant and has been further emphasized by the current SARS-CoV2 pandemic. The pathways, dynamics and conditions determining of pathogen transmission is of pivotal relevance to develop epidemic crisis and global risk assessments plans by healthy authorities. The various knowledges required includes those on the physicochemical and biological properties of pathogen containing aerosol particles as they have been studied in this thesis.

4 Materials

4.1 Chemicals, Solutions and Buffers

Name/ Substance	Composition/ Producer
Acetit acid, 1%	J.T. Baker
Chicken erythrocytes with citrate	Lohmann Tierzucht
Citrate buffer	DCS
Diaphorase/NAD+	Roche (Mannheim, Germany)
Ethanol (EtOH)	Carl Roth (Karlsruhe, Germany)
Epon	EMS (Hatfield Pennsylvania)
Glutaraldehyde, 2.5%	EMS (Hatfield Pennsylvania)
Glycerol	Invitrogen (Carlsbad, California)
Glycogen (Mytilus edulis)	Sigma-Aldrich (St. Louis, Missouri)
Gold	Q150R Quorum Technologies (Lewes, GB)
H_2O_2	Omnilabs, (Hamburg, Germany)
Hexamethyldisilane	Sigma-Aldrich (St. Louis, Missouri)
Histoplaque 1199	Sigma-Aldrich (St. Louis, Missouri)
Isopropanol (2-propanol)	Fluka
Iodotetrazolium chloride/sodium lactate	Roche (Mannheim, Germany)
MassRuler DNA Ladder Mix, 80-10 000 bp	Fermentas/Thermo Scientific
Osmeon, 2%	EMS (Hatfield Pennsylvania)
Paraformaldehyde (PFA)	BioChemica (Billingham, UK)
Percoll	Sigma-Aldrich (St. Louis, Missouri)
PBS (1x)	Sigma-Aldrich, (St. Louis, Missouri)
PBS (10x)	26,8 mM KCl (Carl Roth, Karlsruhe, Germany) 17,6 mM KH_2PO_4 (Merck, Darmstadt, Germany) 1,37 M NaCl (Merck, Darmstadt, Germany)

	51,3 mM Na_2HPO_4 $2H_2O$ (Merck, Darmstadt, Germany) ad. 1 L aqua dest. pH 7.4
PBS-Tween (0.05 %)	0.05 % Tween-20 (Serva, Heidelberg, Germany) in 1x PBS
Solvent-free glue	UHU (Bühl, Germany)
Triton X-100 (0.1% in PBS)	Omnilabs (Hamburg, Germany)
TrueBlue™ Peroxidase Substrate	Sera care (Milford, Massachussetts)
Uranylacetat (2%)	EMS (Hatfield, Pennsylvania)

4.2 Cell culture media and Additives

Name/ Substance	Composition/ Producer
Growth medium mycobacteria	7H9 broth (BD Bioscience, Franklin Lakes, New Jersey) 0.05 % Tween 80 (Serva, Heidelberg, Germany) 10 % OADC (BD Bioscience, Franklin Lakes, New Jersey)
Freezing medium mycobacteria	50 % growth medium mycobacteria 50 % Glycerol (Invitrogen, Carlsbad, California)
Agar plate mycobacteria	7H11 agar (BD Bioscience, Franklin Lakes, New Jersey) 10 % FCS (BD Bioscience, Franklin Lakes, New Jersey)
Growth media neutrophils	RPMI Medium (Invitrogen, Carlsbad, California) 10% FCS (Sigma-Aldrich, St. Louis, Missouri) 2 mM Glutamine (Invitrogen, Carlsbad, California)
Name/ Substance	Composition/ Producer
Avicel (microcrystalline cellulose)	FCM BioPolymer
Avicel-Overlay medium	50 % Overlay medium 50 % Avicel solution (2.5% Avicel in 1xPBS)

Bovine serum albumin, 35% in DPBS	Sigma-Aldrich (St. Louis, Missouri)
Dulbecco's Modified Eagle Medium (DMEM)	Sigma-Aldrich (St. Louis, Missouri)
Dulbecco's PBS (1x)	Sigma-Aldrich (St. Louis, Missouri)
Fetal calf serum (FCS)	Biochrom
Growth Medium MDCK cells	MEM, Sigma-Aldrich (St. Louis, Missouri) 10 % FCS, Sigma-Aldrich (St. Louis, Missouri) 1 % L-Glutamin, Sigma-Aldrich (St. Louis, Missouri) 1% penicillin and streptomycin, Sigma-Aldrich (St. Louis, Missouri)
Infection medium MDCK	MEM, Sigma-Aldrich (St. Louis, Missouri) 0.2 % BSA, Sigma-Aldrich (St. Louis, Missouri) 1 % L-Glutamin, Sigma-Aldrich (St. Louis, Missouri)
Minimal Essential Medium (MEM)	Sigma-Aldrich (St. Louis, Missouri)
Modified Eagle Medium (2xMEM)	GIBCO, ThermoFisher Scientific (Waltham, Massachusetts)
Overlay medium for plaque assay	2x MEM 0.4 % BSA 2 % L-glutamin 2% penicillin and streptomycin
Penicillin and streptomycin (P/S, 100x)	Sigma-Aldrich (St. Louis, Missouri)
Reduced Serum Medium (Opti-MEM)	GIBCO, ThermoFisher Scientific (Waltham, Massachusetts)
Trypsin-EDTA (1x)	Sigma-Aldrich (St. Louis, Missouri)

4.3 Enzymes and Kits

Name/ Substance	Composition/ Producer
DNA-Polymerase Phusion	NEB (Ipswich, Massachusetts)
DNAse I, RNase free	Roche (Basel, Switzerland)

dNTP-Mix (10 mM each)	QIAGEN (Hilden, Germany)
QIAamp Viral RNA Mini Kit	QIAGEN (Hilden, Germany)
SuperScript™ III Reverse Transcriptase	Invitrogen (Carlsbad, California)
Trypsin-TPCK	Sigma-Aldrich (St. Louis, Missouri)
LIVE/DEAD™ BacLight™ Bacterial Viability Kit	ThermoFisher Scientific (Waltham, Massachusetts)

4.4 Primer for Detection

Name	Sequence (5'→3')
NP fw	*gaagttgggggggg* AGCAAAAGCAGG GTA
NP rev	*ccgccgggttatt* AGTAGAAACAAGG GTATTTTT

4.5 Bacterial stocks

Name	Origin / Description
M. bovis BCG strains Pasteur (BCG)	Camille Locht, Institute Pasteur, Lille, France

4.6 Virus stocks

Name	Origin / Description
A/Hamburg/05/09 (pH1N1) → HH05	Clinical isolate from 2009 pandemic Sigrid Baumgarte, Institut für Hygiene und Umwelt, Hamburg, Deutschland
H5N1-HA$_{monobasic}$	7+1 reassortant virus of A/PR/8/34 (H1N1) and the HA of A/Vietnam/11/94 (H5N1) without the multibasic HA cleavage site (H5 control). Thijs Kuiken/Debby van Riel, Erasmus Medical Center, Rotterdam, Netherlands
A/Netherlands/213/03 (H3N2)	Clinical isolate from 2003 Erasmus University Rotterdam, Rotterdam Niederlande, Dr. Thijs Kuiken

4.7 Antibodies

Name	Origin	Producer	Application
Anti-NP	Mouse monoclonal	Abcam (ab43821)	1:1000 plaque assay 1:500 histology
Anti-mouse IgG-HRP	Rabbit polyclonal	SouthernBiotech (6170-05)	1:2000 plaque assay
Anti-Kir5	Rabbit monoclonal	Abcam (Cambridge, UK)	1:1000 Histology
Anti-mouse IgG Alexa 594	Goat polyclonal	ThermoFisher Scientific (Waltham, Massachusetts)	1:500 Histology
Anti-rabbit IgG Alexa 488	Donkey polyclonal	ThermoFisher Scientific (Waltham, Massachusetts)	1:500 Histology

4.8 Consumables

Consumables were purchased if not indicated otherwise from the following companies: Falcon, Sarstedt, Biozym, Nunc.

Name	Producer
Cantilever OMCL-AC160TS	Olympus (Tokyo, Japan)
Lithium chloride	ThermoFisherScientific (Waltham, Massachusetts)
Mesh copper grid	Electron Microscopy Sciences (EMS), (Hatfield, Pennsylvania)
Omnifix® Syringes (3 ml / Luer Lock Solo)	B. Braun Melsungen AG (Melsungen, Germany)
Omnifix® Syringes (10 ml / Luer Lock Solo)	B. Braun Melsungen AG (Melsungen, Germany)
Potassium chloride	ThermoFisherScientific (Waltham, Massachusetts)
Sodium nitrate	ThermoFisherScientific (Waltham, Massachusetts)

4.9 Equipment

Name	Producer
Aerodynamic Particle Spectrometer	APS 3221, TSI (Shoreview, Minnesota)
Atomic Force Microscopy	Oxford Instruments, Asylum Research, (Santa Barbara, California)
Cascade Impactor	Copley Scientific (Nottingham, UK)
Centrifuge Multifuge 3S-R	Heraeus (Hanau, Germany)
Centrifuge Varifuge 3.0R	Heraeus (Hanau, Germany)
Centrifuge 5424R	Eppendorf (Hamburg, Germany)
Centrifuge 5424	Eppendorf (Hamburg, Germany)
Centrifuge 5427R	Eppendorf (Hamburg, Germany)
Centrifuge (Coverslip)	
CO_2 incubator BBD6220	Thermo Scientific (Waltham, Massachusetts)
CO_{2i} incubator HERACELL 150	Thermo Scientific (Waltham, Massachusetts)
Dynamic Light Scattering Method	ZetaSizer, Malvern Panalytical (Malvern UK)
HEPA AirClean	Miele (Gütersloh, Germany)
HEPA filter	Patronenfilter- HS- Mikroseal JG-S, HS-Luftfilterbau GmbH (Kiel, Germany)
Jet nebulizer	IH18, Beurer (Ulm, Germany)
Opsys MR ELISA reader	Dynex Technology (Chantilly, Virgina)
pH meter 766 Calimatic	Knick (Berlin, Germany)
Pipettes Eppendorf Reference	Eppendorf (Hamburg,Germany)
Pipetboy Pipetus	Hirschmann Laborgeräte (Eberstadt, Germany)
Precision balance Extend	Sartorius (Göttingen, Germany)
Precision scale ED224S	Sartorius (Göttingen, Germany)
Saftey cabinet Herasafe KS 12	Thermo Scientific (Waltham, Massachusetts)
Safety cabinet Herasafe KS 18	Thermo Scientific (Waltham, Massachusetts)
Scanning Electron Microscopy	Philips XL30ESEM/Point Electronic DISS5 (Philips, Hillsboro, Oregon)

Sperm counting chamber	Marienfeld Superior (Lauda-Königshofen, Germany)
Shaking water bath SW-22	Julabo (Seelbach, Germany)
Transmission Electron Microscope	Philips CM120/ Gatan MSC 794 (Hillsboro, Oregon)
Ultra-wave nebulizer	U22 Microair, Omron (Kyoto, Japan)
Water purification system Milli Q	Merck (Darmstadt, Germany)
Zeiss LSM 510 fluorescent confocal microscope	Zeiss (Oberkochen, Germany)

References

1. Aliabadi, A. A., Rogak, S. N., Bartlett, K. H. & Green, S. I. Preventing Airborne Disease Transmission : Review of Methods for Ventilation Design in Health Care Facilities. *Adv. Prev. Med.* **2011**, (2011).

2. Herfst, S. *et al.* Drivers of airborne human-to-human pathogen transmission. *Curr. Opin. Virol.* **22**, 22–29 (2017).

3. Sturm, R. Theoretical model of clearance in the tracheobronchial airways of healthy subjects and smokers. 1–8 (2018). doi:10.21037/jphe.2018.03.04

4. Owen, M. K., Ensor, D. S. & Sparks, L. Airborne particle sizes and sources found in indoor air. *Atmos. Environ.* **26**, 2149–2162 (1992).

5. Kim, K., Kabir, E. & Jahan, S. A. Airborne bioaerosols and their impact on human health. **7**, 23–35 (2017).

6. Douwes, J., Thorne, P., Pearce, N. & Heederik, D. Bioaerosol Health Effects and Exposure Assessment : Progress and Prospects. *Ann. occup. Hyg.* **47**, 187–200 (2003).

7. Sturm, R. Modeling the deposition of bioaerosols with variable size and shape in the human respiratory tract – A review. *J. Adv. Res.* **3**, 295–304 (2012).

8. Hinds, W. C. *Aerosol Technology; Proberties, behavior and measurment of airborne particles*. (Wiley Interscience, 1999).

9. Jones, R. M. & Brosseau, L. M. Aerosol Transmission of Infectious Disease. *J. Occup. Environ. Med.* **57**, 501–508 (2015).

10. Fernstrom, A. & Goldblatt, M. Airobiology and Its Role in the Transmission of Infectious Diseases. *J. Pathog.* **2013**, 13 (2012).

11. Richard, M. & Fouchier, R. A. M. Influenza A virus transmission via respiratory aerosols or droplets as it relates to pandemic potential. 68–85 (2016). doi:10.1093/femsre/fuv039

12. Gralton, J., Tovey, E., McLaws, M.-L. & Rawlinson, W. D. The role of particle size in aerosolised pathogen transmission : A review. *J. Infect.* **62**, 1–13 (2011).

13. Dery, R. Water balance of the respiratory tract during ventilation with a gas mixture saturated at body temperature. *Candian Anaesth. Soc. J.* **20**, 719–727 (1973).

14. Fabian, P., Brain, J., Houseman, E. A., Gern, J. & Milton, D. Origin of Exhaled Breath Particles from Healthy and Human Rhinovirus-Infected Subjects 1 1. *J. Aerosol Med. Pulm. Drug Deliv.* **24**, 137–147 (2011).

15. Jennison, M. W. & Edgerton, H. E. Droplet Infection of Air: High Speed Photography of Droplet Production by Sneezing. *Aerobiology* **17**, 106–128 (1942).

16. Tang, J. W. *et al.* Airflow Dynamics of Human Jets : Sneezing and Breathing - Potential Sources of Infectious Aerosols. *PLoS One* **8**, 1–7 (2013).

17. Wells, W. F. Airborne Contagion and Air Hygiene: an Ecological Study of Droplet Infection. *Harvard Univ. Press* 423 p (1955).

18. Kwon, S. *et al.* Chemosphere Study on the initial velocity distribution of exhaled air from coughing and speaking. *Chemosphere* **87**, 1260–1264 (2012).

19. Han, Z. Y., Weng, W. G. & Huang, Q. Y. Characterizations of particle size distribution of the droplets exhaled by sneeze. (2013).

20. Milton, D. K., Fabian, M. P., Cowling, B. J., Grantham, M. L. & Mcdevitt, J. J. Influenza Virus Aerosols in Human Exhaled Breath : Particle Size , Culturability , and Effect of Surgical Masks. *PLoS Pathog.* **9**, (2013).

21. Lindsley, W. G. *et al.* Measurements of Airborne Influenza Virus in Aerosol Particles from Human Coughs. **5**, (2010).

22. Holmgren, H., Ljungström, E., Almstrand, A.-C., Bake, B. & Olin, A.-C. Size distribution of exhaled particles in the range from 0.01 to 2.0 μm. *J. Aerosol Sci.* **41**, 439–446 (2010).

23. Fabian, P., Mcdevitt, J. J., Dehaan, W. H., Fung, R. O. P. & Cowling, B. J. Influenza Virus in Human Exhaled Breath : An Observational Study. (2008). doi:10.1371/journal.pone.0002691

24. Papineni, R. & Rosenthal, F. The size distribution of droplets in the exhaled breath of healty human subjects. *J. Aerosol Med.* **10**, (2009).

25. Lighthart, B. The ecology of bacteria in the alfresco atmosphere. *FEMS Microbiol. Ecol.* **23**, 263–274 (1997).

26. Tong, Y. & Lighthart, B. The annual bacterial particle concentration and size distribution in the ambient atmosphere in a rural area of the Willamette Valley, Oregon. *Aerosol Sci. Technol.* **32**, 393–403 (2000).

27. Mi, E. *et al.* Impact of Asian dust events on airborne bacterial community assessed by molecular analyses. *Atmos. Environ.* **45**, 4313–4321 (2011).

28. Molesworth, A., Cuevas, L., Morse, A. & Herman, J. Dust clouds and spread of infection. *Lancet* **359**, 81–82 (2002).

29. Lee, E., Yoon, T., Lee, M., Han, S. & Ka, J. Inactivation of environmental mycobacteria by free chlorine and UV. *Water Res.* **44**, 1329–1334 (2010).

30. Ko, G., First, M. W. & Burge, H. a. Influence of relative humidity on particle size and UV sensitivity of Serratia marcescens and Mycobacterium bovis BCG aerosols. *Tuber. Lung Dis.* **80**, 217–228 (2000).

31. Shahid, M., Abubakar, M., Hameed, S. & Hassan, S. Avian influenza virus (H5N1); effects of physico-chemical factors on its survival. *Virol. J.* **6**, 38 (2009).

32. Wathes, C. M., Howard, K. & Webster, a J. The survival of Escherichia coli in an aerosol at air temperatures of 15 and 30 degrees C and a range of humidities. *J. Hyg. (Lond).* **97**, 489–96 (1986).

33. Takayama, K., Armstrong, E. L. E. E., Davidson, L. A., Kunugi, K. A. & Kilburn, J. O. Effect of Low Temperature on Growth , Viability , and Synthesis of Mycotic Acids of Mycobacterium tuberculosis Strain H37Ra ' 2. **118**, 113–117 (1978).

34. Olender, S. *et al.* Low prevalence and increased household clustering of Mycobacterium tuberculosis infection in high altitude villages in Peru. *Am. J. Trop. Med. Hyg.* **68**, 721–727 (2003).

35. Schaffer, F. L., Soergel, M. E. & Straube, D. C. Survival of airborne influenza virus: effects of propagating host, relative humidity, and composition of spray fluids. *Arch. Virol.* **51**, 263–273 (1976).

36. Bjørnstad, O. N., Metcalf, C. J. E. & Grenfell, B. T. Urbanization and humidity shape the intensity of influenza epidemics in U.S. cities. **79**, 75–79 (2018).

37. Shaman, J. & Kohn, M. Absolute humidity modulates influenza survival , transmission , and seasonality. **106**, (2009).

38. Lowen, A. C., Mubareka, S., Steel, J. & Palese, P. Influenza virus transmission is dependent on relative humidity and temperature. *PLoS Pathog.* **3**, 1470–1476 (2007).

39. Steel, J., Palese, P. & Lowen, A. C. Transmission of a 2009 pandemic influenza virus shows a sensitivity to temperature and humidity similar to that of an H3N2 seasonal strain. *J. Virol.* **85**, 1400–1402 (2011).

40. Löffler, Petrides & Heinrich. *Biochemie & Pathobiochemie*. (2009).

41. Koblinger, L. & Hofmann, W. Analysis of human lung morphometric data for stochastic aerosol deposition calculationso Title. *Phys Med Biol.* **30**, 541–56 (1985).

42. Labiris, N. R. & Dolovich, M. B. Pulmonary drug delivery. Part I: Physiological factors affecting therapeutic effectiveness of aerosolized medications. *Br. J. Clin. Pharmacol.* **56**, 588–599 (2003).

43. Munkholm, M. & Mortensen, J. Mucociliary clearance : pathophysiological aspects. 171–177 (2014). doi:10.1111/cpf.12085

44. Jeffery, P. K. & Li, D. Airway mucosa: Secretory cells, mucus and mucin genes. *Eur. Respir. J.* **10**, 1655–1662 (1997).

45. Bustamante-Marin, X. M. & Ostrowski, L. E. Cilia and Mucociliary Clearance. 1–17 (2017).

46. Hiemstra, P. S., Mc Cary, P. B. & Bals, R. The innate immune function of airway epithelial cells in inflammatory lung disease. *Eur Respir J* **45**, 1150–1162 (2015).

47. Boe, D. M., Boule, L. A. & Kovacs, E. J. Innate immune responses in the ageing lung. *J. Transl. Immunol.* 16–25 (2017). doi:10.1111/cei.12881

48. Verreault, D., Moineau, S. & Duchaine, C. Methods for sampling of airborne viruses. *Microbiol. Mol. Biol. Rev.* **72**, 413–444 (2008).

49. Andersen, A. (US A. C. C. New Sampler for the Collection, Sizing, and Enumeration of Viable Airborne Particles. (1958).

50. Mcgarrity, B. G. J. & Dion, A. S. Detection of airborne polyoma virus. 9–13 (1978).

51. Thomas, B. G. & Thomas, G. An adhesive surface sampling technique for airborne

viruses. 273–282 (1970).

52. Thomas, B. Y. G., Down, P. & Thomas, G. Air sampling of smallpox virus. (1974).

53. Parker, J. Airborne excretion of foot-and-mouth disease virus volume sampler (Litton Model M (Modified), Litton Systems Inc ., Minneapolis ,. (1969).

54. Bausum, H. T., Schaub, S. A., Kenyon, K. F. & Mitchell, J. Comparison of Coliphage and Bacterial Aerosols at a Wastewater Spray Irrigation Site. **43**, 28–38 (1982).

55. Dahlgren, C. M., Decker, H. M. & Harstad, J. B. A Slit Sampler for Collecting T-3 Bacteriophage and Venezuelan Equine Encephalomyelitis Virus. 1959–1961 (1959).

56. Kuehne, R. W. & Gochenour, W. S. A Slit Sampler for Collecting T-3 Bacteriophage and Venezuelan Equine Encephalomyelitis Virus. 106–107 (1961).

57. Willeke, K., Lin, X. & Grinshpun, S. a. Improved Aerosol Collection by Combined Impaction and Centrifugal Motion. *Aerosol Sci. Technol.* **28**, 439–456 (1998).

58. Drake, J. W. Rates of spontaneous mutation among RNA viruses. *Genetics* **90**, 4171–4175 (1993).

59. Matrosovich, M., Matrosovich, T., Garten, W. & Klenk, H. D. New low-viscosity overlay medium for viral plaque assays. *Virol. J.* **3**, 1–7 (2006).

60. Dallenga, T. *et al.* M. tuberculosis-Induced Necrosis of Infected Neutrophils Promotes Bacterial Growth Following Phagocytosis by Macrophages. *Cell Host Microbe* **22**, 519-530.e3 (2017).

61. Dallenga, T. & Schaible, U. E. Neutrophils in tuberculosis – first line of defence or booster of disease and targets for host directed therapy? *Pathog. Dis.* **74**, (2016).

62. Dallenga, T. *et al.* Targeting neutrophils for host-directed therapy to treat tuberculosis. *Int. J. Med. Microbiol.* **308**, 142–147 (2017).

63. Liu, P. Y. *et al.* Real-Time measurement of single bacterium's refractive index using optofluidic immersion refractometry. in *Procedia Engineering* (2014). doi:10.1016/j.proeng.2014.11.743

64. WHO. *Global Tuberculosis Report*. *World Health Organization, Geneva* (2019).

65. Loddenkemper, R., Lipman, M. & Zumla, A. Clinical Aspects of Adult Tuberculosis. *Cold Spring Harb Perspect Med* **6**, 1–25 (2016).

66. Flynn, J. L. & Chan, J. Tuberculosis : Latency and Reactivation. *Infect. Immun.* **69**, 4195–4201 (2001).

67. Hu, H. Y., Wu, C. Y., Huang, N., Chou, Y. J. & Chang, Y. C. Increased risk of tuberculosis in patients with end-stage renal disease : a population-based cohort study in Taiwan , a country of high incidence of end-stage renal disease. 191–199 (2019). doi:10.1017/S0950268813000551

68. O'Leary, S. M. *et al.* Cigarette smoking impairs human pulmonary immunity to mycobacterium tuberculosis. *Am. J. Respir. Crit. Care Med.* **190**, 1430–1436 (2014).

69. Müller, M., de Wit, E. & Hoal, E. G. Past, present and future directions in human genetic susceptibility to tuberculosis. *FEMS* (2009). doi:10.1111/j.1574-695X.2009.00600.x

70. Brosch, R. *et al.* A new evolutionary scenario for the Mycobacterium tuberculosis complex. *PNAS* **99**, (2002).

71. C.Gortázara, L.M.Fernández-Calleb, J.A.Collazos-Martínezb, O.Mínguez-Gonzálezb & P.Acevedoa. Animal tuberculosis maintenance at low abundance of suitable wildlife reservoir hosts: A case study in northern Spain. *Prev. Vet. Med.* **146**, 150–157 (2017).

72. Blouin, Y. *et al.* Significance of the Identification in the Horn of Africa of an Exceptionally Deep Branching Mycobacterium tuberculosis Clade. *PLoS One* **7**, (2012).

73. Echeverria-Valencia, G., Flores-Villalva, S. & Clara, E. *Virulence Factors and Pathogenicity of Mycobacterium*. (2018).

74. Raffetseder, J. *et al.* Replication rates of mycobacterium tuberculosis in human macrophages do not correlate with mycobacterial antibiotic susceptibility. *PLoS One* **9**, 1–10 (2014).

75. Gegenbacher, M. & Kaufmann, S. H. E. Mycobacterium tuberculosis : Success through dormancy. *FEMS* **36**, 514–532 (2012).

76. Simeone, R., Bottai, D. & Brosch, R. ESX/type VII secretion systems and their role in host-pathogen interaction. *Curr. Opin. Microbiol.* **12**, 4–10 (2009).

77. Bottai, D. *et al.* Disruption of the ESX-5 system of Mycobacterium tuberculosis causes loss of PPE protein secretion , reduction of cell wall integrity and strong attenuation. *Mol. Microbiol.* **83**, 1195–1209 (2012).

78. Portal-Celhay, C. *et al.* Mycobacterium tuberculosis EsxH inhibits ESCRT-dependent CD4+ T-cell activation. *Nat. Microbiol.* **2**, (2017).

79. Tufariello, J. M., Chapman, J. R., Kerantzas, C. A., Wong, K. & Vilchèze, C. Separable roles for Mycobacterium tuberculosis ESX-3 effectors in iron acquisition and virulence. *PNAS* (2016). doi:10.1073/pnas.1523321113

80. Tinaztepe, E. *et al.* Role of Metal-Dependent Regulation of ESX-3 Secretion in Intracellular Survival of Mycobacterium tuberculosis. *Am. Soc. Microbiol.* **84**, 2255–2263 (2016).

81. Korb, V., Chuturgoon, A. & Moodley, D. Mycobacterium tuberculosis: Manipulator of Protective Immunity. *Int. J. Mol. Sci.* **17**, 131 (2016).

82. Orme, I. M. A new unifying theory of the pathogenesis of tuberculosis. *Tuberculosis* **94**, 8–14 (2014).

83. Jo, E., Yang, C., Choi, C. H. & Harding, C. V. Intracellular signalling cascades regulating innate immune responses to Mycobacteria : branching out from Toll-like receptors. *Cell Microbiol.* **9**, 1087–1098 (2007).

84. Liu, C. H., Liu, H. & Ge, B. Innate immunity in tuberculosis: Host defense vs pathogen evasion. *Cell. Mol. Immunol.* **14**, 963–975 (2017).

85. Winau, F. *et al.* Apoptotic vesicles crossprime CD8 T cells and protect against tuberculosis. *Immunity* 105–11715 (2006).

86. Underhill, D. M., Ozinsky, A., Smith, K. D. & Aderem, A. proinflammatory signaling in macrophages. *PNAS* **96**, 14459–14463 (1999).

87. Jamwal, S. V, Mehrotra, P., Singh, A., Siddiqui, Z. & Basu, A. Mycobacterial escape from macrophage phagosomes to the cytoplasm represents an alternate adaptation mechanism. *Sci. Rep.* 1–9 (2016). doi:10.1038/srep23089

88. Mahamed, D. *et al.* Intracellular growth of Mycobacterium tuberculosis after macrophage cell death leads to serial killing of host cells. *Elife* **6**, 1–26 (2017).

89. Parasa, V. R. *et al.* Modeling Mycobacterium tuberculosis early granuloma formation in experimental human lung tissue. *DMM Dis. Model. Mech.* **7**, 281–288 (2014).

90. Davis, J. M. *et al.* Real-time visualization of Mycobacterium-macrophage interactions leading to initiation of granuloma formation in zebrafish embryos. *Immunity* **17**, 693–702 (2002).

91. Pagán, A. J. & Ramakrishnan, L. Immunity and immunopathology in the tuberculous granuloma. *Cold Spring Harb. Perspect. Med.* **5**, 1–19 (2015).

92. Flynn, J. A. L. *et al.* Tumor necrosis factor-α is required in the protective immune response against mycobacterium tuberculosis in mice. *Immunity* **2**, 561–572 (1995).

93. Smith, D., Hänsch, H., Bancroft, G. & Ehlers, S. T-cell-independent granuloma formation in response to Mycobacterium avium: Role of tumour necrosis factor-α and interferon-γ. *Immunology* **92**, 413–421 (1997).

94. Hemmati, M. *et al.* Additive effect of recombinant Mycobacterium tuberculosis ESAT-6 protein and ESAT-6/CFP-10 fusion protein in adhesion of macrophages through fibronectin receptors. *J. Microbiol. Immunol. Infect.* **49**, 249–256 (2016).

95. Dheda, K. *et al.* Lung Remodeling in Pulmonary Tuberculosis. *J. Infect. Dis.* **192**, 1201–1210 (2005).

96. Orme, I. M. & Basaraba, R. J. The formation of the granuloma in tuberculosis infection. *Semin. Immunol.* **26**, 601–609 (2014).

97. Ehlers, S. & Schaible, U. E. The granuloma in tuberculosis: Dynamics of a host-pathogen collusion. *Front. Immunol.* **3**, 1–9 (2012).

98. Stewart, G. R., Robertson, B. D. & Young, D. B. Tuberculosis: A problem with persistence. *Nat. Rev. Microbiol.* **1**, 97–105 (2003).

99. Turner, R. D. & Bothamley, G. H. Cough and the transmission of tuberculosis. *J. Infect. Dis.* **44**, 1–19 (2014).

100. Wurie, F. B., Lawn, S. D., Booth, H., Sonnenberg, P. & Hayward, A. C. Bio-aerosol production by patients with tuberculosis during normal tidal breathing : implications for transmission risk : a cohort study. *Lancet* **386**, S81 (2016).

101. Clark, S. O., Hall, Y., Kelly, D. L. F., Hatch, G. J. & Williams, A. Survival of

Mycobacterium tuberculosis during experimental aerosolization and implications for aerosol challenge models. *J. Appl. Microbiol.* 350–359 (2011). doi:10.1111/j.1365-2672.2011.05069.x

102. Escombe, A. R. *et al.* The Detection of Airborne Transmission of Tuberculosis from HIV-Infected Patients , Using an In Vivo Air Sampling Model. (2007). doi:10.1086/515397

103. Riley, R. L. *et al.* Ultraviolet Irradiation of Infected Air: Comparative Infectiousness of Different Patients. *Am. Rev. Respir. Dis.* **85**, (1962).

104. Peccia, J. & Hernandez, M. UV-Induced Inactivation Rates for Airborne Mycobacterium bovis BCG. *J. Occup. Environ. Med.* **1**, 430–435 (2004).

105. Brambilla, C., Llorens-fons, M., Julián, E., Noguera-ortega, E. & Luquin, M. Mycobacteria Clumping Increase Their Capacity to Damage Macrophages. *Front. Microbiol.* **7**, 1–12 (2016).

106. Eum, S. Y. *et al.* Neutrophils are the predominant infected phagocytic cells in the airways of patients with active pulmonary TB. *Chest* **137**, 122–128 (2010).

107. Lowe, D. M., Redford, P. S., Wilkinson, R. J., O'Garra, A. & Martineau, A. R. Neutrophils in tuberculosis: Friend or foe? *Trends Immunol.* **33**, 14–25 (2012).

108. Fennelly, K. P. *et al.* Cough-generated Aerosols of Mycobacterium tuberculosis A New Method to Study Infectiousness. **169**, 604–609 (2004).

109. Corleis, B. *et al.* Escape of Mycobacterium tuberculosis from oxidative killing by neutrophils. *Cell. Microbiol.* **14**, 1109–1121 (2012).

110. Ferry, R. M., Brown, W. F. & Damon, E. B. Studies of the loss of viability of bacterial aerosols. III. Factors affecting death rates of certain non-pathogens. *J. Hyg. (Lond)*. **56**, 389–403 (1958).

111. Snider, D. E., Kelly, G. D., Cauthen, G. M., Thompson, N. J. & Kilburn, J. O. Infection and disease among contacts of tuberculosis cases with drug-resistant and drug-susceptible bacilli. *Am. Rev. Respir. Dis.* **132**, 125–32 (1985).

112. Peccia, J. *et al.* Effects of Relative Humidity on the Ultraviolet Induced Inactivation of Airborne Bacteria Effects of Relative Humidity on the Ultraviolet Induced Inactivation of Airborne Bacteria. *Aerosol Sci. Technol.* **6826**, 728–740 (2001).

113. Turner, R. D. *et al.* Tuberculosis Infectiousness and Host Susceptibility. *J. Infect. Dis.* **216**, (2017).

114. Nardell, E. A. Transmission and Institutional Infection Control of Tuberculosis. *Cold Spring Harb Perspect Med* **6**, (2015).

115. Gannon, B. W., Hayes, C. M. & Roe, J. M. Survival rate of airborne Mycobacterium bovis. *Res. Vet. Sci.* **82**, 169–172 (2007).

116. WHO. WHO Fact Sheed. (2018). Available at: https://www.who.int/en/news-room/fact-sheets/detail/influenza-(seasonal).

117. Modrow, S., Falke, D., Truyen, U. & Schätzl, H. *Molekulare Virologie*. (2003).

118. Taubenberger, J. & Morens, D. The Pathology of Influenza Virus Infections. *Annu Rev Pathol* **3**, 499–522 (2008).

119. Knipe, D. M. u. P. M. H. *Fields Virology*. (2006).

120. Hause, B. M. *et al.* Characterization of a Novel Influenza Virus in Cattle and Swine : Proposal for a New Genus in the Orthomyxoviridae Family. *MBio* **5**, 1–10 (2014).

121. Briese, T., Chowdhary, R., Hutchison, S. K., Popov, V. & Street, C. Are Novel Members of the Family Orthomyxoviridae. *J. Virol.* **88**, 5298–5309 (2014).

122. Allison, A. B. *et al.* Cyclic Avian Mass Mortality in the Northeastern United States Is Associated with a Novel Orthomyxovirus. *J. Virol.* **89**, 1389–1403 (2015).

123. Tong, S. *et al.* New World Bats Harbor Diverse Influenza A Viruses. *PLoS Pathog.* **9**, (2013).

124. Nayak, D. P., Balgoun, R. A., Yamada, H., Zhou, Z. H. & Barman, S. Influenza virus morphogenesis and budding. *Virus Res.* **143**, 147–161 (2009).

125. Dadonaite, B., Vijayakrishnan, S., Fodor, E., Bhella, D. & Hutschinson, E. Filamentous Influenza Viruses. *J Gen Virol* **97**, 1755–1764 (2018).

126. Campbell, P. J. *et al.* The M Segment of the 2009 Pandemic Influenza Virus Confers Increased Neuraminidase Activity , Filamentous Morphology , and Efficient Contact Transmissibility to A / Puerto Rico / 8 / 1934-Based. *J. Virol.* **88**, 3802–3814 (2014).

127. Bouvier, N. M. & Palese, P. The Biology of Influenza Viruses. *Vaccine* **26**, (2011).

128. Horimoto, T. & Kawaoka, Y. Influenza: lessons from past pandemics, warning of current incidents. *Nat. Rev. Microbiol.* **3**, 591–600 (2005).

129. Flick, R. & Hobom, G. Interaction of influenza virus polymerase with viral RNA in the ' corkscrew ' conformation. *J. Gen. Virol.* **80**, 2565–2572 (1999).

130. Jagger, B. W. *et al.* An Overlapping Protein-Coding Region In Influenza A Virus Segment 3 Modulates the Host Response. *Science (80-.).* **337**, 199–204 (2013).

131. Yamayoshi, S., Watanabe, M. & Goto, H. Identification of a Novel Viral Protein Expressed from the PB2 Segment of Influenza A Virus. *Jounal Virol.* **90**, 444–456 (2016).

132. Wise, H. M. *et al.* Identification of a Novel Splice Variant Form of the Influenza A Virus M2 Ion Channel with an Antigenically Distinct Ectodomain. *PLoS Pathog.* **8**, (2012).

133. Dias, A. *et al.* The cap-snatching endonuclease of influenza virus polymerase resides in the PA subunit. *Nature* **458**, (2009).

134. Selman, M., Dankar, S. K., Forbes, N. E., Jia, J. & Brown, E. G. Adaptive mutation in influenza A virus non-structural gene is linked to host switching and induces a novel protein by alternative splicing. *Emerg. Microbes Infect.* **42**, 0 (2012).

135. Toricelli, M., Melo, F. H. M., Peres, G. B., Silva, D. C. P. & Jasiulionis, M. G. Timp1 interacts with beta-1 integrin and CD63 along melanoma genesis and confers anoikis resistance by activating PI3-K signaling pathway independently of Akt phosphorylation.

Mol. Cancer **12**, 22 (2013).

136. Mostafa, A., Abdelwhab, E. M., Mettenleiter, T. C. & Pleschka, S. Zoonotic Potential of Influenza A Viruses : A Comprehensive Overview. *Viruses* 1–38 (2018). doi:10.3390/v10090497

137. Neumann, G., Noda, T. & Kawaoka, Y. Emergence and pandemic potential of swine-origin H1N1 influenza virus Gabriele. *Nature* **459**, 931–939 (2009).

138. Chu, V. C. & Whittaker, G. R. Influenza virus entry and infection require host cell N-linked glycoprotein. *PNAS* **101**, (2004).

139. Shi, Y., Wu, Y., Zhang, W., Qi, J. & Gao, G. Enabling the 'host jump': structural determinants of receptor-binding specificity in influenza A viruses. *Nat Rev Microbiol* **12**, 822–831 (2014).

140. Nicholls, J. M., Bourne, A. J., Chen, H., Guan, Y. & Peiris, M. Sialic acid receptor detection in the human respiratory tract : evidence for widespread distribution of potential binding sites for human and avian influenza viruses. *Respir. Res.* **1**, 1–10 (2007).

141. Lakadamyali, M., Rust, M. & Zhuang, X. Endocytosis of influenza viruses. *Microbes infect* **6**, 929–936 (2009).

142. Sun, X. & Whittaker, G. R. *Entry of influenza virus*. (2013).

143. Whittaker, G. R., Kann, M. & Helenius, A. Viral Entry into the Nucleus. *Annu. Rev. Cell Dev. Biol.* **16**, 627–651 (2000).

144. Dou, D. *et al.* Influenza A Virus Cell Entry , Replication , Virion Assembly and Movement. *Front. Immunol.* **9**, 1–17 (2018).

145. Thangavel, R. R. & Bouvier, N. M. Animal models for influenza virus pathogenesis, transmission and immunology. *J Immunol Methods* **0**, 60–79 (2014).

146. Aquarium, N. E. & Island, P. Are Seals Frequently Infected with Avian Influenza Viruses? *J. Virol.* **51**, 863–865 (1984).

147. Hinshaw, V. S. *et al.* Characterization of Two Influenza A Viruses from a Pilot Whale Anbtigenieinto. **58**, 655–656 (1986).

148. Guo, Y. *et al.* Charactertization of a new avian-like influenza A virus from horses in China. *Virology* **188**, 245–255 (1992).

149. Englund, L. Studies of influenza viruses H10N4 and H19 N7 of avian origin in mink. *Vet. Microbiol.* **74**, 101–107 (2000).

150. Mänz, B., Schwemmle, M. & Brunotte, L. Adaptation of Avian Influenza A Virus Polymerase in Mammals To Overcome the Host Species Barrier. *J. Virol.* **87**, 7200–7209 (2013).

151. Wei, K. *et al.* Influenza a virus acquires enhanced pathogenicity and transmissibility after serial passages in Swine. *J. Virol.* **88**, 11981–94 (2014).

152. Varble, A. *et al.* Influenza a virus transmission bottlenecks are defined by infection route

and recipient host. *Cell Host Microbe* **16**, 691–700 (2014).

153. Webster, R. G., Bean, W. J., Gorman, O. T. & Chambers, T. M. Evolution and Ecology of Influenza A Viruses. *Microbiol. Rev.* **56**, 152–179 (1992).

154. Joseph, U. *et al.* Adaptation of Pandemic H2N2 Influenza A Viruses in Humans. *J. Virol.* **89**, 2442–2448 (2015).

155. Allen, J. D. & Ross, T. M. H3N2 in fluenza viruses in humans : Viral mechanisms , evolution , and evaluation. *Hum. Vaccin. Immunother.* **0**, 1–8 (2018).

156. Parrish, C. R., Murcia, P. R. & Holmes, C. Influenza Virus Reservoirs and Intermediate Hosts : Dogs , Horses , and New Possibilities for Influenza Virus Exposure of Humans. *J. Virol.* **89**, 2990–2994 (2015).

157. Tellier, R. Aerosol transmission of influenza A virus: a review of new studies. *J. R. Soc. Interface* **6**, S783–S790 (2009).

158. Brankston, G., Gitterman, L., Hirji, Z., Lemieux, C. & Gardam, M. Transmission of influenza in human beings. *Lancet* **7**, 257–265 (2007).

159. Zhang, H. *et al.* Airborne spread and infection of a novel swine-origin influenza A (H1N1) virus. *Virol. J.* **10**, 204 (2013).

160. Killingley, B. & Nguyen-Van-Tam, J. Routes of influenza transmission. *Influenza Other Respi. Viruses* **7**, 42–51 (2013).

161. Richard, M. & Fouchier, R. A. M. Influenza A virus transmission via respiratory aerosols or droplets as it relates to pandemic potential. 1–18 (2015). doi:10.1093/femsre/fuv039

162. Hemmes, J. H., Winkler, K. C. & Kool, S. M. Virus survival as a seasonal factor inInfluenza and Poliomyelitis. *Nature* **188**, 430–431 (1960).

163. Yang, W. & Marr, L. C. Dynamics of Airborne influenza A viruses indoors and dependence on humidity. *PLoS One* **6**, (2011).

164. Marr, L. C., Tang, J. W., Van Mullekom, J. & Lakdawala, S. S. Mechanistic insights into the effect of humidity on airborne influenza virus survival, transmission and incidence. *J. R. Soc. Interface* **16**, (2019).

165. Yan, J. *et al.* Infectious virus in exhaled breath of symptomatic seasonal influenza cases from a college community. **115**, 4–9 (2018).

166. Mubareka, S. *et al.* Transmission of Infleunza Virus via Aerosols and Fomites in the Guinea Pig Model. *J Infect Dis* **18**, 1199–1216 (2013).

167. Brown, J. R. *et al.* Influenza virus survival in aerosols and estimates of viable virus loss resulting from aerosolization and air-sampling. *J. Hosp. Infect.* (2015). doi:10.1016/j.jhin.2015.08.004

168. Wang, S. *et al.* Label-free imaging, detection, and mass measurement of single viruses by surface plasmon resonance. *Proc. Natl. Acad. Sci.* **107**, 16028-16–32 (2010).

169. Wolfe, N. D., Dunavan, C. P. & Diamond, J. Origins of major human infectious diseases.

Nature **447**, 279–283 (2007).

170. Imai, M. *et al.* Transmission of influenza A/H5N1 viruses in mammals. *Virus Res.* **178**, 15–20 (2013).

171. Denney, L. & Ho, L. ScienceDirect Review Article : Special Edition The role of respiratory epithelium in host defence against influenza virus infection *. *Biomed. J.* **41**, 218–233 (2018).

172. Baumgartner, E. A. *et al.* Seasonality, timing, and climate drivers of influenza activity worldwide. *J. Infect. Dis.* **206**, 838–846 (2012).

173. Lofgren, E., Fefferman, N. H., Naumov, Y. N., Gorski, J. & Naumova, E. N. Influenza seasonality: underlying causes and modeling theories. *J. Virol.* **81**, 5429–5436 (2007).

174. Ng, S. & Gordon, A. Influenza Burden and Transmission in the Tropics. *Curr. Epidemiol. Reports* 89–100 (2015). doi:10.1007/s40471-015-0038-4

175. Shaman, J., Pitzer, V. E., Viboud, C., Grenfell, B. T. & Lipsitch, M. Absolute humidity and the seasonal onset of influenza in the continental United States. *PLoS Biol.* **8**, (2010).

176. Bonilla, E., Valero, N., Chacín-Bonilla, L. & Medina-Leendertz, S. Melatonin and viral infections. *J. Pineal Res.* **36**, 73–79 (2004).

177. Dowell, S. F. Seasonal variation in host susceptibility and cycles of certain infectious diseases. *Emerg. Infect. Dis.* **7**, 369–374 (2001).

178. Ferguson, N. M., Galvani, A. P. & Bush, R. M. Ecological and immunological determinants of influenza evolution. *Nature* **422**, 428–433 (2003).

179. Weinberger, D. M. *et al.* Influenza epidemics in iceland over 9 decades: Changes in timing and synchrony with the United States and Europe. *Am. J. Epidemiol.* **176**, 649–655 (2012).

180. Harper, B. Y. G. J. Airborne micro-organisms : survival tests with four viruses. 479–486 (1961).

181. Lowen, A. C. & Steel, J. Roles of Humidity and Temperature in Shaping Influenza Seasonality. *J. Virol.* **88**, 7692–7695 (2014).

182. Yang, W., Elankumaran, S. & Marr, L. C. Relationship between Humidity and Influenza A Viability in Droplets and Implications for Influenza's Seasonality. *PLoS One* **7**, 1–8 (2012).

183. Delort, A.-M. & Amato, P. *Microbiology of Aerosols*. (John Wiley & Sons, Inc., 2017).

184. DWD. https://cdc.dwd.de/portal/.

185. RKI. https://survstat.rki.de/.

186. Bundesamt, S. *https://www-genesis.destatis.de/genesis/online*. (2019).

187. Soebiyanto, R. P. *et al.* Associations between meteorological parameters and influenza activity in Berlin (Germany), Ljubljana (Slovenia), Castile and León (Spain) and Israeli districts. *PLoS One* **10**, 1–21 (2015).

188. Jain, S. *et al.* Community-Acquired Pneumonia Requiring Hospitalization among U.S. Adults. *N. Engl. J. Med.* 150714140110004 (2015). doi:10.1056/NEJMoa1500245

189. Müller-Westermeier, G. Das Klima in Deutschland. *Klimastatusbericht 2001* 9–11 (2001).

190. Engvall, K., Wickman, P. & Norbäck, D. Sick building syndrome and perceived indoor environment in relation to energy saving by reduced ventilation flow during heating season: a 1 year intervention study in dwellings. *Indoor Air* **15**, 120–6 (2005).

191. Yang, W., Elankumaran, S. & Marr, L. C. Concentrations and size distributions of airborne influenza A viruses measured indoors at a health centre, a day-care centre and on aeroplanes. *J. R. Soc. Interface* **8**, 1176–1184 (2011).

192. Hogan, C. J. J. *et al.* Sampling methodologies and dosage as- sessment techniques for submicrometre and ultrafine virus aerosol particles. *J. Appl. Microbiol* **99**, 1422–1434 (2005).

193. Yaari, R., Katriel, G., Huppert, A., Axelsen, J. B. & Stone, L. Modelling seasonal influenza: The role of weather and punctuated antigenic drift. *J. R. Soc. Interface* **10**, (2013).

194. Fares, A. Seasonality of Tuberculosis. *J Glob Infect Dis* **3**, 46–55 (2011).

195. Soetens, L. C., Boshuizen, H. C. & Korthals Altes, H. Contribution of seasonality in transmission of mycobacterium tuberculosis to seasonality in tuberculosis disease: A simulation study. *Am. J. Epidemiol.* **178**, 1281–1288 (2013).

196. Wingfield, T. *et al.* The Seasonality of Tuberculosis , Sunlight , Vitamin D , and Household Crowding. *J. Infect. Dis.* **210**, (2014).

197. Ring, S. *et al.* Blocking IL-10 receptor signaling ameliorates Mycobacterium tuberculosis infection during influenza-induced exacerbation. *JCI Insight* **4**, (2019).

List of Publications

In review Scientific Reports

'Enhanced tenacity of mycobacterial aerosol from necrotic neutrophils',

E. Pfrommer, C. Dreier, G. Gabriel, T. Dallenga, R. Reimer, K. Schepanski, R. Scherließ, U. E. Schaible, T. Gutsmann

Manuscript in preparation

'Respiratory virus infection modelling using novel in vitro generated human nasopharynx-like tissue'

E. Pfrommer, A. Münscher, C. Dreier, M. Spohn, R. Reimer, C. Schneider, G. Pilnitz-Stolze, L. Bußmann, N. Möckelmann, T. Waßenhoven, L. Hsieh, D. Indenbirken, A. Grundhoff, G. Gabriel, U. Schaible, Thomas Dobner and W. Ching

Manuscript in preparation

'Weather conditions shape Influenza season'

E. Pfrommer, M. Faust, T. Gutsmann, G. Gabriel, U. Schaible, K. Schepanski

Eidesstattliche Versicherung

Declaration on oath

Hiermit erkläre ich, Karoline Elisabeth Pfrommer, an Eid statt, dass ich die vorliegende Dissertationsschrift selbst verfasst und keine anderen als die angegebenen Quellen und Hilfsmittel benutzt habe. Infektions-Experimente für Abbildung 19 und 20A wurden von Carola Dreier unter meiner Anleitung durchgeführt. Das Nasopharynx basierte Gewebemodel wurde von Wilhelm Ching entwickelt und Proben für die Experimente aus Abbildungen 18 - 21 bereitgestellt.

I, Karoline Elisabeth Pfrommer, hereby declare, on oath, that I have written the present dissertation by my own and have not used other than the acknowledged resources and aids. Infections experiments from figure 19 and 20A were performed by Carola Dreier. The nasopharyngeal tissue culture model was developed by Wilhelm Ching and samples for all experiments were provided (Figure 18 till 21).

Ort und Datum	Unterschrift
city and date	*signature*

Bestätigung der Korrektheit der englischen Sprache

Confirmation of the correctness of the English language

Ort und Datum	Unterschrift
city and date	*signature*

Acknowledgements

I would like to thank my supervisors, who have been extremely supportive during my thesis. They helped me to accomplish my goals and without them I would have not made it so far. They always gave me the freedom to explore my ideas and shared my enthusiasm for unconventional solutions.

I had the chance to work in 4 different teams and to meet many amazing and supportive people but I would like to thank in particular:

Rudolf Reimer and Carola Schneider, who showed me the world of Electron Microscopy and sparked my love for this technique and the wonders of pictures.

Christian Nehls, who helped me to creatively develop my experiments, especially the biophysical ones and always had time for a coffee in the sun.

Caroline Pfeifer and Maja Ziegler who always where there for me, when it got tough and had an open door for me.

Matthias Faust, Jamie Banks and Stefanie Feuerstein, who were patient enough to help me with python.